PREPARATION AND CHARACTERIZATION OF SOME MOLECULAR AND GLASSY SEMICONDUCTORS

A thesis submitted by

ABDELRAZIK ELFAKI HAMEDELNIEL

in candidature for the degree

of

Master of Philosophy

of the University of London

The Bourne Laboratory,
Royal Holloway & Bedford New College,
(University of London),
Egham, Surrey, TW20 0EX,
U.K.

May 1987

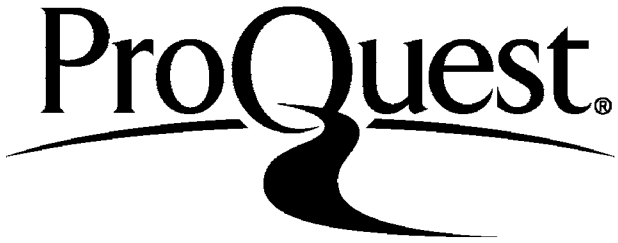

ABSTRACT

This work concerns mainly the characterization of oxonol dyes, cyanine dyes and their complexes, especially with tetrathiafulvalene (TTF). Some work has also been done on titanium (IV) doped iron (III) oxide. Cyclic voltammetry shows that TTF and its derivative dibenzo TTF can be reversibly oxidized to its radical cation and dication in non-aqueous solution. The equilibrium potentials for two one-electron oxidation steps in acetonitrile/tetrabutylammonium perchlorate (TBAP) were measured and found to be E(0,+.) = 0.302V and E(+.,++) = 0.770V for TTF and E(0,+.) = 0.540V and E(+.,++) = 0.900V for dibenzo TTF. Unlike cyanine dyes, oxonols are irreversibly oxidized and equilibrium potentials were measured by extrapolation of potential-sweep rate curves. Also using cyclic voltammetry, the rates of electron-transfer were calculated for TTF and dibenzo TTF as well as an electrochemical reduction series for some charge-transfer compounds relative to hydrogen reduction potential.

The complex TTF/oxonol dye was prepared electrochemically at the optimum conditions. Its solubility and sensitivity towards pH changes were measured. Cyclic voltammetry shows that the complex is irreversibly oxidized and at lower voltages compared to its constituents TTF and oxonol dye. Electrical measurements show that the complex is a semiconductor ($\sigma \simeq 9.8 \times 10^{-4} \Omega^{-1}\ cm^{-1}$) and the energy gap is 0.516 eV.

First ionization potentials measured by photoelectron spectroscopy for TTF, dibenzo TTF and TTF-oxonol dye complex give approximately the same value which suggests that, the solution chemistry of these compounds is different from their gaseous state behaviour. MNDO

calculations were used for geometry optimization, charge-density distribution, heats of formation and ionization potentials. Coupling constants and g-factors were calculated for TTF, its dibenzo derivative and its dye complexes using esr spectroscopy.

Charge-transfer complexes, particularly TTF/TCNQ show some degree of response towards polluting gases such as sulphur dioxide and carbon monoxide as determined by their conductivity changes when the gases were passed over the surface. They may therefore be used as gas sensors if certain modifications in structure or electrode design could be made.

Titanium (IV) Iron (III) oxide mixture shows a reasonable conductivity of $1.4 \times 10^{-3} \Omega^{-1} cm^{-1}$ but unfortunately a compressed pellet electrode is not mechanically stable. This problem can be solved by sintering the oxides with glass powder which resulted in a high resistance electrode in which some pH/voltage measurements have been done.

ACKNOWLEDGEMENT

I would like to express my sincere and grateful thanks to Professor D.B. Hibbert for his guidance and encouragement throughout this work. My thanks are also extended to Dr. J. Sandall for providing invaluable guidance at the late stages of this work. I am also grateful to Dr. M. Grossel and his group for providing the organic dyes, to Dr. L. Sutcliffe for some esr measurements, to Professor A. Finch for many valuable discussions and to the rest of the staff at the Bourne Laboratory for their help and co-operation during this work.

I would also like to acknowledge the British Council and University of Khartoum (Sudan) for financing this work and finally, my thanks to Mrs. E. Kearsey and Mrs. J. Evans for persisting with a difficult manuscript.

I dedicate this thesis

to my parents, Elfaki and Amina

and to my wife Sara.

CONTENTS

LIST OF FIGURES

LIST OF TABLES

CHAPTER 1

General Introduction

1.1 Historical Background of Organic Metals.

Organic solids are usually thought of as electrical insulators. Recent discoveries of molecular crystals and polymers that exhibit metallic levels of conductivity have drastically altered the situation. Such materials have been termed 'molecular metals' ($\sigma \sim 10\text{-}10^4\ \Omega^{-1}\ cm^{-1}$).[1] They have provided new insights into the solid state properties of organic systems and offer prospects of many technological applications in the future.

Although metallic in nature, they have low conductivity compared to a metal such as copper. However, while some organic metals become superconducting (absence of electrical resistance) at low temperature, copper never does. The first organic metal, reported in 1954[2], was a perylene-bromine complex.

Most of the studies are now concerned mainly with charge-transfer complexes[3], which have been studied extensively since the beginning of the century[4,5]. Familiar donors include alkali metals, amines, or aromatic molecules; among familiar acceptors are halogen atoms, quinones, or electron deficient alkenes, heterocycles or aromatic molecules.

The first evidence that crystalline charge-transfer complexes could be electrically conducting dates back to the early 1960's[6,7]. Then Little[8] proposed a model for high temperature organic superconductors involving conduction along linear hydrocarbon chains surrounded by polarizable dye molecules.

The preparation of a new donor, tetrathiafulvalene (TTF)[9] in 1970 led, two years later, to discovery of some derivatives which are metallic at room temperature[10-13]. Many were surprised to learn that TTF/TCNQ (Tetrathiafulvalene/Tetracyanoquinodimethane) had

metallic conductivity, rising to $10^4\ \Omega^{-1}\ cm^{-1}$ around 60K, at which point a metal-semiconductor transition occurred[11,9]. This discovery caused many chemists, physicists, and theoreticians to enter the field of organic metals. Unitl 1979, when the first organic superconductor was discovered[14], research focused on the synthesis of new TTF and TCNQ derivatives and other novel donor and acceptor systems.

During this period, there has been equal interest in polymeric hydrocarbons with extensive - electron delocalization, where there is the possibility of a narrow conduction band, derived from the π-orbitals. Polyacetylene has received most attention; in the pure state the material is an insulator ($\sigma_{rt} \sim 10^{-9}\ \Omega^{-1}\ cm^{-1}$) with a relatively large band gap, but Heeger, MacDiarmid and co-workers[15,16,17] showed in 1977 that doping with strong oxidizing and reducing agents increase the conductivity of polyacetylene to $\sigma_{rt} \sim 500\ \Omega^{-1}\ cm^{-1}$. Since then there has been much work on polyacetylene and its derivatives[18].

Two other related classes of one-dimensional conductors include polymers of the main group elements, for example, $(SN)_x$[19] and linear-chain chelated transition metal compounds where intrachain overlap involves the ligand - system as well as metal-metal interactions[20]. For more information on such materials see references 21-23.

The electron wave-function overlap for 3- types of conducting materials are shown in Figure (1)[24]. Some examples of molecular metals are shown in Table (1) and the necessary conditions to design an organic conductor were also summarized.

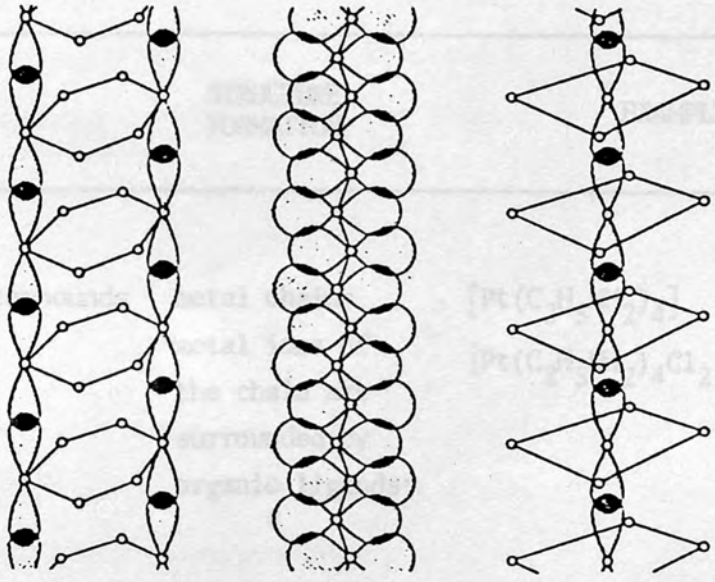

Figure (1) 1.1.1 Electron wave function overlap for carbon atom π electrons in:

a) a molecular stack

b) a polymer chain and

c) metal ion d-orbitals in a metal organic compound.

Only some functions are shown in (a) for clarity.

1.1.2 Table (1):

Examples of Molecular Metals.

TYPE	STRUCTURE FORMATION	EXAMPLES
1. chain compounds	metal chains "metal ions of the chain are surrounded by organic ligands"	$[Pt(C_2H_5NH_2)_4]$ - $[Pt(C_2H_5NH_2)_4Cl_2]\ Cl_4$
2. conjugated polymers	polymerization	(i) poly-sulphur nitride (SN_X) (ii) polyacetylene
3. charge-transfer complexes	complexes formed from donors and acceptors.	Donors: TTF and its derivatives Acceptors: TCNQ and its derivatives

1.1.3 The necessary conditions to design organic conductor composed of donor (D) and acceptor (A) are[25]:

1. Enforce a segregated mode of stacking (....DD....11....AA....) in the solid state, which can be shown clearly as:

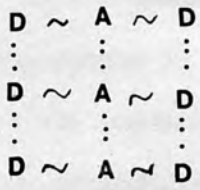

and the crystal lattice of organic metals consist of segregated stacks of planar (D_{2h}) donors and planar (D_{2h}) acceptors.

2. Control the A:D stoichiometry.
3. Partial degree of electron-transfer.
4. Symmetry of donor and acceptor must be considered.
5. Stabilized the delocalized state ($D^{+\delta}D^{+\delta}..11..A^{-\delta}A^{-\delta}$) below the localized one ($D^{+}D..11..A^{+}A$).
6. Permit and control the degree of interchain coupling.

1.2 Definition of Insulators, Semiconductors and Metals in terms of energy gap and range of conductivity.

When a set of N- atoms or ions is condensed from the gas phase to form a crystalline solid, the discrete electronic energy levels of the individual atoms interact and spread into bands of allowed energy separated by forbidden energy gaps[26]. For pure accurately stoichiometric compounds three limiting cases arise:

(a) Some solids are electrical insulatros (e.g. pure MgO) for these, each occupied band is exactly filled with its quota of

electrons and there is a large forbidden energy gap ΔE^{o} to the next allowed level which is thus completely empty (Fig. 2d). The energy gap in this case is more than 1.2 eV.

(b) The second case for pure compounds is when the forbidden energy gap is within an order of magnitude of thermally accessible energies (0.1 to 1.5 eV). Such compounds are insulators at low temperatures but, as the temperature is raised, increasing numbers of electrons are promoted to the conduction band and the compound becomes a semiconductor, with a conductivity which increases exponentially with temperature. Both the electrons in the conduction band and the positive holes in the almost filled band contribute to this conductivity, Fig. (2c). Semiconductivity will either be intrinsic or extrinsic and this will be discussed later.

(c) The third limiting case describes the situation in metals: here either the highest occupied band is only partly filled with electrons (e.g. Na) or two bands overlap, allowing electrons from an otherwise full band to leak over into the next higher band (e.g. Mg). In both cases there are levels to which electrons can move under the influence of an applied potential and the metal is a good electronic conductor (Fig. (2a) and (2b)).

The range of electrical conductivity for the above 3- mentioned cases are as follows[27]:

metals:	10^{4} - 10^{6}	Ω^{-1} cm^{-1}
semiconductors:	10^{-9} - 10^{3}	" "
insulators:	10^{-22} - 10^{-10}	" "

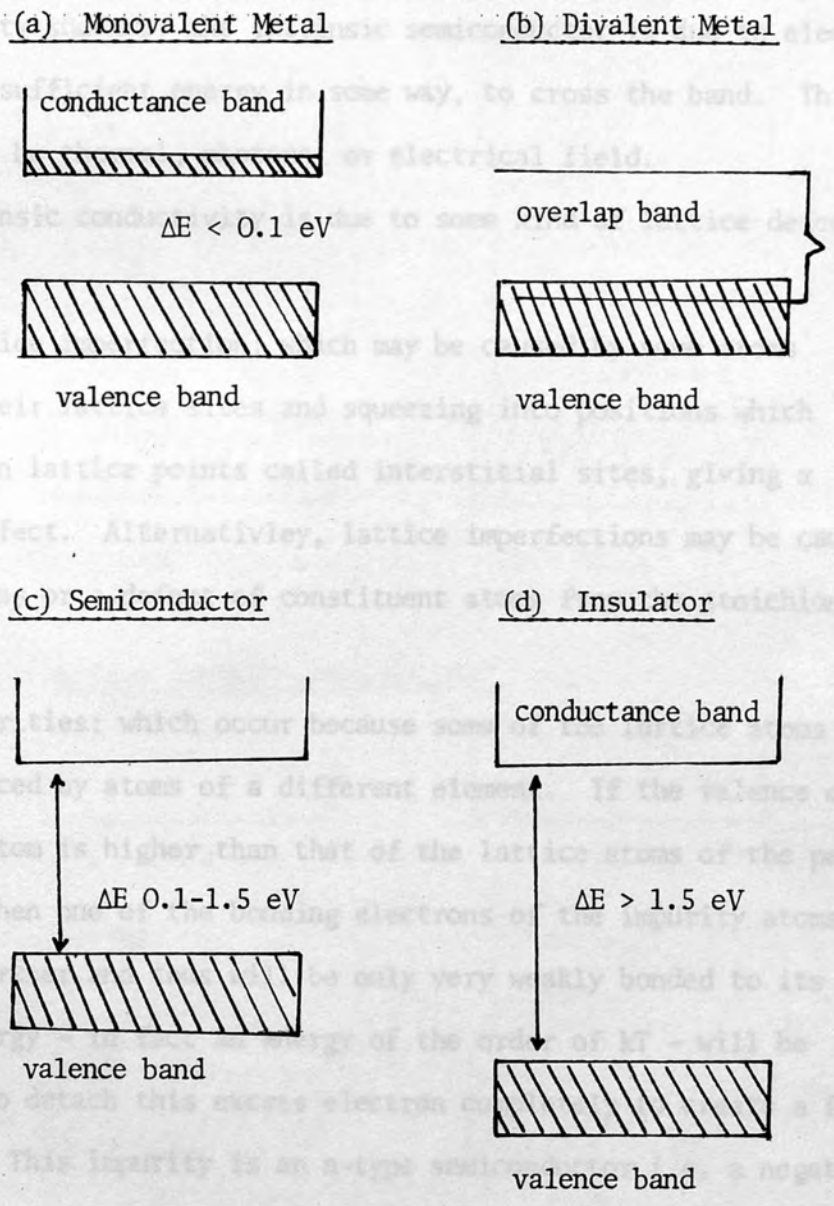

Figure (2) 1.2.1 Energy gap diagrams in metals, semiconductors and insulators.

1.2.2 Intrinsic and Extrinsic Semiconduction.

A semiconductor may be either intrinsic or extrinsic[27]. Conductivity shown by the intrinsic semiconductor is due to electrons acquiring sufficient energy in some way, to cross the band. This energy may be thermal, photons, or electrical field.

Extrinsic conductivity is due to some kind of lattice defect such as:

(a) Lattice imperfection: which may be caused by some atoms leaving their lattice sites and squeezing into positions which are between lattice points called interstitial sites, giving a Frenkel defect. Alternativley, lattice imperfections may be caused by an excess or a defect of constituent atoms from the stoichiometric formula.

(b) Impurities: which occur because some of the lattice atoms have been replaced by atoms of a different element. If the valence of the impurity atom is higher than that of the lattice atoms of the parent crystal, then one of the bonding electrons of the impurity atoms will have no partner and thus will be only very weakly bonded to its atom. Little energy - in fact an energy of the order of kT - will be required to detach this excess electron completely to create a free electron. This impurity is an n-type semiconductor i.e. a negative charge carrier. A p-type semiconductor is a type where the impurity atoms have a valence below that of the host lattice atoms. This is shown diagramatically in Fig. (3a) and (3b).

a) p-Type Impurity Semiconductor

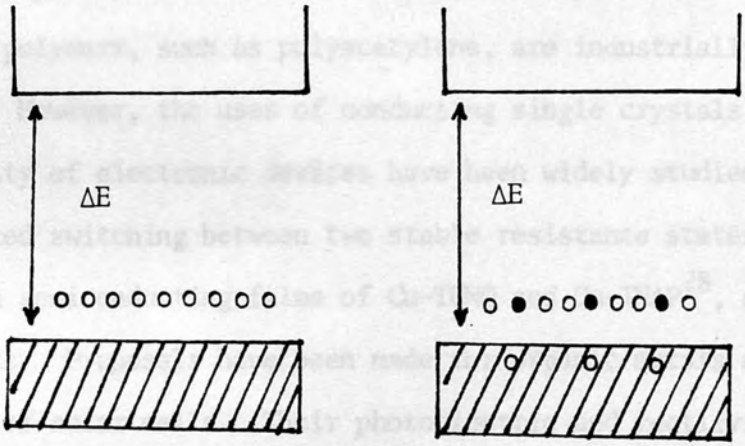

b) n-Type Impurity Semiconductor

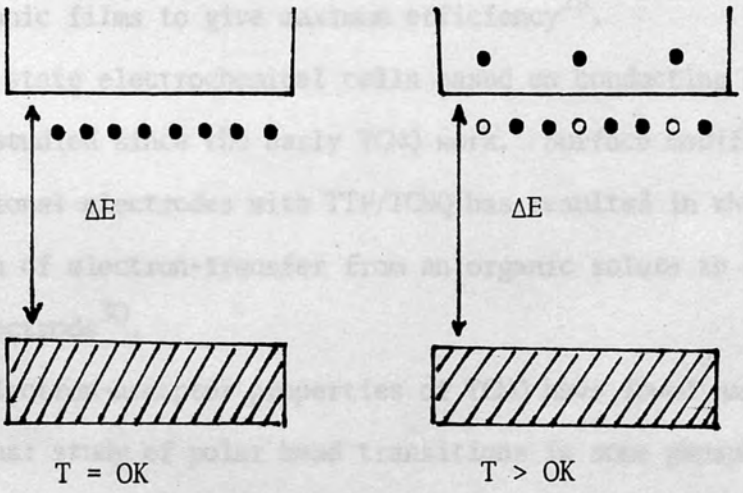

Figure (3) 1.2.3 Mechanism of conductance in impurity type of semiconductors.

1.3 Some Applications of Organic Semiconductors.

TTF-TCNQ and its derivatives have not found extensive applications partly because of frailty of the crystals whereas conducting polymers, such as polyacetylene, are industrially more adaptable. However, the uses of conducting single crystals in microcircuity of electronic devices have been widely studied. Photo-induced switching between two stable resistance states has been observed in semiconducting films of Cu-TCNQ and Cu-TNAP[28], and in some $TCNQF_4$ salts. Proposals have been made for organic metals as components of solar cells. Their photoelectric and rectifying behaviour resembles that of a conventional Schottky barrier or MIS (metal-insulator-semiconductor) devices, and research in this area is now concentrated on optimising the nature and distribution of dopants in the organic films to give maximum efficiency[29].

Solid state electrochemical cells based on conducting complexes have been studied since the early TCNQ work. Surface modification of conventional electrodes with TTF/TCNQ has resulted in the first observation of electron-transfer from an organic solute to a compacted organic electrode[30].

The electron-acceptor properties of TCNQ have found many diverse applications: study of polar head transitions in some phospholipids[31], for characterising electron donor properties of metal oxides used in catalysts[32], and for determining the critical micelle concentration of surfactants[33]. If superconductivity can be achieved at higher temperatures than those required to date then the technological potential is enormous; more efficient electronic motors, very powerful electromagnets and supercomputers that exploit the small heat output of superconducting circuit elements have all been considered[34].

1.4 The Physics of Transitions among Insulators, Semiconductors, Metals and Superconductors.

The most exciting advances of the past few years have come from studies of tetramethyltetraselenafulvalene (TMTSF) salts[3]. In 1978, the complex TMTSF-2,5-dimethyl TCNQ was found to be the first organic compound in which a truly conducting state is stabilized under pressure down to 1K; at ambient pressure a sharp-metal-to-insulator transition occurs at 42K[35,36].

Two theories were advanced to explain the low temperature conductivity of TMTSF-DMTCNQ. The Fermi surface may be semimetallic due to interchain hydridization making a quazi-two-dimentional solid[37] or, on the other hand, there may be gradual growth at low temperatures of a superconducting pairing between electron states[36].

According to the crystal structure and segregated mode of stacking, conducting organic charge-transfer complexes may be linked to arrays of one-dimensional molecules with more than the complement of electrons required for valence bonding. In principle, the extra electrons will partially fill a conduction band whose width is determined by the interactions between neighbours.

The behaviour of such a system was discussed inthe mid-1950's when Peierls[38] pointed out that, at a low temperature, a quazi-one-dimensional metal could not sustain long range order but would be unstable with respect to lattice distortions. In the simplest terms, the conducting chain would be stretched in one region and contracted in another, so that the conducting electrons become localized, with a filled electron band at a lower energy and an empty band at a higher energy. A variation of charge density in phase with the lattice distortion, such as this, is known as a charge density wave, and the

associated energy gap results in an insulating, or at best, a semiconducting solid.

As part of the explanation of superconductivity, however, Frohlich[39] pointed out in 1954 that if charge density waves were coupled to the vibration of the underlying lattice, a charge density wave could travel freely through the crystal, affording a superconductivity rather than an insulating state.

When the number of electrons in a chain is commensurate with the number of lattice sites, a metal-to-insulator transition can be expected to occur readily as the electron charge density wave becomes static because of the high potential energy which must be overcome in order for electrons to move to new equilibrium positions along the chain.

On the other hand, a charge density wave incommensurate with the lattice will not be locked to the lattice and will be free to translate to new positions, so acting as a charge carrier, without adversely affecting the energetics of its relationship to the lattice. Thus a mechanism for high conductivity is available and for a truly incommensurate system a superconducting state will exist[39]. A spin modulation, without a lattice modulation, provides another possible instability for one-dimensional conductors. Here, the electron spin density distorts along the chain, in the extreme case giving an antiferromagnetic arrangement of spins.

Lattice defects and impurities can also lead to random electrostatic potentials that will tend to spin the charge density wave to the underlying lattice and favour Peierls distortions.

1.5 Studies of Organic Conductors

In recent years there have been extensive research activities focussed on macromolecules with extended π-electron systems. Semiconductivity, as a property of crystalline organic substances containing π-electrons, was established in the first instance for phthalocyanine and isodibenzanthrone and pyranthrone. It was supposed in each case that the current carriers were mobile π-electrons, and support for this view came from the observation of Inokuchi[40] that the thermal energy gap decreases with increase in the number of π-electrons in the molecule.

In the early 1960's Masahtro[41] studied the paramagnetic and electronic properties of polyacetylene. In 1963, R.G. Kepler[42] carried out magnetic susceptibility measurements for a wide variety or organic salts based on the anion radical of TCNQ.

A correlation between the magnetic and electrical properties has been observed. It was found that, salts which exhibit the higher conductivities also exhibit a temperature independent paramagnetic contribution to their susceptibility, but in the less conducting materials, the odd electron associated withthe TCNQ anion radicals are paired in quazimolecular states consisting of a singlet ground state and a triplet state lying slightly above the ground state.

In 1971 Sharp and Johansson[43] prepared ion-selective solid state electrodes from ion-radical salts of TCNQ. The technique used was a compressed pellet of the ground salts and attached to a bright platinum base with graphite paste as adhesive and as electrical contact.

They found that, copper-selective and the silver selective

electrodes showed only a few interferences and behaved according to Nernst's equation over 5 and 6 decades of activities, respectively.

John[11] (1973), prepared the new compound TTF/TCNQ in 1:1 ratio. They concluded that, the electron transport properties of TTF/TCNQ are of interest for several reasons: a) TTF is highly symmetric (point group D_{2h}) and thus random potentials due to asymmetric orientation are less likely than for other cations previously investigated, b) TTF is highly polarizable because of the presence of sulphur and thus coulomb repulsion between electrons on neighbouring TCNQ sites should be considerably less than suggested for other TCNQ complexes prepared with nitrogen-containing heterocyclic cations of similar size to TTF[44].

The first ionization potential of TTF as measured by electron impact ionization was found to be 6.95 ± 0.1 eV[45]. At the same time the energy required to remove a second electron from TTF was suggested to be low by R.N. Compton and Co-workers[46] (1974). This suggestion was due to an observation of stable TTF^{2+} in a medium-resolution magnetic mass spectrometer. They also studied the electron affinity of TCNQ using cesium collisional ionization technique described in reference 47.

In 1975 E.M. Engler at the Watson Research Centre in New York[48] studied the ionization potentials and donor properties of selenium analoges of tetrathiafulvalence. Using cyclic-voltammetry they found that diselenadithiafulvalene (DSeDTF) and tetraselenafulvalene were more difficult to oxidize, that is they are weaker donors, than TTF. Their results were also confirmed by the energy of charge-transfer absorption upon complex formation with an acceptor and calculated

association constants.

Since selenium possess a lower ionization energy than sulphur 10.4 vs. 9.8 eV)[49], it also forms much weaker π-bonds to carbon (e.g. C=S π band strength, 3.00 eV vs. C=SC, 2.15 eV)[50]. It is the balance between these two opposing factors which may be responsible for the different trends in ionizaiton energy observed on replacing sulphur with selemium in these heteroaromatic systems.

The low ionization energy in the TTF system probably derives from its ability to distribute charge on all four sulphurs by π-bonding to carbon as illustrated by resonance structures below. Some molecular orbital calculations have been done to illustrate this point.

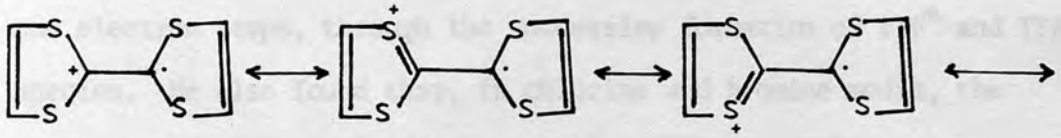

In 1977, Robert C.W. showed the effect of electron-transfer on TTF/TCNQ complexes. His study concluded that, the percent electron transfer in such complexes could have considerable influence on final electrical conductivity since electron-transfer in turn may influence the ease of a Peierls transition to an insulating state, the ability to form closely packed homogeneous stacks of cations and anions, and electronic interactions in homogeneous cation and anion stacks once formed. There are two ways to affect electron-transfer: to vary electron acceptor or donor strengths[52] and alter the stoichiometry.

In 1979 Allen J. Bard et al studied some properties of compact pellets of TTF/TCNQ in aqueous media as an electrode[53]. They found that the electrode was stable over a potential range of about 0.9 V, within this region the electrode exhibits residual Faradaic currents of less than 1-2 $\mu A/cm^2$ and the oxidation and reduction of soluble redox couples at this electrode could be carried out.

Another technique was used by F.B. Kaufman and co-workers[54], in which a linear phenoxytetrathiafulvalene polymer is physically adsorbed onto a metallic substrate by spin-coating to produce a polymer-modified electrode whose electrochemical and optical properties are distinctly different from those of the metallic substrate.

The electrochemistry of TTF in various aqueous media by using carbon paste electrode, was studied by Marian in 1982[55]. In metal-acetate, the oxidation of solid TTF procedes, as in solution, in two one electron steps, through the successive formation of $TTF^{+\cdot}$ and TTF^{++} species. He also found that, in chlorine and bromine media, the formation of several mixed valence salts $(TTF)Cl_{0.7}$, $(TTF)Br_{0.05}$ is detected on the current-voltage curves.

At the same time Henning and co-workers[56] prepared some electrodes by covering the conductive substrate (pt, Ta, Si, SnO_2) with 10 µL of 2% by weight Na/ion/EtOH solution and allowing the EtOH to evaporate. The TTF was incorporated into the film by immersing the electrode in an aqueous solution of 1 mM TTFCl for 10 minutes. Their study suggests that these films might be useful as protective layers on semiconductor electrodes to incorporate catalysts onto electrode surfaces.

Recently cyanine dyes have been examined as possible candidates for solar energy conversion in the form of monolayers and thin films

on glass substrates[57]. Absorption and emission characteristics of cyanine dyes were studied at the same time. They found that the efficiency of the cyanine dyes depends upon their emission properties and also on their photostability.

Unfortunately, it is commonly observed that the cyanine dyes with polymethine chains in the molecular framework degrade in light.

Williams[58], studied selenium - and sulphur - based organic superconductors. They were especially concerned with the novel structural features that characterized these systems and allow the development of structure-property correlations. Other studies[59] involve the range of electrical conductivity of TCNQ, which is started as an insulator (pyrene-TCNQ), a semiconductor (morphulinium-TCNQ), TTF/TCNQ the first organic metal, to HMTSF-TCNQ (Hexamethylenetetra-selenafulvalene), the first organic compound to remain metallic as the temperature approaches zero.

1.6 Aim of the Research

The major aim of this work is to characterize some novel conducting materials. The materials used include organic dyes, both anionic (oxonols) and cationic (cyanines), donors (tetrathiafulvalenes) and acceptors (tetracyanoquinodimethanes).

Cyclic voltammetry, conduction measurements, electron spin resonance, photoelectron spectroscopy and chemical analysis techniques were used to characterise these organic dyes and their complexes. In addition the novel materials were tested to make a sensor for polluting gases (e.g. sulphur dioxide, carbon monoxide).

Titanium-doped iron oxide glassy discs were treated under different conditions. Their electrical conductivity, response to pH changes were measured.

CHAPTER 2

Electrochemical Studies of Ti-doped Iron (III) Oxide Glassy Discs.

Electrochemical Studies of Ti-doped Iron (III) Oxide Glass Mixture

2. Introduction

Inorganic semiconductors play an important role in many industrial devices. Electrolysis of water to give hydrogen and oxygen is an obvious example, but chlorine production, fuel cells and even certain corrosion reactions involving gas electrodes are of particular interest. The materials presently used as inert electrodes at noble potentials in acid media include graphite, lead alloys, lead dioxide and platinum or ruthenium based coating on titanium[60].

Glass coating techniques have been used successfully for many years to provide a protective coating for mild steel vessels used in handling of acidic media[61].

In general a glass mixed with semiconductor oxides will be supposed to conduct if it has two continuous phases - a conducting oxide phase and a non-conducting glassy phase which fill up all pores. This condition will be satisfied if the oxide has some solubility in the glassy phase to enable liquid phase sintering[62] to take place. Very few of the known semiconducting oxides possess adequate conductivity and corrosion resistance in acidic media[63,64,65].

Work on iron oxide was initiated by Borom of the University of California in 1967[66]. He and his group studied the reactions between metallic iron and cobalt oxide bearing sodium disilicate glass. Their research was aimed to confirm the theory that chemical bonding occurs between a glass and metal when thermodynamic equilibrium relative to the low-valent oxide of the metal is present at the interface[67,68]. They also reported quantitative and definitive studies of the

electrochemistry of a model glass-metal system, i.e. iron and sodium disilicate glass containing cobalt oxide.

It has been shown that reactions may occur in glass containing reducible oxide-metal systems that are not at equilibrium, which are galvanic or electrochemical in nature and thus require both electronic and ionic transport mechanisms. Thus saturation of the glass at the glass-metal substrate interface with the oxide of the metal can be achieved only by solution of an oxide formed by preoxidation of the metal.

Recently $NiCo_2O_4$ has been developed as an electrode material to produce pure O_2 on a small scale, particularly for use in developing countries for medical purposes[69,70,71]. Tseung and his group of the City University[72] studied the role of lower metal oxide/higher metal oxide couples in determining the minimum voltage required for the evolution of oxygen, together with other essential requirements such as electrical resistivity, electrode microstructure, corrosion resistance and catalytic properties. Their survey of various metal oxides based on the above criterion suggested that $NiCo_2O_4$ is of particular interest and teflon bonded electrodes based on this material gave over 1300 A/m^2 at 1.63 V vs. dhe, 70°C, 5N KOH.

They also studied hydrogen evolution on teflon bonded Pt black, platinized Pt and Pt foil electrodes in 5N H_2SO_4, 25°C. Their study showed that teflon bonded electrodes gave a higher performance than the other electrodes. Tafel plots on such electrodes are complicated by the formation of higher oxides, gas bubbles, and emptying of the electrocatalyst pores, and it is suggested that potentiostatic pulse techniques can give more reliable results, provided the electrodes

are fully preanodized to form the higher metal oxide.

Preliminary attempts to develop inexpensive, protective conducting coatings on mild steel for use as insoluble anodes were studied by the same group. They managed to show that 3% Ti-Fe_2O_3 plus 20% glass pellets fired at 1250^{o}C have low resistivity and low porosity at which chlorine could be evolved in HCl. Their results showed that a Ti-doped glass coating did not give 100% protection to the mild steel. They suggest that improvement in the coating technique or the use of a more acid resistant metal could provide inexpensive, stable electrochemical anodes for a whole range of aqueous electrosynthesis processes.

To investigate further, we studied in this report titanium doped iron (III) oxide glass mixture at different compositons and heated in different conditions. An electrode of a compressed pellet was constructed and examined to be used as ion-selective electrode, especially towards hydrogen ion-concentration. Ion-selective electrodes can be defined as an electrochemical sensors that allow potentiometric determination of the activity of certain ions in the presence of other ions, and the suitable solid state materials should have the following properties:

a) Ion-exchange should be rapid and reversible for at least one ion.

b) Ion-exchange should attain local thermodynamic equilibrium.

c) They should be ionic conductors with resistance small compared to the imput impedence of the measuring device.

2.1 Preparation of discs.

All the staring materials were of Analar Grade. Iron (III) oxide is 99.9% pure from Ventron (Alfa division), titanium dioxide (BDH

Chemicals Ltd.) and 120 mesh glass powder. The mixed oxides were prepared by direct mixing of the three oxides and by co-precipitation[60] of the hydroxides from solution acidified with HCl, using excess ammonia. The precipitates were washed and heated to 1000°C for 2 hrs. in air. Different discs were prepared by pressing about 0.75-1.5 grams of the mixture into a 1 cm steel die at 10-15 tons cm^{-2}.

These discs were fired in air at 1200°C for different intervals. The composition of the mixture was changed and the conditions of heating were also changed each time. The resistivity of the oxide pellets (Table (4)) was measured by using 8020A model Digital Multimeter (John Fluke HFG. Co., Inc.). Using aluminium foils attached at both sides of the disc for an easy electrical contact.

2.2 Electrical Measurements Results.

Table (2) shows the range of electrical conductivity for pellets of different composition with constant 20% by weight of glass powder compared to that of pure iron (III) oxide. Table (3) represents oxides with constant composition, but different heating conditions. The effect of increasing titanium percent on conductivity of titanium doped iron (III) oxide disc was also shown in Fig. (4).

Table (2)

2.3 The Effect of Increasing Ti % in Conductivity of Ti-doped Iron (III) Oxide Discs Heated in Air (1200°C.)

	Composition	Conductivity (Ω^{-1} cm^{-1})
1.	Fe_2O_3	2.5×10^{-7}
2.	1.96% Ti-Fe_2O_3 20% glass	5.1×10^{-6}
3.	2.91% Ti-Fe_2O_3 20% glass	8.1×10^{-6}
4.	3.84% Ti-Fe_2O_3 20% glass	1.5×10^{-4}
5.	4.76% Ti-Fe_2O_3 20% glass	4.3×10^{-6}
6.	7.68% Ti-Fe_2O_3 2o% glass	1.0×10^{-4}
7.	3.84% Ti-Fe_2O_3 (no glass)	1.4×10^{-3}

Table (3)

2.4 The Effect of Heating Conditions in Conductivity of Ti-doped Iron (III) Oxide Disc.

	Composition	Heating Conditions	Conductivity (Ω^{-1} cm^{-1})
1.	3.84% Ti-Fe_2O_3 20% glass	2.5 hrs. (Air)	9.3×10^{-1}
2.	3.84% Ti-Fe_2O_3 20% glass	overnight (Air)	1.5×10^{-4}
3.	3.84% Ti-Fe_2O_3 20% glass	overnight (vacuum)	7.8×10^{-4}
4.	3.84% Ti-Fe_2O_3 20% glass	overnight (Argon)	6.4×10^{-5}

2.5 Electrochemical Studies

Some of the pressed discs were mounted: one side of the disc was coated with silver paste-epoxy adhesive (RS Components Limited). A nickel mesh screen was pressed onto the silver-epoxy coating and copper wire was fixed to the nickel screen using the same material. Using a plastic cover as a mould, the electrode was then encapsulated in epoxy resin (Araldite). Side and front views were shown in Fig. (5). The whole assembly was used as a working electrode in a 3-electrode cell, together with Calomel electrode reference and a sheet of platinum auxillary electrode - dipped in 0.1 M hydrochloric

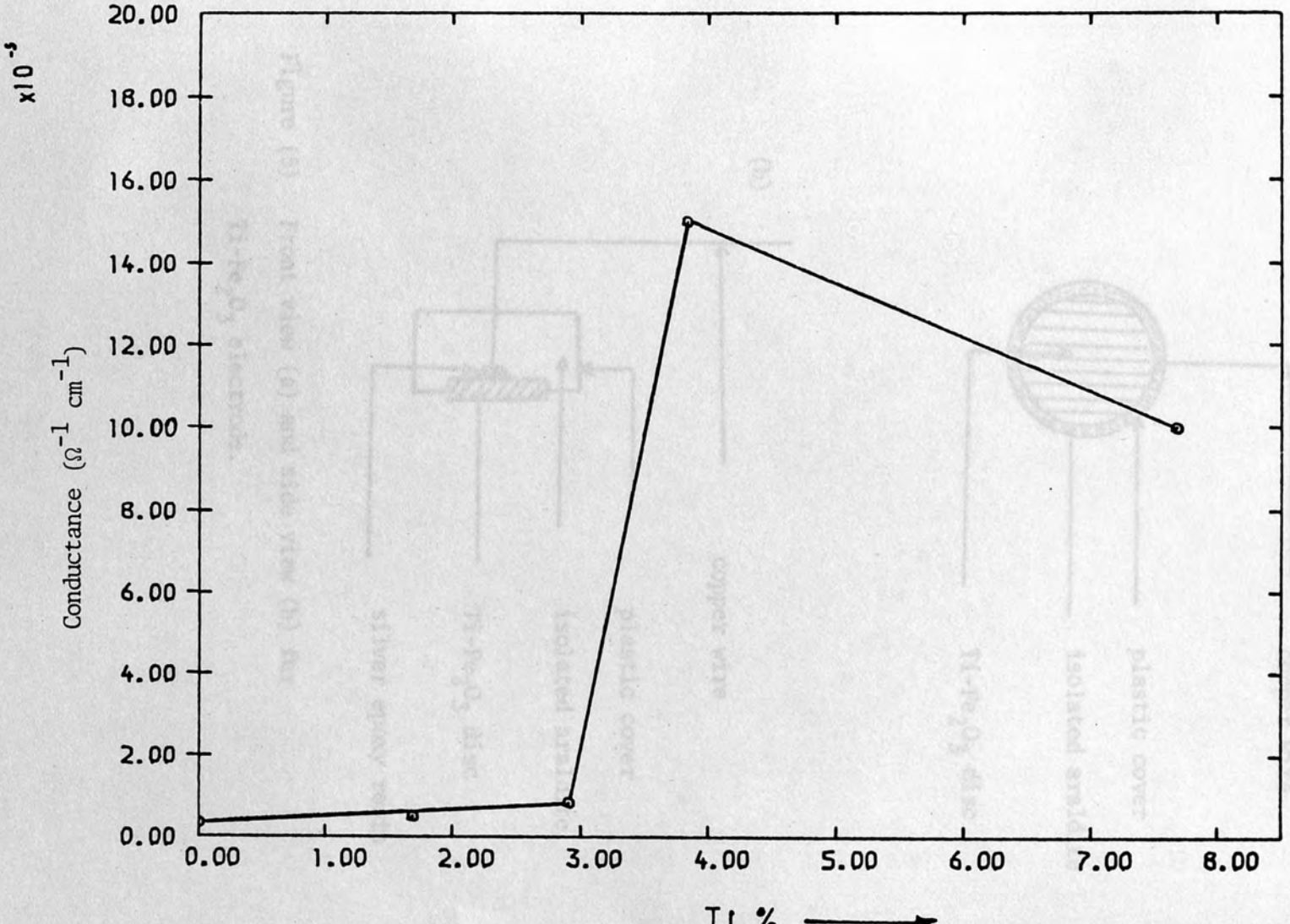

Figure (4) Effect of increasing Ti % in conductivity of Ti-Fe_2O_3 disc

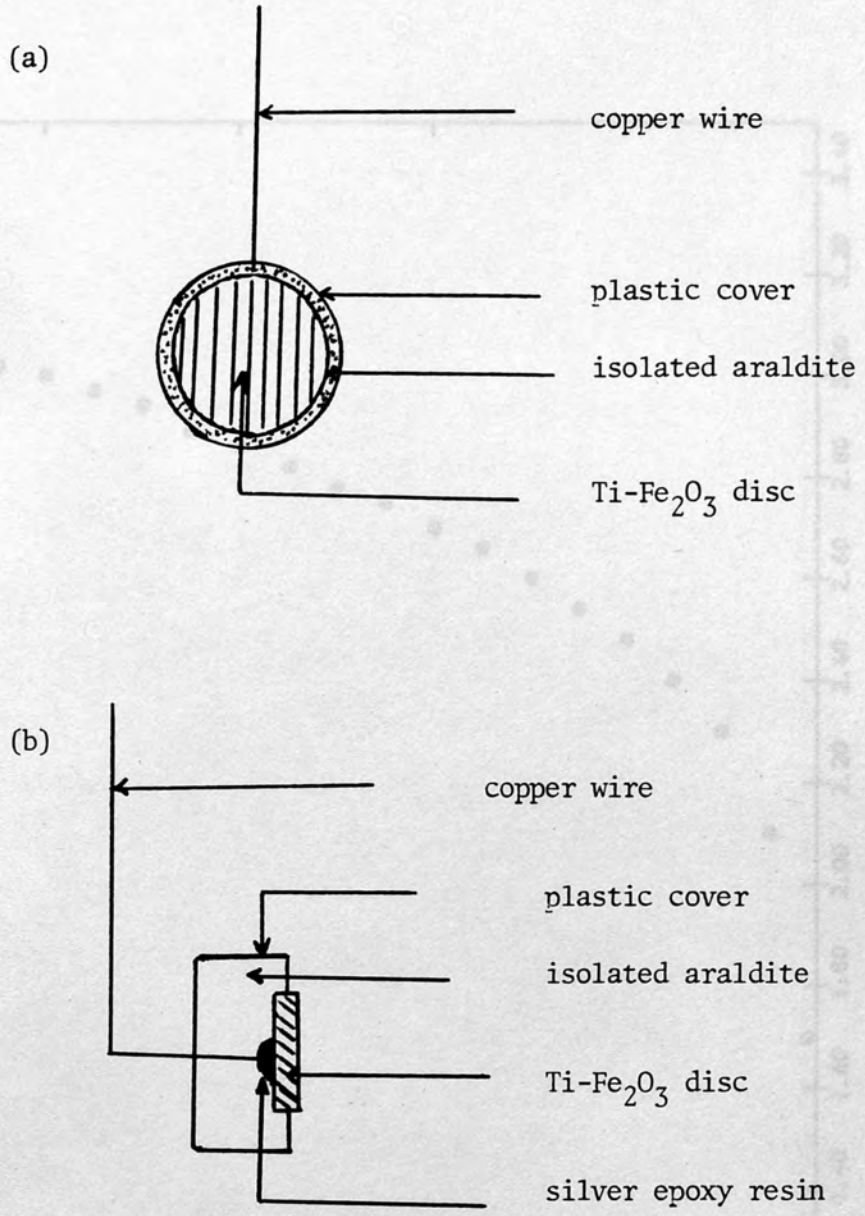

Figure (5) Front view (a) and side view (b) for Ti-Fe_2O_3 electrode.

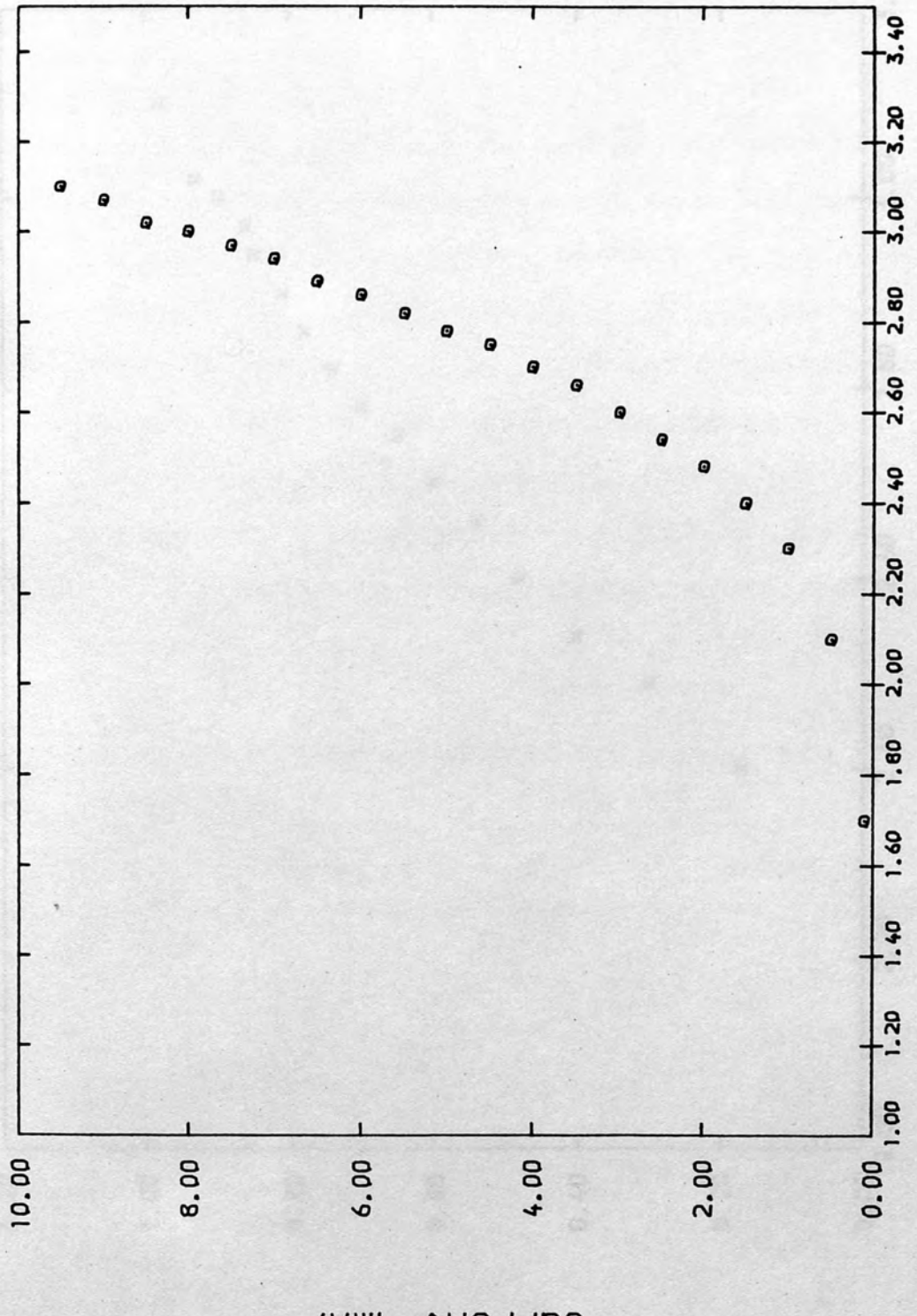

Figure (6) Graph of voltage vs current for glassy oxide electrode

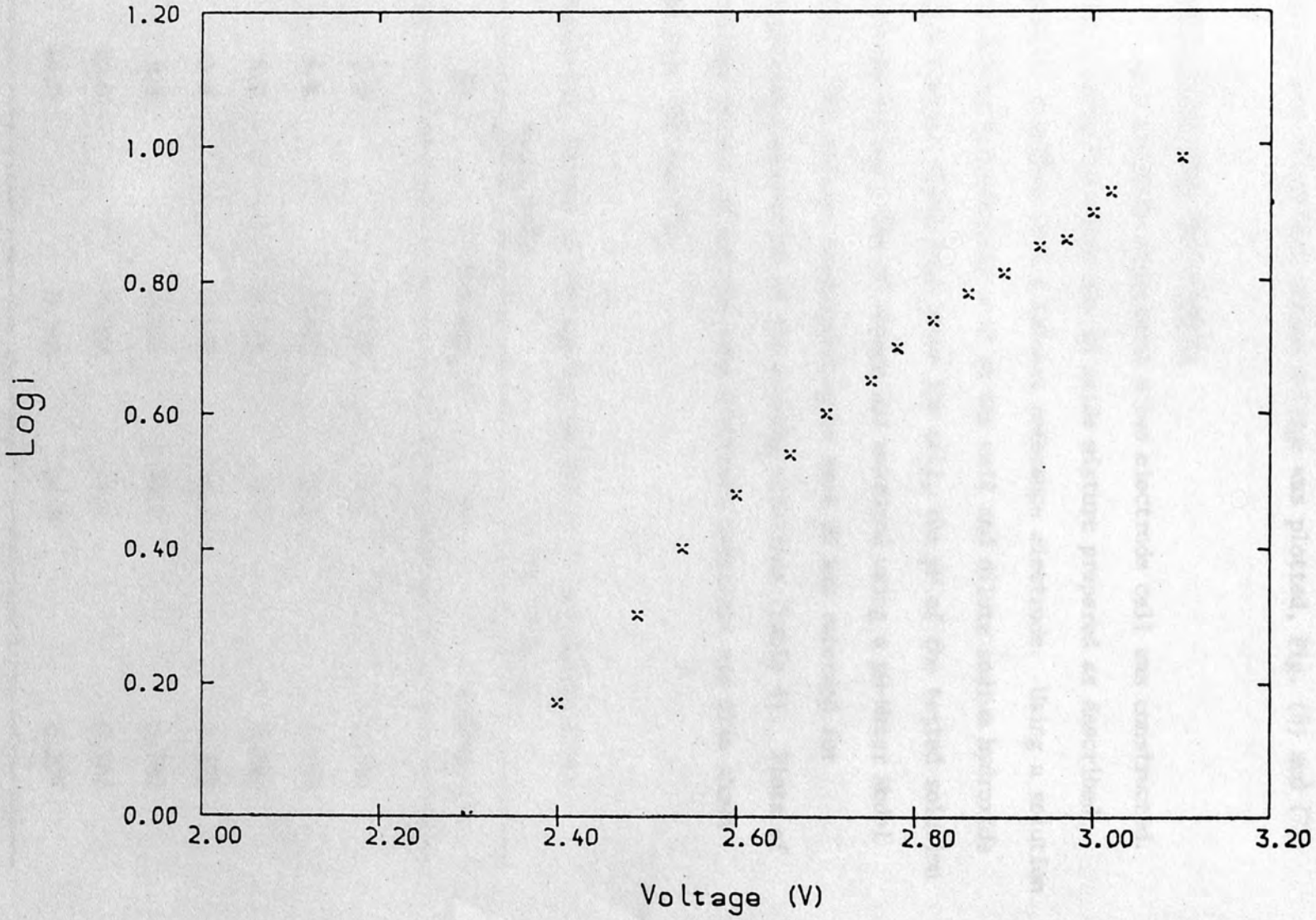

Figure (7) Graph of voltage vs Logi for glassy oxide electrode

acid. A current passed with the corresponding voltage was recorded, and graphs of current versus voltage was plotted, Fig. (6) and (7).

2.6 PH/Voltage Measurements

In a separate experiment a two electrode cell was constructed. The working electrode was an oxide mixture prepared as described before, together with a Calomel reference electrode. Using a solution of dilute hydrochloric acid in the cell and dilute sodium hydroxide in a burette fixed just above the cell, the pH of the tested solution was controlled. The pH change was measured using a pH-Meter Model E512. The voltage corresponding to each pH was recorded for different composition of the working electrode (Table 4). Plots of voltage versus pH for the same electrode materials are also shown in Fig. (8) and (9).

Table (4) Values of Voltage vs. pH for Different Oxides Discs.

Fe_2O_3 only.		3.84% Ti-Fe_2O_3.	
pH	Voltage (V)	pH	Voltage (V)
3.8	0.133	3.1	0.499
4.6	0.153	4.1	0.433
5.5	0.144	6.0	0.400
6.8	0.122	8.5	0.379
8.8	0.104	10.2	0.362
10.0	0.088	11.2	0.352
14.0	0.053	14.0	0.299

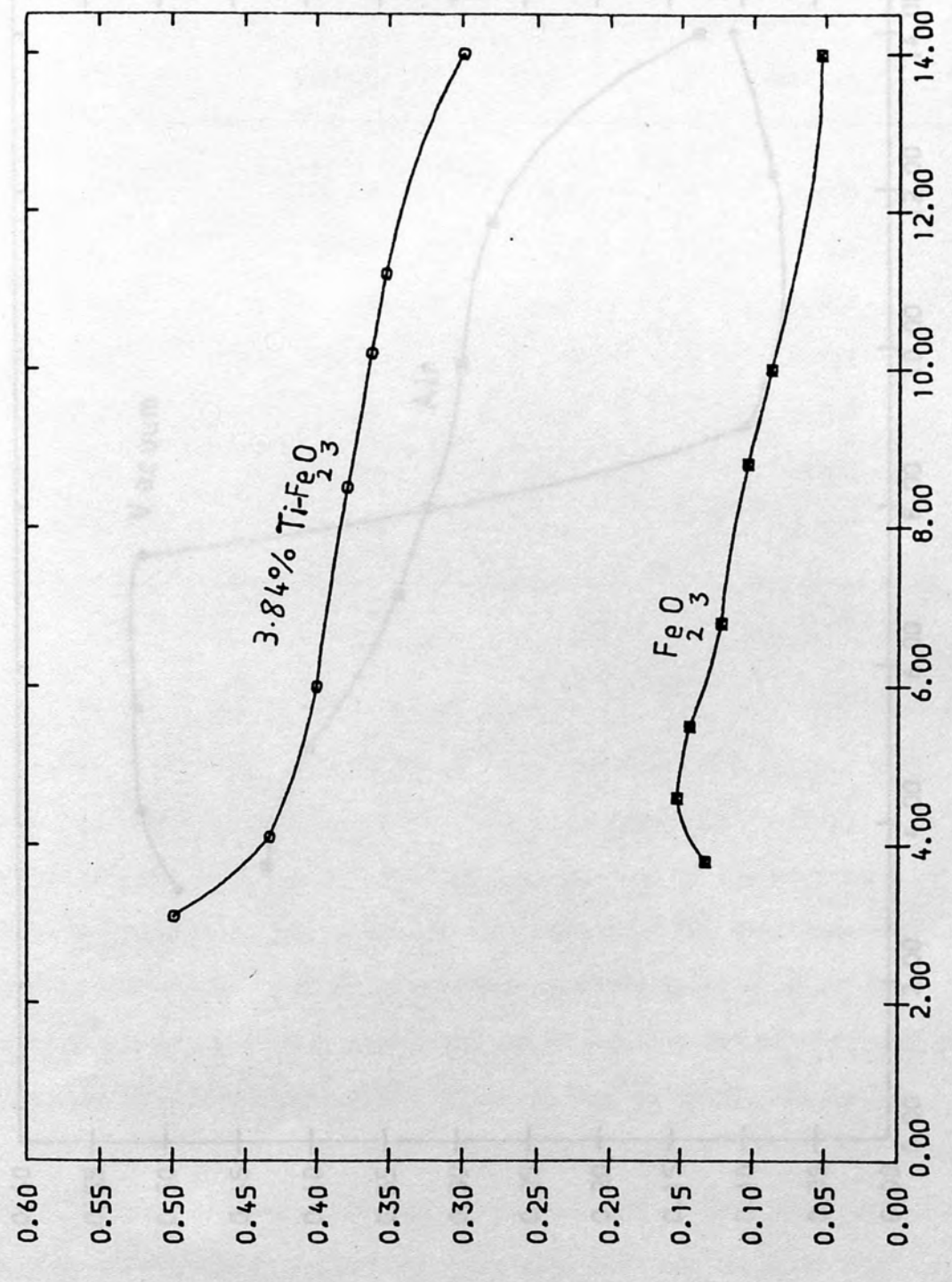

Figure (8) Plots of pH vs voltage for Fe_2O_3 and 3.84% Ti-Fe_2O_3 electrodes

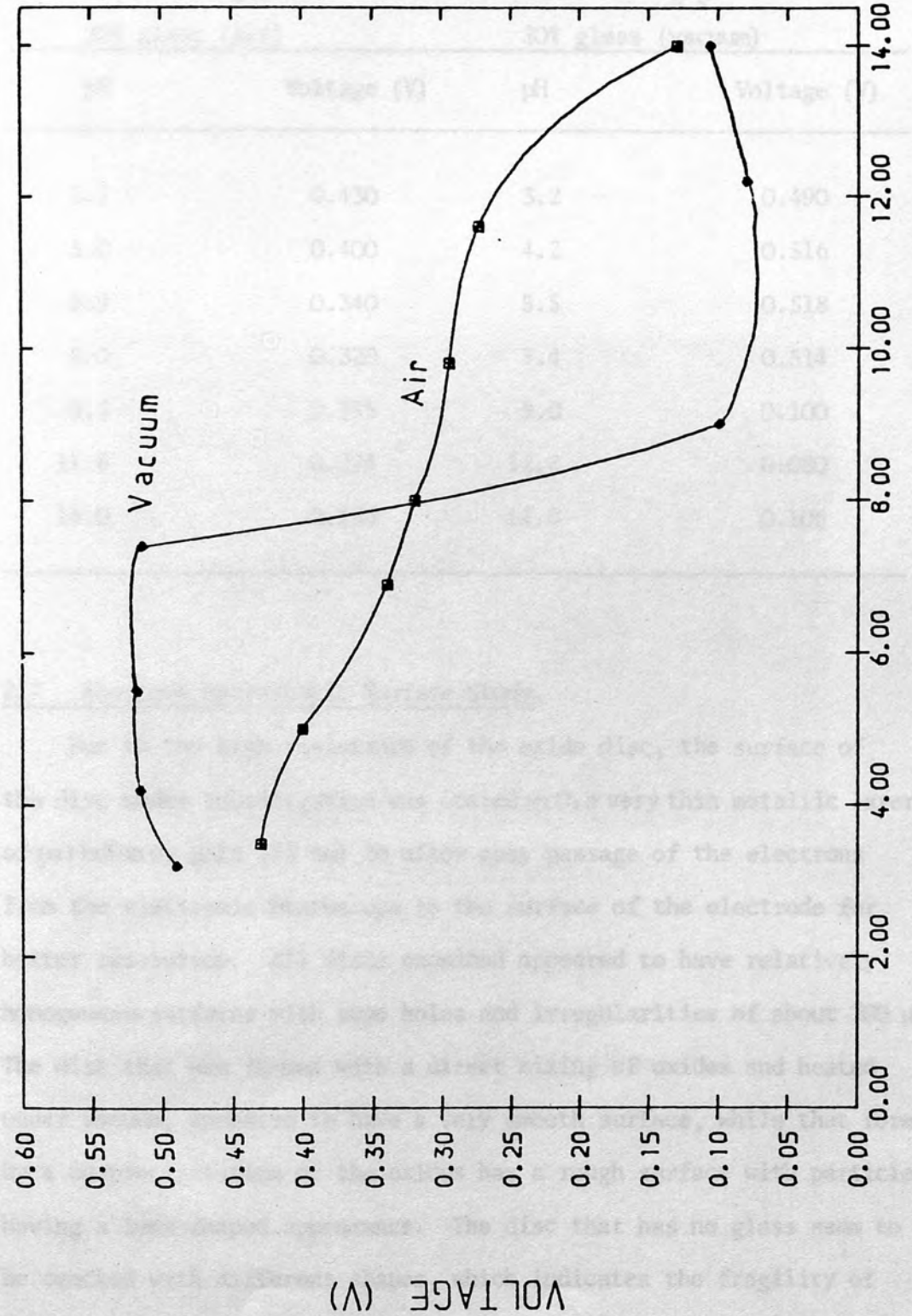

Figure (9) Plots of pH vs voltage for glassy 3.84% Ti-Fe_2O_3 electrodes (heated in air and vacuum)

Table 4. (Continued)

3.84% Ti-Fe_2O_3 + 20% glass (Air)		3.84% Ti-Fe_2O_3 + 20% glass (vacuum)	
pH	Voltage (V)	pH	Voltage (V)
3.5	0.430	3.2	0.490
5.0	0.400	4.2	0.516
6.9	0.340	5.5	0.518
8.0	0.320	7.4	0.514
9.8	0.295	9.0	0.100
11.6	0.274	12.2	0.080
14.0	0.130	14.0	0.106

2.7 Electron Microscopic Surface Study.

Due to the high resistance of the oxide disc, the surface of the disc under investigation was coated with a very thin metallic layer of palladium or gold (23 nm) to allow easy passage of the electrons from the electronic microscope to the surface of the electrode for better resolution. All discs examined appeared to have relatively homogeneous surfaces with some holes and irregularities of about 200 μM. The disc that was formed with a direct mixing of oxides and heated under vacuum, appeared to have a very smooth surface, while that formed by a co-precipitation of the oxides has a rough surface with particles having a lens-shaped appearance. The disc that has no glass seem to be cracked with different shapes, which indicates the fragility of the mixture and the importance of glass to make a mechanically stable

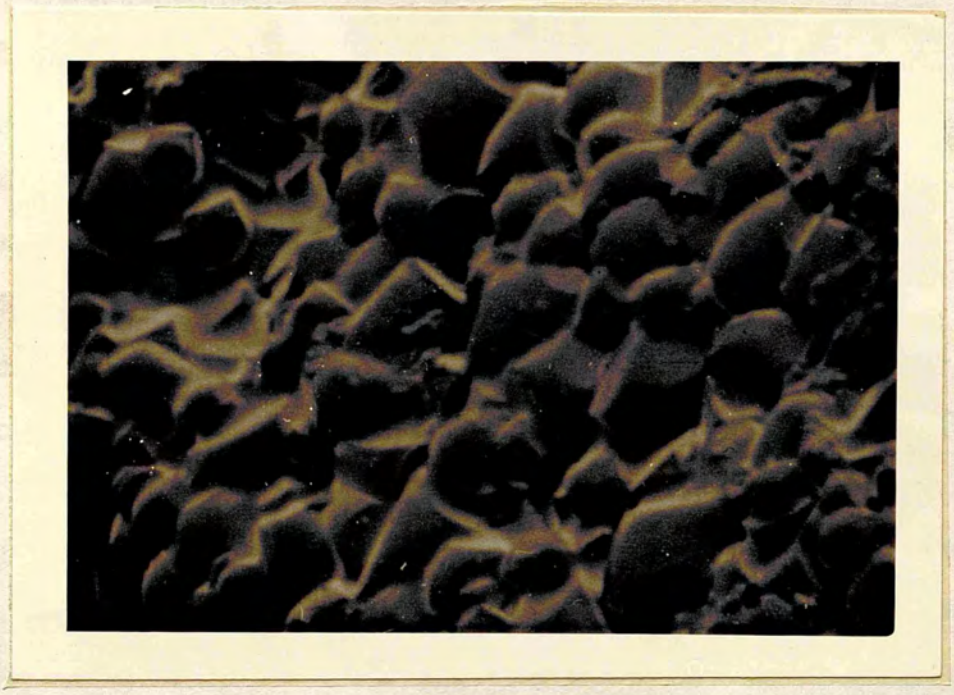

Figure (10): An electron-microscope surface analysis of glassy Ti-Fe_2O_3 electrode

electrode. The homogenity of the mixture was supported by the electron emission experiment run by Dr. D.B. Hibbert of the Chemistry Department, Royal Holloway and Bedford New College, under whom this research was conducted. In his experiment no separate emission from glass powder appeared on the screen. A photograph of an electrode surface is shown in Figure (10).

2.8 Discussion

The iron (III) oxide discs had very low conductivity of about $2.5 \times 10^{-7}\ \Omega^{-1}\ cm^{-1}$. When doped with a certain percentage of titanium-oxide (3.84% Ti-Fe_2O_3), the conductivity remarkably increased ($1.4 \times 10^{-3}\ \Omega^{-1}\ cm^{-1}$) owing to the effect of titanium dioxide which acts as an impurity in the iron (III) oxide matrix. Introduction of Ti^{4+} to Fe^{3+} host lattice is a typical n-type semi-conductor. Titanium (IV) has one more valence electron than iron (III), hence when it is incorporated substitutionally, one electron per titanium is introduced into the bonding structure of the host lattice. At low temperature the excess electrons remain in the vicinity of the titanium impurities, but as the temperature raised, these electrons are free to move and as a result, the iron host lattice can conduct current.

Although the mixed oxides discs have a reasonable conductivity, unfortunately they were so fragile that they can easily be broken during handling. Addition of glass powder of about 20% by weight, brings about a mechanically stable electrode, but it decreases the conductivity by about ten fold ($1.5 \times 10^{-4}\ \Omega^{-1}\ cm^{-1}$).

Heating conditions will affect the properties and surface structure of the mixed oxide discs. Discs that were heated overnight under vacuum seem to have the highest conductivity ($7.8 \times 10^{-4}\ \Omega^{-1}\ cm^{-1}$). The decrease in conductivity for glassy electrodes may be explained by the fact that, a discontinuity of the two phases (glass phase and metal oxide phase) might exist within the bulk of the electrode or disc despite the fact that electron microscopy shows a homogeneous surface distribution. This discontinuity could lead to contact resistance.

Discs that were heated in air have a lower conductivity ($1.4 \times 10^{-4}\ \Omega^{-1}\ cm^{-1}$), possibly due to interferences of some molecules in air such as oxygen or hydrogen in form of water vapour. Heating under vacuum may cause more vacancies and imperfection which could lead to a higher conductivity. The same explanation will be expected for discs which were heated under argon, but in a lesser extent. That might explain why discs heated under argon have lower conductivity than those which were heated under vacuum.

Increasing the percentage of titanium in titanium doped iron (III) oxide discs leads to an observable increase in disc conductivity. The highest % of titanium (7.68%) expected to give the highest conductivity, but this is not the case, the highest conductivity was found around the region 3.84% which indicates that, there may

be an optimum amount of the impurity oxide to give a reasonable conductivity.

From the current-voltage curve it was observed that, the current started to flow around 1.7 V versus SCE which is the voltage at which chlorine gas is expected to evolve. This value is compatible with that found by Tseung[60] which was 1.6 V versus RHE. The linearity of the curve in the region (1.7 - 2.6 V) is due to the high resistance of the electrode.

The possibility of glassy oxide discs to be used as hydrogen ion-selective electrodes is limited. This was observed from the pH versus voltage curves in which there were no reasonable change of voltage with increasing pH of the tested solution. The very limited response found is not Nernstian in nature, since the slopes of all graphs were very different from the value calculated from Nerust equation (60 mV). The slopes for the four tested electrodes (Fe_2O_3, 3.84% Ti-Fe_2O_3 with and without glass, heated in vacuum) were as follows: -1.07×10^{-2}, -1.25×10^{-2}, -2.0×10^{-2} and $4.4 \times 10^{-3}\ V^{-1}$ respectively.

The oxide disc heated under vacuum has very little response in acidic media, but there was an observable sharp change in voltage in changing the pH of the solution from acidic to basic. This can be explained by the fact that, there is a specific surface structure which was only affected by OH^- groups and it will not react with any excess hydrogen in acidic media. The possible mechanism suggested is that the surface acquires OH groups which are thermodynamically favourable to react with OH^- to generate water rather than react with hydrogen to give the same product. This can

be represented as follows:

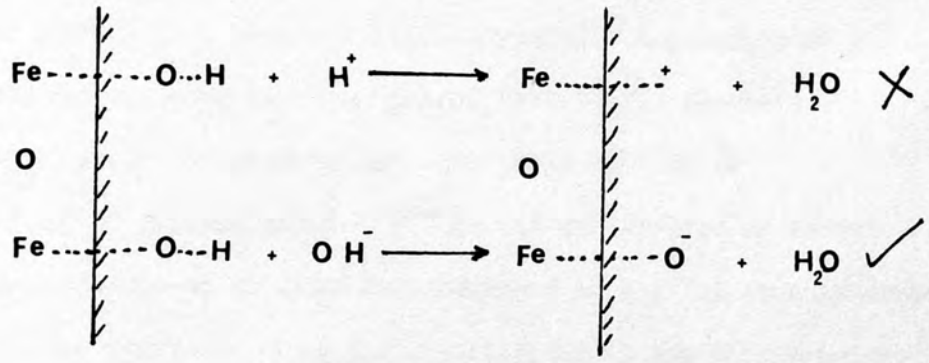

Thermodynamic equilibrium can be attained after generation of water molecules in basic media.

In general, it was shown clearly that, using glass powder as well as the right amount of impurity (doped oxide) with semiconducting oxides were important for sintering at high temperature and for reasonable electrical conductivity.

Some Difficulties Involved In This Work.

1. The major difficulty is the high resistance of the electrodes which prevent any reasonable currents being passed.

2. Mixing the oxides homogeneously is a very sensitive process and it needs much care.

CHAPTER 3

Investigation by Cyclic Voltammetry of the Electrochemical Properties of TTF, Some Organic Dyes and Their Derivatives.

3. Cyclic Voltammogram Instrumentation and Cell Design

In the last fifteen years, cyclic voltammetry has become a popular tool for studying electrochemical reactions. The method was applied to study the organic dyes and their derivatives. Voltammetry may be defined generally[73] as the measurement of current-voltage relationships at an electrode immersed in a solution containing an electroactive species. More specifically, it is the determination of the potential of a single electrode during the course of a sustained electron-transfer reaction at the electrode surface. This technique requires:

1. Waveform generator to produce the excitation signal.
2. A potentiostat to apply this signal to an electrochemical cell.
3. A current to a voltage converter to measure the resulting current.
4. An X-Y recorder or oscilloscope to display the voltammogram.

The first three items are normally incorporated into a single electronic device although modular instruments are also used. Figure (11) shows a circuit diagram for cyclic voltammetry. Data were typically obtained via an X-Y Recorder at slow scans i.e. 1.0 Vs^{-1} or less and storage oscilloscope at faster rates. Scan rates up to 20,000 Vs^{-1} have been used, however rates faster than 100 Vs^{-1} were rarely practical because of iR drop and charging current.

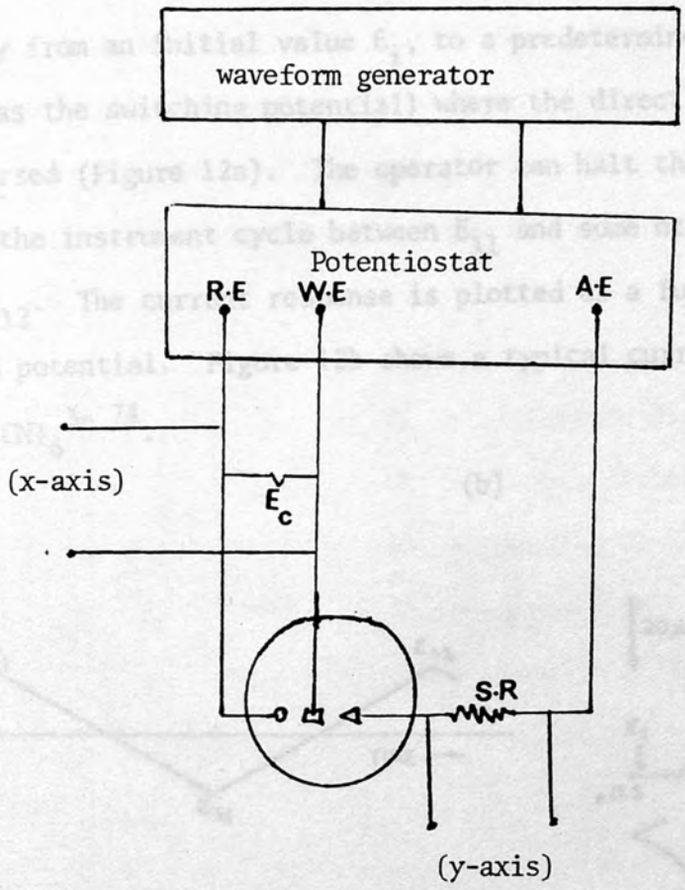

W·E = Working Electrode

R·E = Reference Electrode

A·E = Auxillary

E_c = Voltage Controlled

S·R = Standard Resistance.

Figure (11) Circuit for cyclic-voltammetry.

3.1 The C.V. Experiment

The voltage applied to the "working" electrode is scanned linearly from an initial value E_i, to a predetermined limit, $E_{\lambda 1}$, (known as the switching potential) where the direction of the scan is reversed (Figure 12a). The operator can halt the scan anywhere or let the instrument cycle between $E_{\lambda 1}$ and some other preselected value $E_{\lambda 2}$. The current response is plotted as a function of the applied potential. Figure 12b shows a typical current-voltage curve for $Fe(CN)_6^{3-}$ [74].

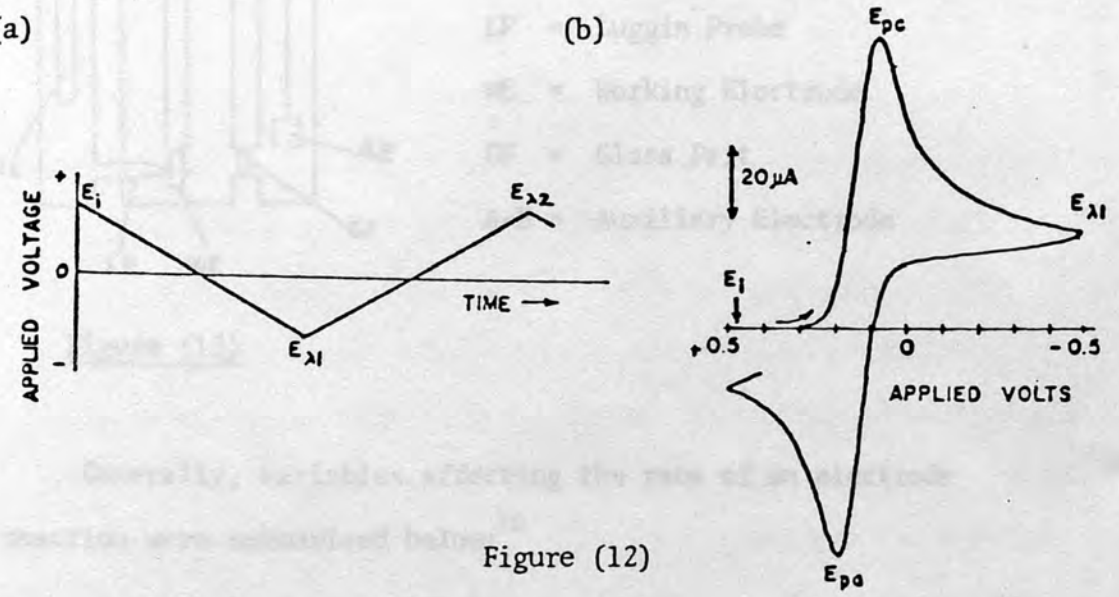

Figure (12)

3.2 Electrochemical Cell

Modern potentiostats utilize a three-electrode configuration as it is shown in Fig. (13). The potentiostat applies the desired potential between a working and a reference electrode. The working electrode is the one at which the reactions(s) of interest takes place. The current required to sustain the reactions at the working electrode is provided by the auxiliary electrode. The arrangement[75] prevents large currents from passing through the reference electrode

that could change its potential. The reference electrode is typically a SCE place near the working electrode or connected to it using a fine tube called a Luggin tube to decrease iR drop in the solution. The working and auxiliary electrodes are platinum sheets placed in the solution and usually separated by a fine porous membrane to decrease the diffusion of reacted species between working and auxiliary electrodes.

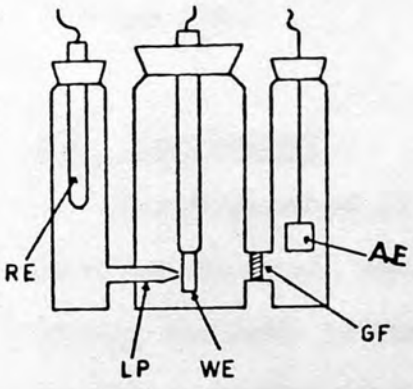

3-Compartment Electrochemical Cell

RE = Reference Electrode

LP = Luggin Probe

WE = Working Electrode

GF = Glass Frit

A-E = Auxiliary Electrode

Figure (13)

Generally, variables affecting the rate of an electrode reaction were summarized below:[76]

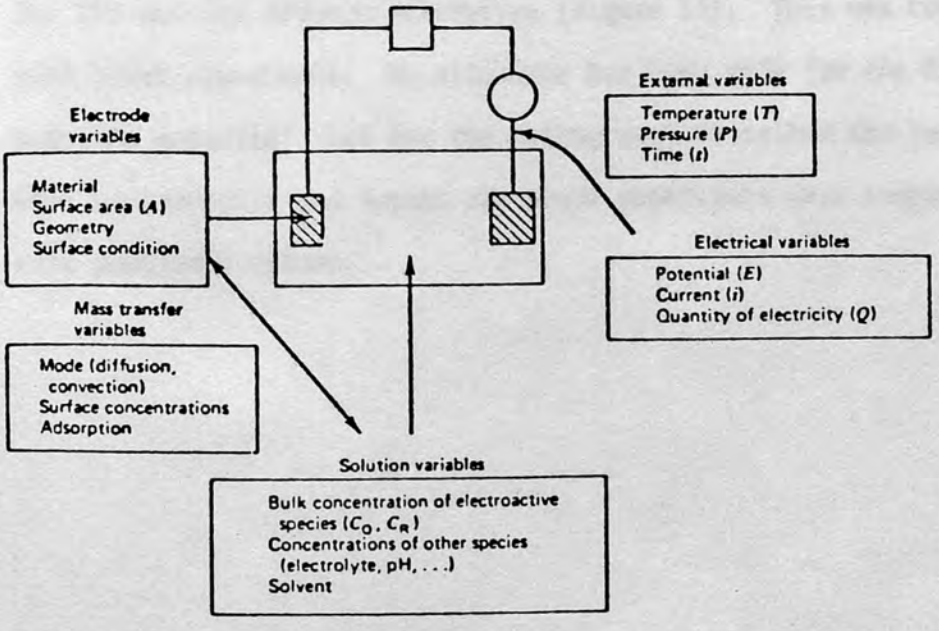

Figure (14)

3.3 Materials

Tetrathiafulvalene (TTF) was purchased from Aldrich Chemical Company (97%) and used without further purification. Acetonitrile was spectroscopic grade quality which had been distilled over phosphorus pentaoxide. Dibenzo TTF, oxonol dyes and cyanine dyes were supplied by Dr. M. Grossel's group at Royal Holloway and Bedford New College (Co-operative work) and they were prepared by methods (77) and (78).

3.4 Experimental

A certain amount of each dye (about 0.3 gram) was dissolved in 50 ml acetonitrile. Cyclic-voltammograms were recorded at platinum working electrode (Johnson Matthey 99.99%) in a three-electrode cell against an aqueous saturated calomel electrode and platinum foil counter electrode. The supporting electrolyte was tetrabutylammonium perchlorate (TBAP). The voltammogram was run for different dyes with the same skeleton (Figure 15), but different numbers of bridge carbon atoms and different side chain length. The experiment was also run for TTF and its dibenzo derivative (Figure 15). This was compared with blank experiment. No allowance has been made for the liquid junction potential, but for the arrangement described the results were reproducible and formal electrode potentials were comparable with published values.

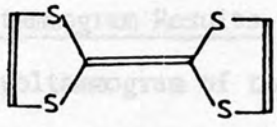

1 TTF

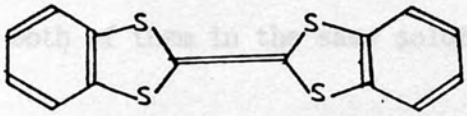

2 DIBENZO TTF

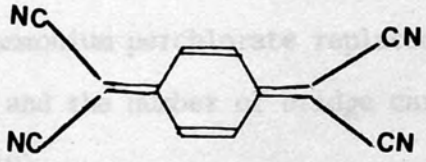

3 TCNQ

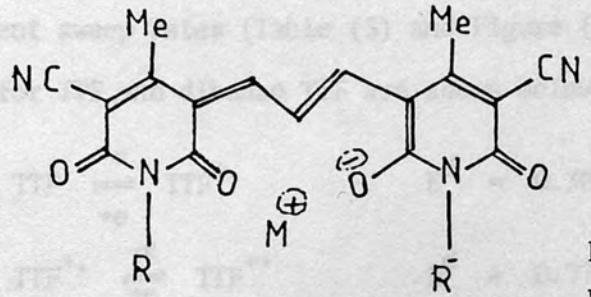

4 OXONOL DYE

R and $\bar{R}$ are alkyl groups

$M^+ = Bu_4N^+-$, Et_4N^+-

$X^- = Br^-$, I^- ...

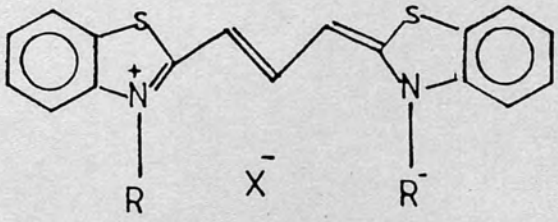

5 CYANINE DYE

Figure (15) Structure of compounds studied.

3.5 Cyclic Voltammogram Results

The cyclic voltammogram of the solvent (acetonitrile) plus the supporting electrolyte (TBAP), N-Et oxonol dye, TTF and a mixture of TTF with the dye are shown in Figure (16). Since the commonly used electrode materials were platinum and nickel, cyclic voltammograms were run for both of them in the same solution (0.01M TBAP in MeCN), Figure (17).

The effect of increasing side chain length in oxidation potentials and in the stability of the resulting species is shown in Figure (18). At the same time the effect of changing the counter ion i.e. tetrabutyl ammonium perchlorate replaced by tetraethyl ammonium perchlorate and the number of bridge carbon atoms are also shown in Figure (19).

Cyclic voltammograms of TTF compared with that of dibenzo TTF are shown in Figure (20). To calculate an accurate standard reduction potential for each compound the cyclic voltammogram was run at different sweep rates (Table (5) and Figure (21). The average values found for TTF and dibenzo TTF are shown below:

$$TTF \underset{+e}{\overset{-e}{\rightleftharpoons}} TTF^{+\cdot} \qquad E^{\phi} = 0.302V$$

$$TTF^{+\cdot} \underset{+e}{\overset{-e}{\rightleftharpoons}} TTF^{++} \qquad E^{\phi} = 0.770V$$

$$DIBTTF \underset{+e}{\overset{-e}{\rightleftharpoons}} DIBTTF^{+\cdot} \qquad E^{\phi} = 0.540V$$

$$DIBTTF^{+\cdot} \underset{+e}{\overset{-e}{\rightleftharpoons}} DIBTTF^{++} \qquad E^{\phi} = 0.900V$$

Since all oxonols under study show only an oxidation peak with small or non-existing corresponding reduction peak, the formal reduction potentials were determined by extrapolating a graph of peak potential versus square root of the sweep rate to zero sweep rate. Table (6) shows the values obtained for oxonol dyes with different side chain length, while Table (7) shows the values obtained for dyes of different numbers of bridge carbon atoms.

Unlike oxonol dyes, cyanines show distinct oxidation reduction peaks (Figure (22)). Their formal reduction potentials were calculated from the average peak potentials and these are summarized in Table (8).

3.5.1

(a) 0.01M TBAP (MeCN)

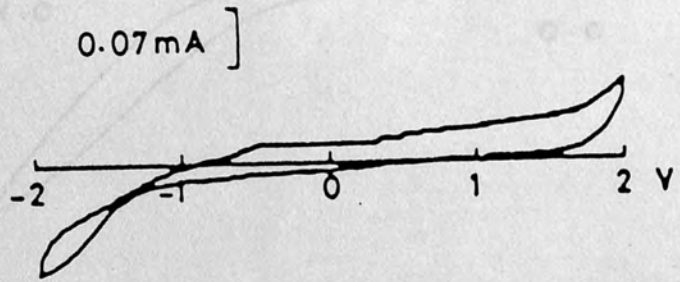

(b) Oxonol Dye

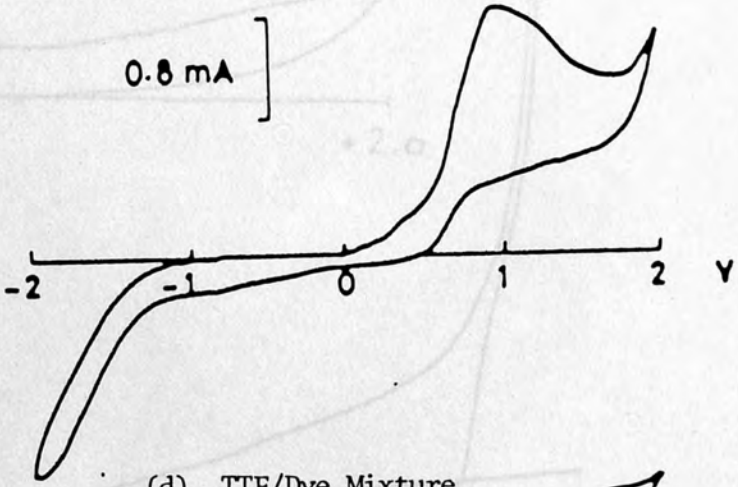

(c) TTF(MeCN)

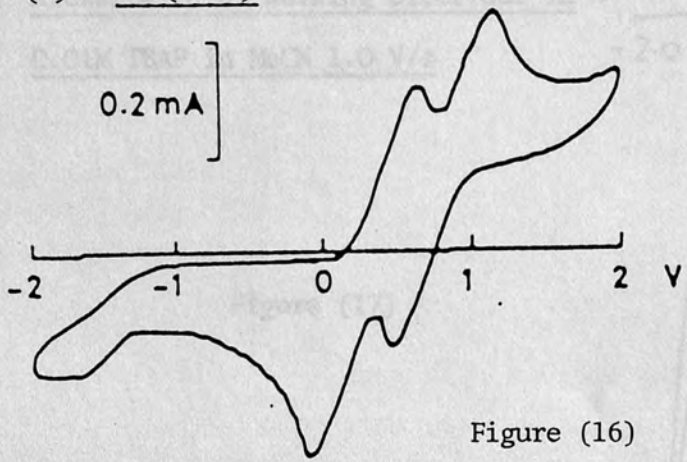

(d) TTF/Dye Mixture

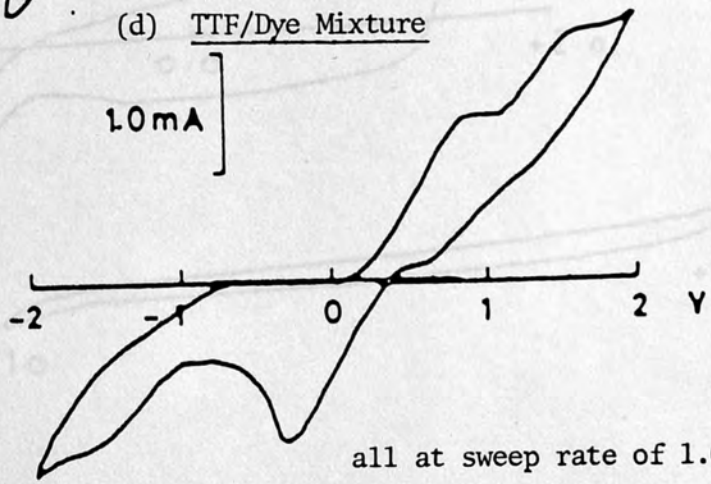

Figure (16)

all at sweep rate of 1.0V/s

3.5.2

(a) Platinum wire as working electrode in 0.01M TBAP in MeCN 0.8 V/s

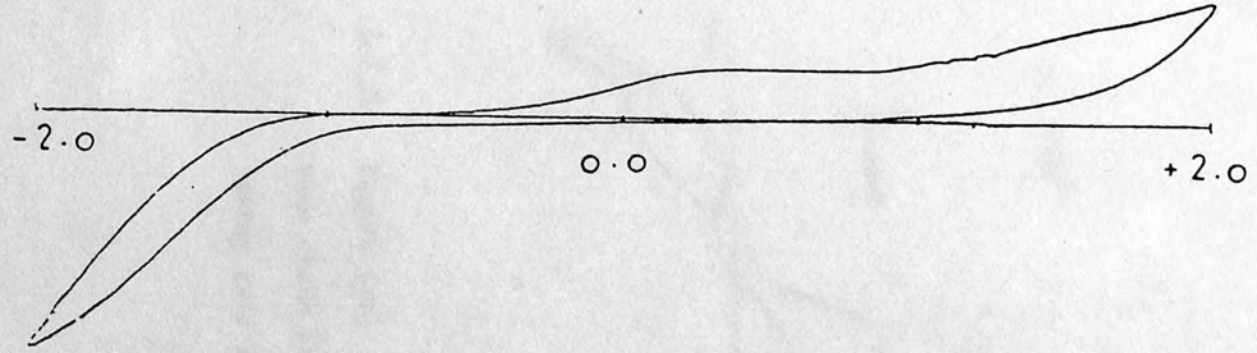

(b) Nickel wire as working electrode in 0.01M TBAP in MeCN 1.0 V/s

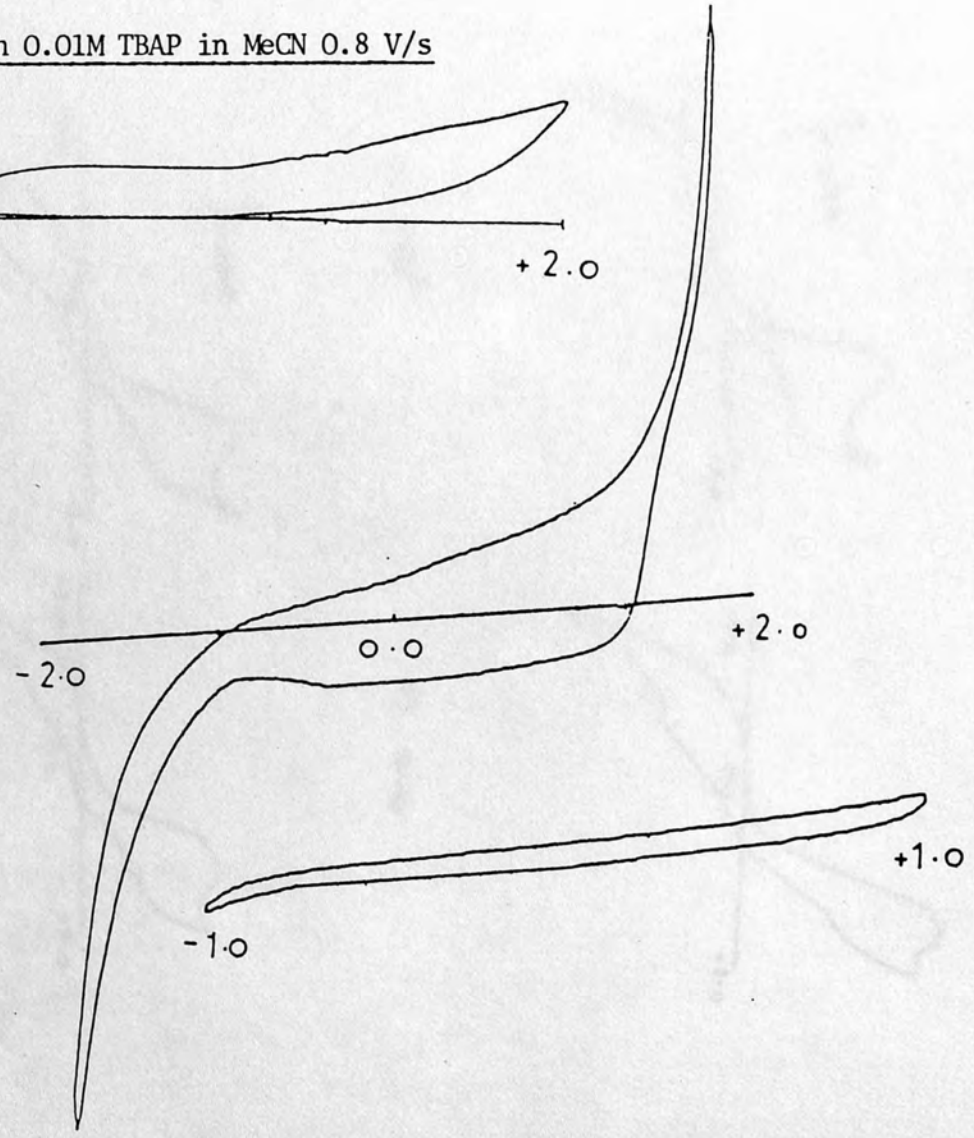

Figure (17)

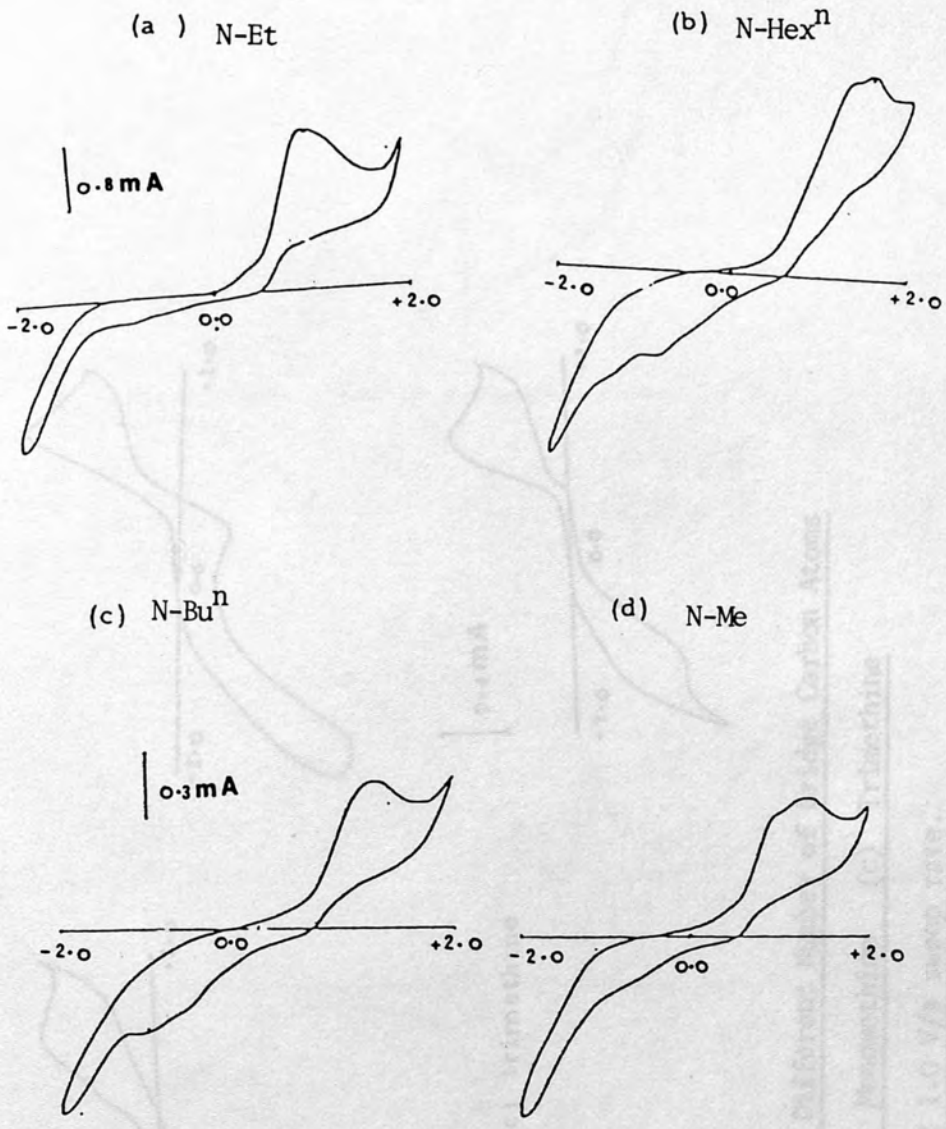

3.5.3. Figure (18) c.v. for oxonol dyes of different side chain length, all in 0.01M TBAP in MeCN at sweep rate of 1.0 mVs^{-1}.

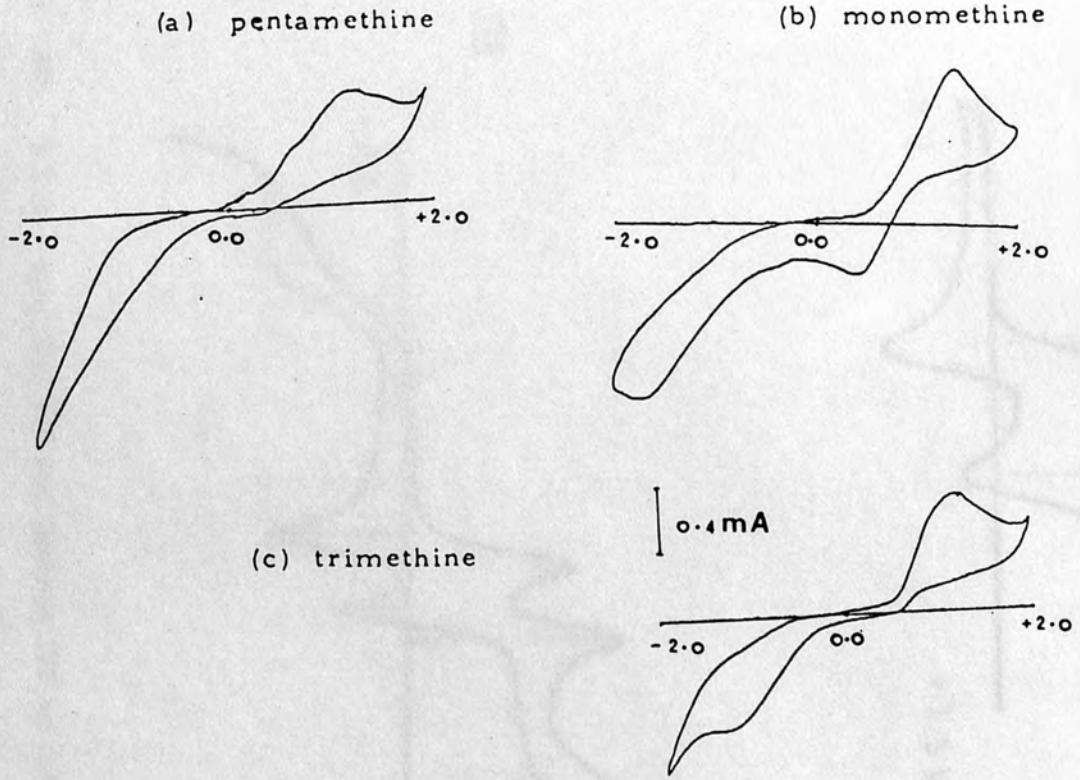

Figure (19)

3.5.4 C.V. for Oxonol Dyes of Different Number of Bridge Carbon Atoms

(a) Pentamethine (b) Monomethine (c) Trimethine

in 0.01M TBAP in MeCN at 1.0 V/s sweep rate.

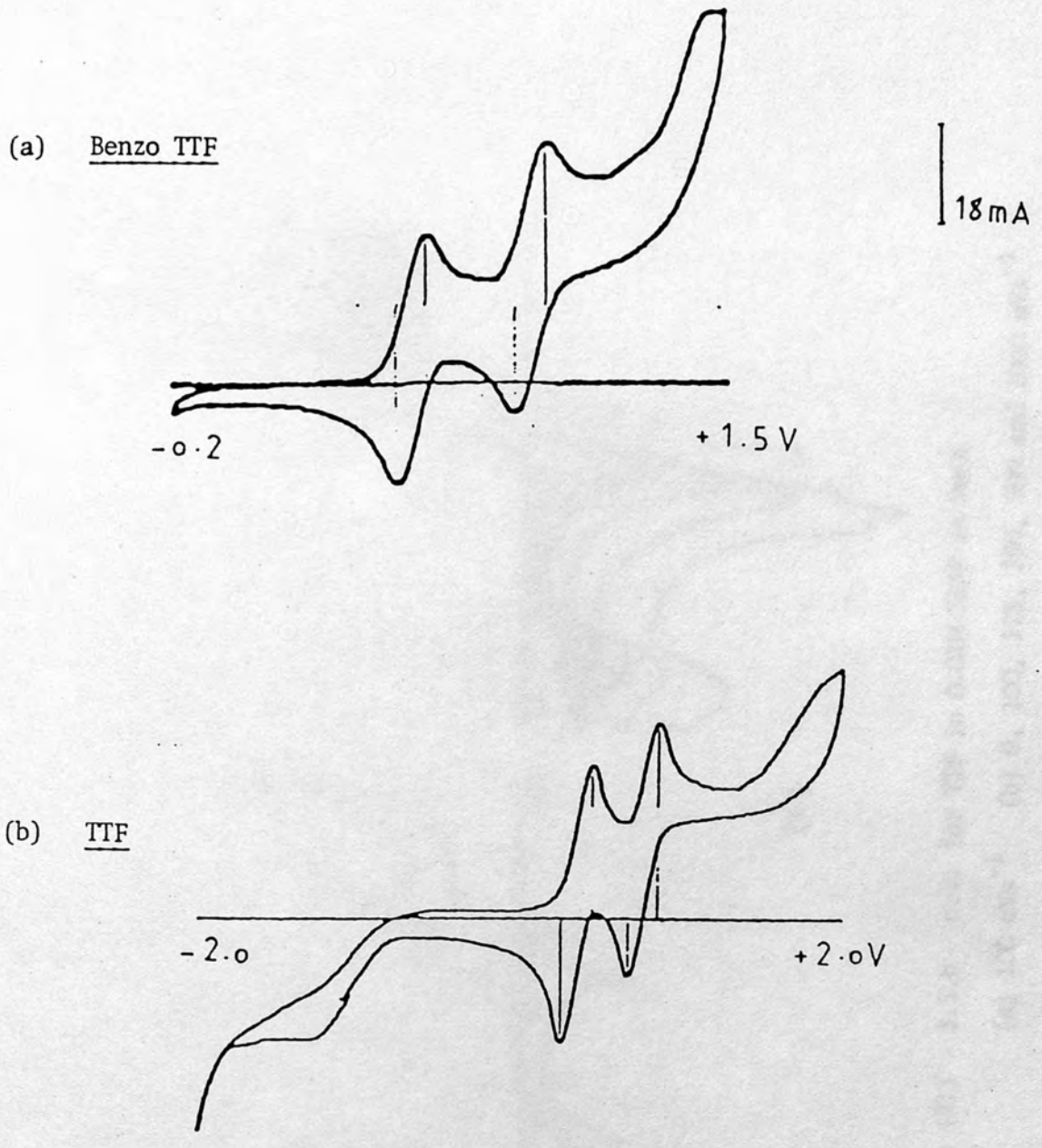

Figure (20) 3.5.5 c.v. for TTF and Dibenzo TTF in 0.01 M TBAP in MeCN at sweep rate of 80 mVs^{-1}

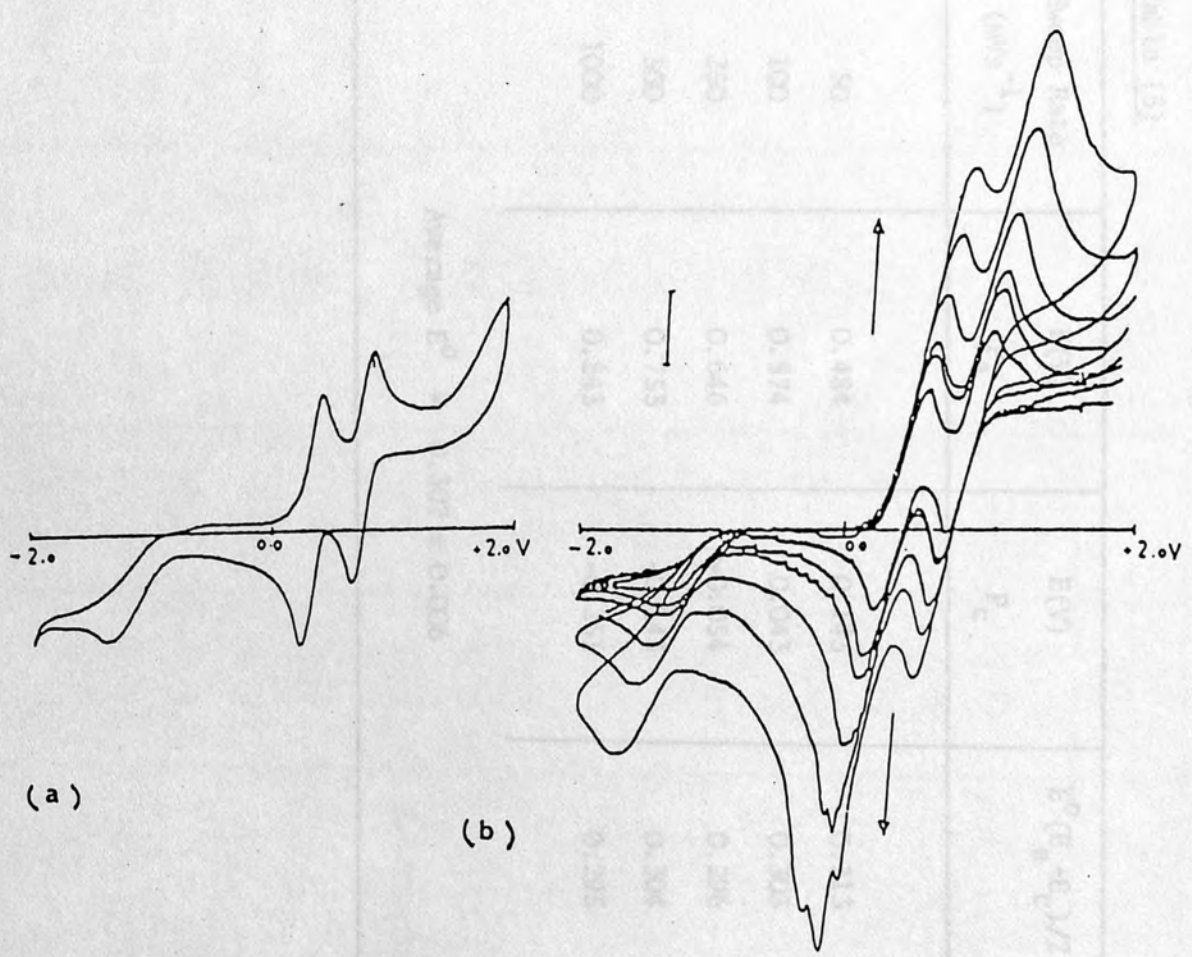

Figure (21) 3.5.6 c.v. for TTF in 0.01M TBAP in MeCN

(a) 100 mVs^{-1} (b) 0, 100, 125, 250, 500 and 1000 mVs^{-1}

3.5.6 Change of Peak Potential with Sweep Rate for TTF in 0.01M TBAP in MeCN.

Table (5)

Sweep Rate (mVs^{-1})	E(V) P_a	E(V) P_c	$E^o(E_a+E_c)/2$
50	0.484	0.143	0.313
100	0.574	0.043	0.303
250	0.646	-0.054	0.296
500	0.753	-0.143	0.304
1000	0.843	-0.251	0.295
	Average E^o = 0.302 ± 0.006		

3.5.7 E^{Φ} Values for Oxonol Dyes with Different Side Chain Length

Table 6

DYE	SWEEP RATE (mVs^{-1}) (V)	$\sqrt{\nu}$	V(V)	E^{Φ} VALUE(V)
N-Me	30	5.48	0.56	
Oxonols	60	7.75	0.60	
	100	10.00	0.64	
	150	12.25	0.68	
	200	14.14	0.71	0.465±0.05V
N-Et	60	7.75	0.64	
Oxonols	80	8.94	0.68	
	100	10.00	0.69	
	200	14.14	0.74	
	250	15.81	0.77	0.539±0.05V
N-Bu^n	60	7.75	0.67	
Oxonols	80	8.94	0.70	
	120	10.95	0.72	
	200	14.14	0.76	0.573±0.03V
N-Hex^n	40	6.32	0.70	
Oxonols	80	8.94	0.75	
	120	10.95	0.78	
	200	14.14	0.80	0.628±0.04V

3.5.8 E^{Φ} Values for Oxonol Dyes of Different Number of Bridge Carbon Atoms.

Table (7)

DYE	SWEEP RATE (mVs^{-1}) (ν)	$\sqrt{\nu}$	V(V)	E^{Φ} VALUE(V)
Monomethine	40	6.32	0.805	
(1-carbon	80	8.94	0.859	
atom)	150	12.25	0.899	
	200	14.14	0.966	0.682±0.05V
Trimethine	40	6.32	0.630	
(3-carbon	60	7.75	0.678	
atoms)	100	10.00	0.684	
	150	12.25	0.725	
	200	14.14	0.765	0.54±0.04V
Pentamethine	40	6.32	0.571	
(5-carbon	80	8.94	0.617	
atoms)	120	10.95	0.698	
	150	12.25	0.752	
	200	14.14	0.778	0.38±0.07V

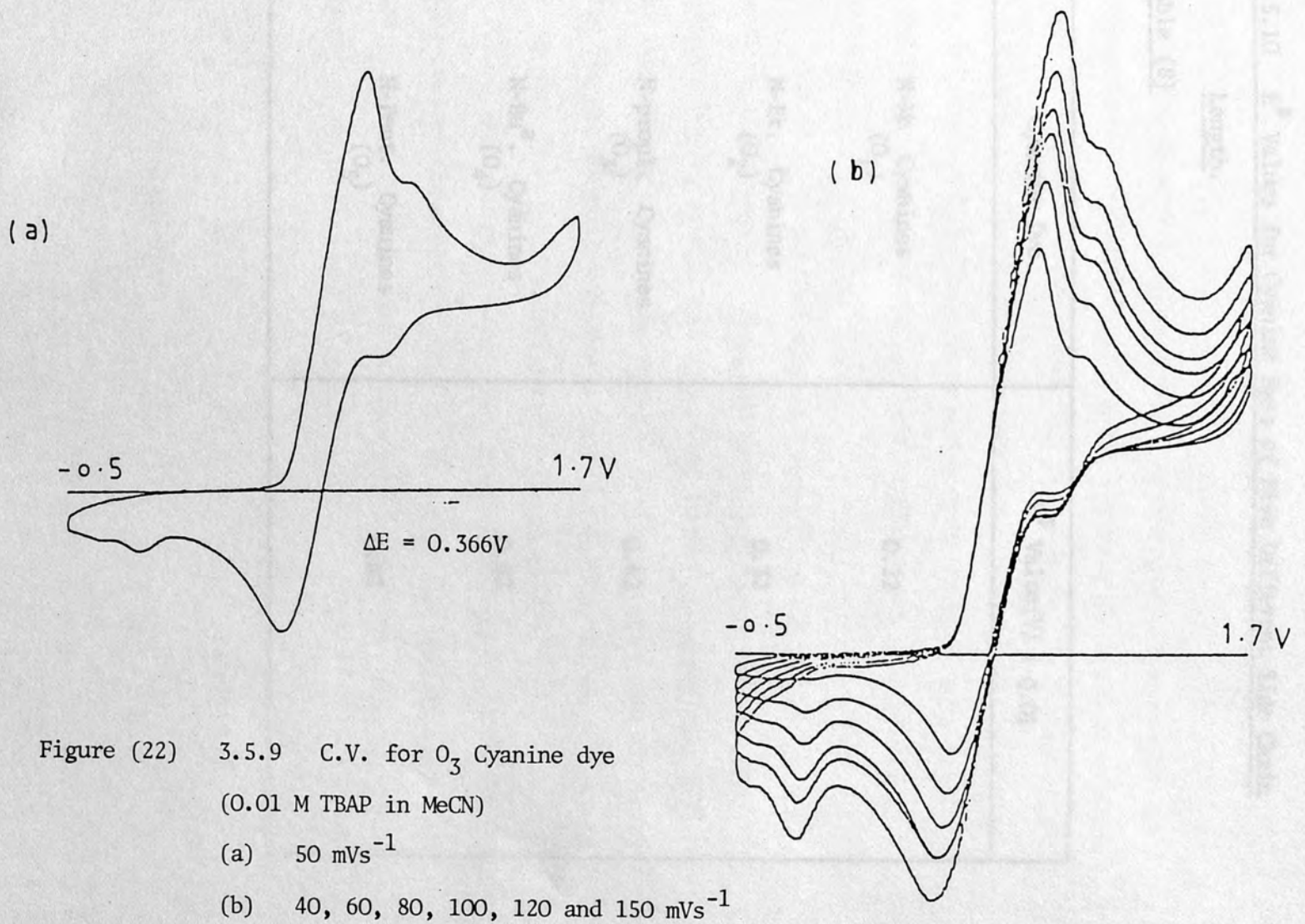

Figure (22) 3.5.9 C.V. for O_3 Cyanine dye

(0.01 M TBAP in MeCN)

(a) 50 mVs^{-1}

(b) 40, 60, 80, 100, 120 and 150 mVs^{-1}

3.5.10 E^{Φ} Values for Cyanine Dyes of Five Different Side Chain Length.

Table (8)

Cyanine Dye	E^{Φ} Value(V) ± 0.01
N-Me Cyanines (O_1)	0.22
N-Et. Cyanines (O_2)	0.32
N-propl. Cyanines (O_3)	0.62
N-Bu^a. Cyanines (O_4)	0.62
N-Pent. Cyanines (O_5)	0.62

3.6 Diagnostic Tests for Reaction Control Using Cyclic Voltammetry.

Using diagnostic tests reported by Pletcher it is possible to obtain some further information about the reaction which is taking place[79]. Pletcher first states that if one wishes to determine if a reaction is diffusion limited, kinetically controlled, or mixed, the relation of I_p(peak-current) and V (peak-voltage) must be considered. This gives various test results which are listed in Table (9).

Thus if I_p is plotted against V and $\sqrt{V}$ one can deduce how the reaction is controlled. These are shown in Figures (23) and (24). Pletcher further states that with peaks caused by adsorption steps (or reactions of an existing adsorbed layer) for which the surface reaction and not mass-transfer is rate determining can be recognised by the fact that I_p is directly proportional to V.

Also for adsorption-desorption steps or oxidation and reductions of the adsorbed layer ΔE_p is zero. All figures show that I_p is not directly proportional to V, and at the same time ΔE was not found to be equal to zero.

Table (9)

Diagnostic Tests for Reaction Control Using Cyclic Voltammetry Results.

Diffusion Limited Electrode Process	Mixed Control	Kinetically Controlled Current
I_p versus $\sqrt{V}$ is linear and passes through the origin.	I_p depends on V but I_p versus $\sqrt{V}$ is non linear.	I_p independent of V.

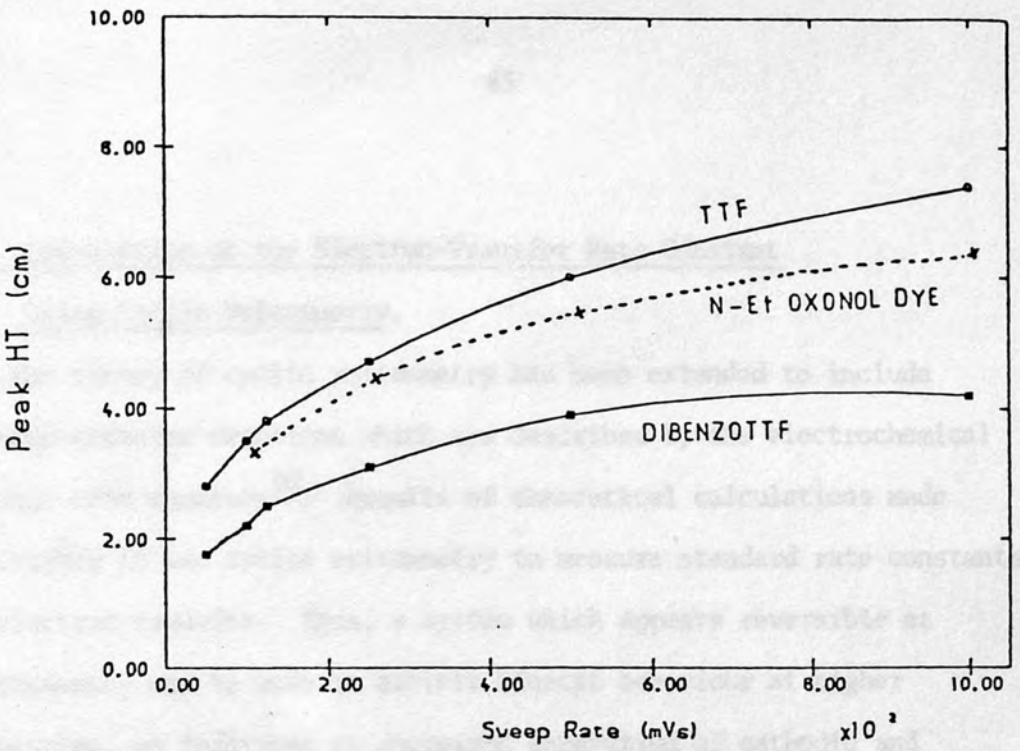

Figure (23) Variation of peak height with sweep rate.

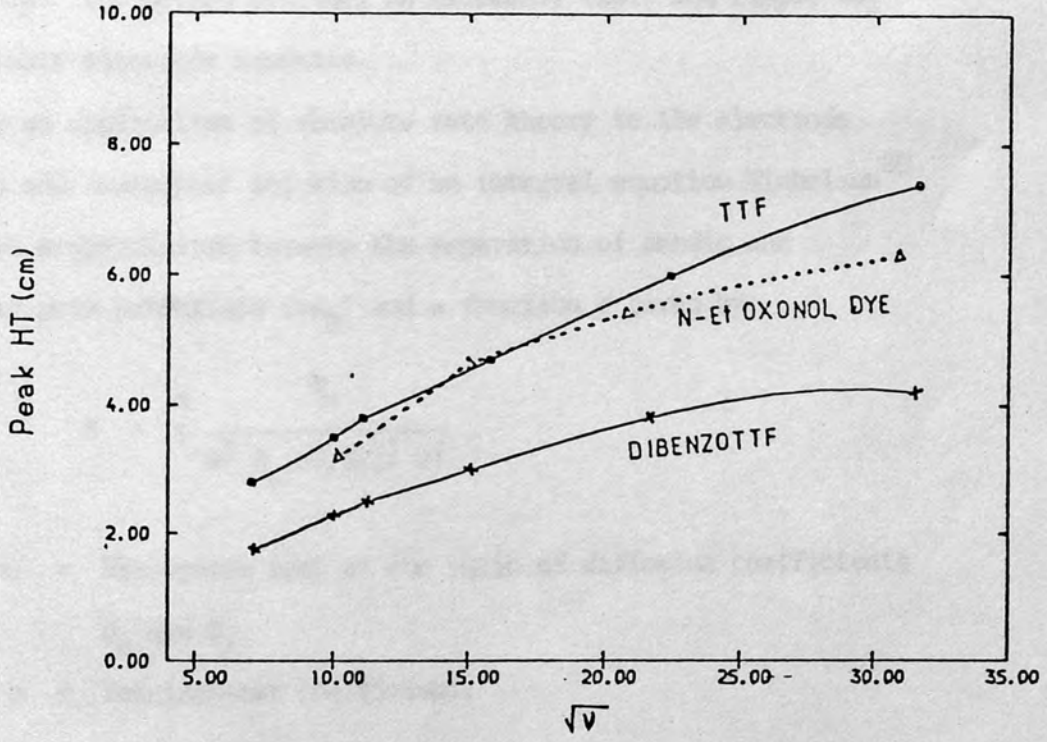

Figure (24) Variation of peak height with square root of sweep rates.

3.7 Calculation of the Electron-Transfer Rate Constant Using Cyclic Voltammetry.

The theory of cyclic voltammetry has been extended to include electron-transfer reactions which are described by the electrochemical absolute rate equation[80]. Results of theoretical calculations made it possible to use cyclic voltammetry to measure standard rate constants for electron-transfer. Thus, a system which appears reversible at one frequency may be made to exhibit kinetic behaviour at higher frequencies, as indicated by increased separation of cathodic and anodic peak potentials. The standard rate constant for electron-transfer is determined from this peak potential separation and frequency. The method provides an extremely rapid and simple way to evaluate electrode kinetics.

By an applicaiton of absolute rate theory to the electrode process and numerical solution of an integral equation Nicholson[80] provides a correlation between the separation of anodic and cathodic peak potentials (ΔE_p) and a function Ψ given by

$$\Psi = \frac{\alpha}{\gamma} \frac{k_s}{\pi^{\frac{1}{2}} D_o (nF/R\Gamma)^{\frac{1}{2}} \nu^{\frac{1}{2}}}$$

where γ = The square root of the ratio of diffusion coefficients D_o and D_r

α = The transfer coefficient.

ν = Sweep rate

k_s = The standard rate constant at $E = E^{\Phi}$

The other terms have their usual significance.

Since the difference in D values is ordinarily small, γ^{α} is unity for many practical situations. Nicholson has also shown that in many situations Ψ is independent of α, as ΔE_p is unchanged due to equal changes to the anodic and cathodic peaks.

Adams simplified the above equation with the following approximations[73]. If $\gamma^{\alpha} = 1$, $D_o = 1 \times 10^{-5}$ cm^2/sec and $F/RT = 39.2$ V^{-1} then if ν is in volts sec^{-1}.

$$\Psi = 28.8 \frac{Ks}{\nu^{\frac{1}{2}}}$$

so using the values of Ψ for various ΔE_p quoted by Nicholson, standard curve can be drawn (Figure 25). Using this curve, the first and second electron-transfer rate constants were calculated for TTF and dibenzoTTF. The results are shown in Table (10) and (11) respectively. The equilibrium potentials for most of the compounds studied are shown in Table (12) and an electrochemical reduction series relative to hydrogen reduction potential is also shown in Table (13).

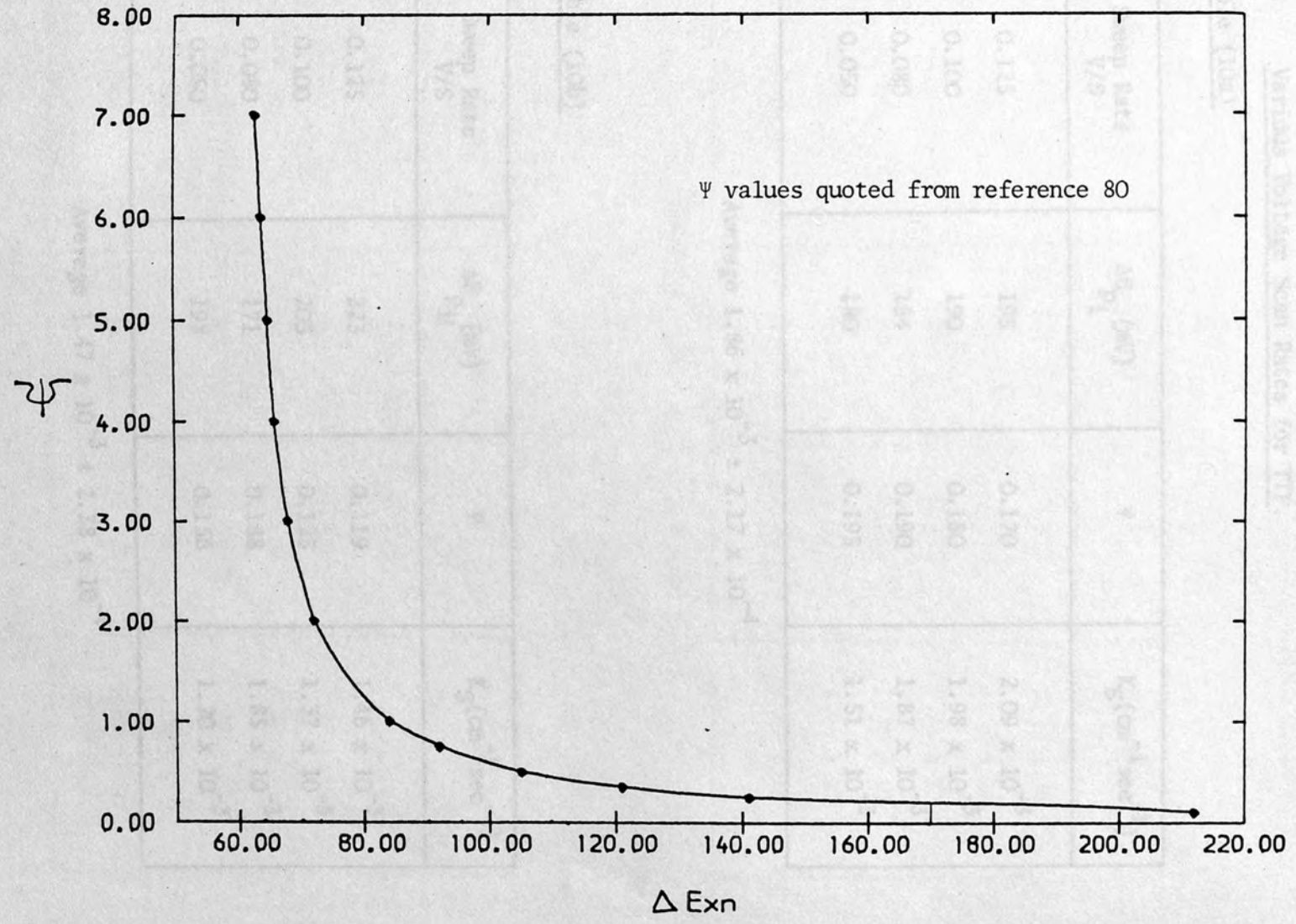

Figure (25) Values of Ψ and its variation with peak potential separation

3.7.1 The Measurements of Electron-Transfer Rate Constant at Various Voltage Scan Rates for TTF.

Table (10a)

Sweep Rate V/S	ΔE_{p_i} (mV)	Ψ	$K_S(cm^{-1}sec^{-1})$
0.125	195	0.170	2.09×10^{-3}
0.100	190	0.180	1.98×10^{-3}
0.080	184	0.190	1.87×10^{-3}
0.050	180	0.195	1.51×10^{-3}

Average $1.86 \times 10^{-3} \pm 2.17 \times 10^{-4}$

Table (10b)

Sweep Rate V/S	$\Delta E_{p_{ii}}$ (mV)	Ψ	$K_S(cm^{-1}sec^{-1})$
0.125	223	0.119	1.46×10^{-3}
0.100	203	0.125	1.37×10^{-3}
0.080	171	0.188	1.85×10^{-3}
0.050	198	0.156	1.20×10^{-3}

Average $1.47 \times 10^{-3} \pm 2.38 \times 10^{-4}$

3.7.2 The Measurements of the Electron-Transfer Rate Constant Calculated at Various Voltage Scan Rate for Dibenzo TTF.

Table (11a)

Sweep Rate V/S	ΔE_{p_i} (mV)	Ψ	$K_S(cm^{-1}sec^{-1})$
0.500	113	0.370	9.08×10^{-3}
0.250	96	0.750	1.30×10^{-2}
0.100	96	0.750	8.24×10^{-3}
0.080	80	1.30	1.28×10^{-2}
0.050	64.8	6.00	4.66×10^{-2}
0.040	64	7.00	4.86×10^{-2}

Average $2.30 \times 10^{-2} \pm 1.7 \times 10^{-2}$

Table (11b)

Sweep Rate V/S	$\Delta E_{p_{ii}}$ (mV)	Ψ	$K_S(cm^{-1}sec^{-1})$
0.500	103	0.570	1.40×10^{-2}
0.250	80	1.300	2.26×10^{-2}
0.100	110	0.410	4.50×10^{-3}
0.080	90	0.800	7.86×10^{-3}
0.050	77.8	1.800	1.34×10^{-2}
0.040	90	0.800	5.55×10^{-3}

Average $1.13 \times 10^{-2} \pm 6.19 \times 10^{-3}$

3.8 Equilibrium Potentials for some Compounds Studied

Table (12)

Electrochemical Reaction	E^{o}(V)
$TCNQ + e = TCNQ^{-}$	0.127[76]
$TTF^{+\cdot} + e = TTF$	0.302
$(\text{N-Et cyanine/I})^{+} + e = (\text{N-Et cyamine / I})$	0.320
$(\text{pent. oxonols}) + e = (\text{pent. oxonols})^{-}$	0.380
$(\text{N-Et oxonols}) + e = (\text{N-Et oxonols})$	0.539
$\text{Dibenzo TTF}^{+\cdot} + e = (\text{Dibenzo TTF})$	0.540
$(\text{N-Hex}^{n}\text{-Cyanine/Br})^{+} + e = (\text{Cyanine/Br})$	0.620
$(\text{N-Hex}^{n}\text{-oxonols}) + e = (\text{N-Hex}^{n}\text{-oxonols})^{-}$	0.628
$TTF^{++} + e = TTF^{\cdot+}$	0.770
$\text{Dibenzo TTF}^{++} + e = \text{Dibenzo TTF}^{\cdot+}$	0.900

3.9 Electrochemical Reduction Series for some Electroactive Organic Compounds.

Table (13)

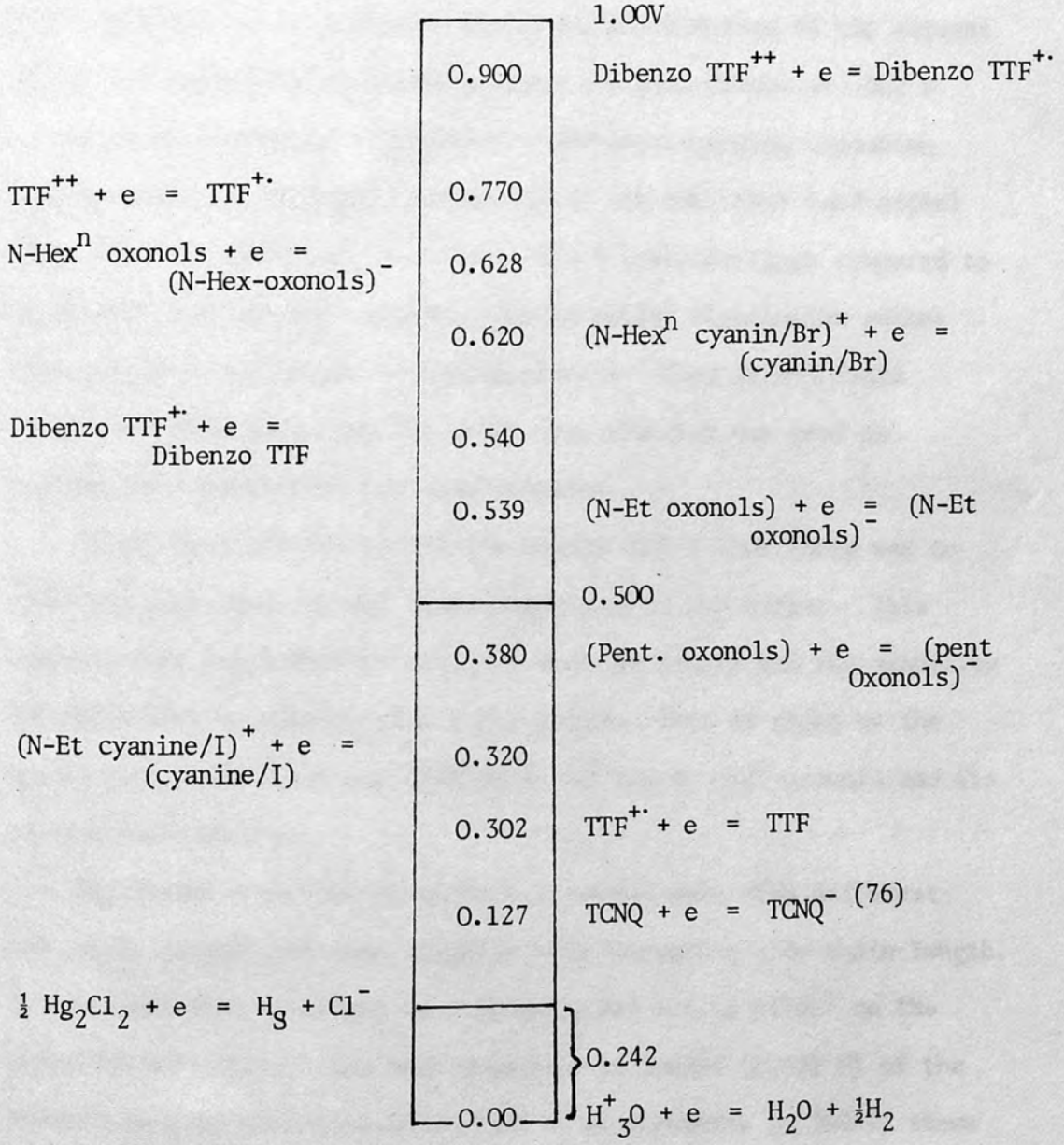

3.10 Discussion

Platinum wire, sheet or mesh proved to be the suitable electrode material for the oxidation of these dyes, since it is stable within a very large range of voltage (-1.5 to 1.8 V) vs. SCE. There are two peaks shown within a region of -2.0 to +2.0 V. The peak which occurs around -1.8 V is most probably due to reduction of the solvent and or the supporting electrolyte while the peak formed at +0.2 V is due to desorption of the solvent. The corresponding oxidation peak is likely to be formed around 2.0 V. On the other hand nickel shows distinct peaks at -1.3 V and +1.3 V (smaller range compared to platinum) which are most probably due to nickel dissolution rather than the expected oxygen evolution process. This is concluded because the same peaks did not occur when platinum was used as working electrode within the same solution.

Oxonol dyes started to oxidize around +0.5 V, but there was no reduction peak shown in the lower homologues of the series. This suggests that the oxidation products were not stable and the stability increases with increasing side chain length. This is shown by the appearance of the reduction peak in N- Bu^n and N- Hex^n oxonols and its absence in N- Et dye.

The formal reduction potentials of oxonol dyes with different side chain lengths increase slightly with increasing side chain length. It does seem that an aliphatic side chain has little effect on the reduction potentials. The high reduction potential (0.682 V) of the monomethine compound compared to that of pentamethine (0.380 V) shows the high stability of the former relative to the latter. The other thing which must be taken into account is that, although the monomethine compound is oxidized at high voltage, it has a stable

products relative to the rest of the series. The trend towards easier oxidation of the oxonol dyes with increasing number of methine groups and decreasing length of alkyl chain at nitrogen reflects an increase in the energy of the HOMO. It is known[81] that increasing the number of methine units in polymethine dyes causes a shift of absorption to longer wavelengths, indicating a narrowing of the gap between HOMO and LUMO. The counter ion as well as the side chain length in cyanine dyes seems to have an effect on the reduction potentials. Generally, cyanine dyes are more easily oxidized with decreasing length of alkyl chain attached to nitrogen. These dyes are known to aggregate in solution[82] even at low concentrations with resulting shifts in bands to higher (H-band aggregation) and lower wavelength (J-band aggregation). The aggregation is sensitive to substituents and it may be this phenomenon that is responsible for the observed changes in E^{Φ}.

Two benzene rings attached to the sides of the symmetrical molecule TTF have an observable effect on the oxidation reduction potential. The reduction potential increases from 0.302 V for TTF to 0.540 V for dibenzo TTF, with a difference of 0.140 V. The same difference was observed from the oxidation reduction process to form the dication radical. A reversible transition between the neutral molecules, mono and dications is clearly seen. The formal electrode potentials agrees with published values (0.32)[53], (0.30)[83], (0.33 V)[84] but E^{Φ} ($TTF^{2+}/TTF^{+\cdot}$) is somewhat greater (0.66 V)[83], 0.70 V[84].

The values of electron-transfer rate constants obtained from the data provided compare well to the range of electron-transfer rate constants normally associated with these types of reactions[76,85].

Although the values obtained are not absolute due to the assumptions made, the consistency of the results suggests that the reaction is totally electrochemical and therefore no side chemical reactions of any consequence are occuring at that voltage. This observation is supported by the repeatability of subsequent cycles after the initial sweep. If any chemical reaction had occurred, the shape of subsequent curves would be different to the initial sweep. At large values of the parameter Ψ mentioned before (K_s large, or ν small), current-voltage curves are independent of kinetic parameters Ψ and α[80]. For this case results are identical to ones obtained previously where the electron-transfer was assumed to be Nernstian[86]. This is in a good agreement of the results obtained for dibenzo TTF at low sweep rate of 40 mVs^{-1} at which Ψ value is 7.0 and the peak separation is 64.0 mV which is nearly a typical Nernstian behaviour. When $\Psi < 7$, the current-voltage curves are dependent on both the values of Ψ and α. For sufficiently small Ψ (K_s very small or ν very large), the back reaction for electron-transfer is unimportant, and the process for oxidation and reduction can be treated separately as the totally irreversible case. For intermediate values of Ψ (a region sometimes referred to as quazi-reversible), the form of the current-voltage curves depends markedly on the exact values of Ψ and α.

The results obtained from TTF and dibenzo TTF may be classified to the last group, since most values of Ψ are between 0.1 and 7.0. The first electron-transfer reaction rates for TTF and dibenzo TTF are faster than the corresponding second rates, but in general, both rates in dibenzo TTF were found to be faster than that of TTF (ten fold increase).

Plots of peak current and peak voltage as suggested by Pletcher[79] showed that, the reaction of the electroactive material on electrode surface is controlled by a mixture of diffusion and kinetics. Since the peak current (Ip) is not directly proportional to the peak voltage, the rate determining step is likely to be the mass-transfer process and not surface reaction. As it was mentioned before ΔE_p is not equal to zero, the reaction is not associated with a simple adsorption-desorption process or a reaction of an adsorbed species.

It is known that TTF/TCNQ is a typical conducting charge-transfer complex. The potential difference (0.175 V) from the electrochemical series can be taken as an optimum value around which the right stoichiometry of charge-transfer occurs. If this potential is taken as reference, then selection of donors and acceptors which form conducting complexes might be possible. Having this idea, N-Et oxonol/TTF with a potential difference of 0.237 V should form a better conducting complex than the higher homologues N- hexyl and pentamethine in which the potential differences are 0.326 and 0.068 V respectively. The same idea can be applied to dibenzo TTF which is expected to form a better complex with the higher homologues rather than lower ones. N-Et cyanine/I, dyes are expected to form charge-transfer complexes with TCNQ, better than N- Hex^n cyanine/Br. The potential difference in the former is 0.193 V, while it is 0.493 V in the latter from the standard TCNQ (0.127 V).

CHAPTER 4

Preparation and Some Properties of TTF/N-Et Oxonol Dye Complex.

4. Electrochemical Preparation of TTF/DYE Complex.

A platinum sheet electrode of approximately 1 cm^2 area was cleaned by dipping into a solution of aqua regia (a mixture of 1:3 nitric acid and hydrochloric acid respectively) for about five minutes, then washing with distilled water, acetone and then distilled water. To complete the removal of any imputities the electrode was used to electrolyse I.0 M sulphuric acid alternately anodic and cathodic for 30 minutes at 1 mA.

The complex between oxonol dye and TTF or its derivative dibenzo TTF was formed electrochemically by the in situ oxidation of neutral TTF in a solution (acetonitrile-tetrabutyl-ammonium perchlorate) containing the dissolved dye. The complex was formed on the anode surface at a current of 2 mA, preferentially at the edges. The coated electrode was then removed from the solution and washed from an excess of the dye or TTF using fresh acetonitrile. The complex was then allowed to dry in air for three hours or in an oven ($80^{o}C$) for an hour. The dry black crystalline material was then scraped from the electrode surface and collected.

The experiment was repeated at different run times and potentiostatically instead of galoanostatically. The optimum conditions for the complex formation were chosen (Table 14) and a microanalysis of the powder was recorded (Table 15).

4.1 Optimum Conditions for Preparation of Oxonol-Dye/TTF Complex Electrochemically.

Table (14)

Complex	Time (hrs.)	Current or Voltage Applied	Conductivity (Ω^{-1} cm^{-1})
TTF/DYE	1.0	2.0 mA	1.13×10^{-4}
TTF/DYE	1.0	1.0 V	4.6×10^{-5}
XTTF/DYE	1.0	2.0 mA	5.9×10^{-5}
TTF/DTE	3.0	1.0 mA	8.7×10^{-5}
TTF/DYE	3.0	1.0 V	very low
TTF/DYE	6.0	2.0 mA	7.4×10^{-7}
TTF/DYE	12.0	2.0 mA	very low

4.2 Microanalysis of TTF/DYE Complex.

Table (15).

Reaction time (hrs.)	Expected %	% Found
1.0	C 54.45 %	54.01 %
	H 3.86 %	3.98 %
	N 9.41 %	9.70 %
12.0	C 58.77 %	51.06 %
	H 4.28 %	4.05 %
	N 11.42 %	10.07 %

4.3 Electron Microscope Analysis of the Crystal Growth of TTF/DYE Complex on Platinum Mesh Electrode Surface.

TTF/DYE crystals formed on the platinum mesh electrode surface were examined under the electronmicroscope. It was observed that, using a current of 1 mA for one hour gave long crystals radiating outwards from a central point and distributed regularly all over the surface as shown in Figure (26). On the other hand using a current of 1 mA for a longer period (2.0 to 3.0 hours) crystals started to build up in three different shapes which are radial, rod and leaf-like. This is shown clearly in Figure (27). Analysis of the emitted X-rays from sulphur in the Electronmicroscope gave no difference in the composition of the different crystallites but this technique would not discriminate between salts of TTF^{+} and TTF^{2+}.

4.4 Solubility of TTF/DYE Complex.

To run any electrochemical experiment on TTF/DYE a solvent must be chosen which will dissolve the supporting electrolyte and not the complex itself. A series of solvents have been tested and their solubility is summarized in Table (16).

Figure (26): Crystal growth of TTF/DYE complex on platinum mesh electrode as shown by electron microscopy (1mA for 1-0 hour)

Figure (27): Crystal growth of TTF/DYE complex on platinum mesh electrode as shown by electron-microscope (1mA for 2 to 3 hours)

Table (16) Solubility of TTF/DYE complex and TBAP in some chosen solvents.

Solvent	Solubility of TBAP	Solubility of TTF/DYE
Distilled water	not soluble	slightly soluble
n-Heptane	not soluble	not soluble
Toluene	not soluble	slightly soluble
Benzene	not soluble	complex is readily dissolved in all four solvents
1,4-dioxan	not soluble	
Methanol	not soluble	
Ketones	not soluble	
Acetonitrile	soluble	Although TTF/DYE is formed in this solvent, it dissolved slowly in it and hence work in acetonitrile must be carried out over a short period of time.

4.5 pH Dependence of the OCV of the TTF/oxonol DYE Complex.

A fresh platinum mesh/TTF-DYE electrode was prepared. The open circuit potential of the electrode was measured against a SCE as a function of pH. Dilute hydrochloric acid (0.1M) and sodium hydroxide (0.1M) were used to control the pH throughout. The pH changes were measured using a PTI-6 Universal Digital pH Meter. The potential was measured for the electrode after preparation, after reduction (1 mA for sufficient time to effect a one electron reduction of the complex), and after an oxidation of a similar electrode. Knowing the weight of the complex on the electrode surface, the time required to oxidize or reduce the whole amount was calculated using the equation:

$$T = \left(\frac{W}{M} \times n F\right) \times 1000 \text{ sec.}$$

where

T = time require for the whole compound to oxidize or reduce.

W = Weight of the complex

M = Molecular weight of the complex

h = number of electrons involved and it assumed as n = 1.

F = Faraday constant.

The results are shown is Figure (28). Intercepts and slopes calculated from pH-voltage curves are also given in Table (17). When the pH was kept constant in the acidic region (pH $\sim$ 1), the voltage was observed to increase initially with time and then level off. This was reversed when a freshly prepared electrode was used into a solution of pH 13.7 (Figure (29)).

Figure (28)

(a)

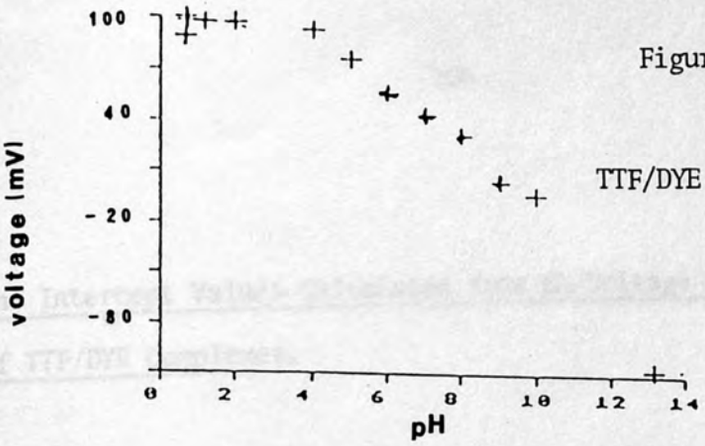

TTF/DYE

(b)

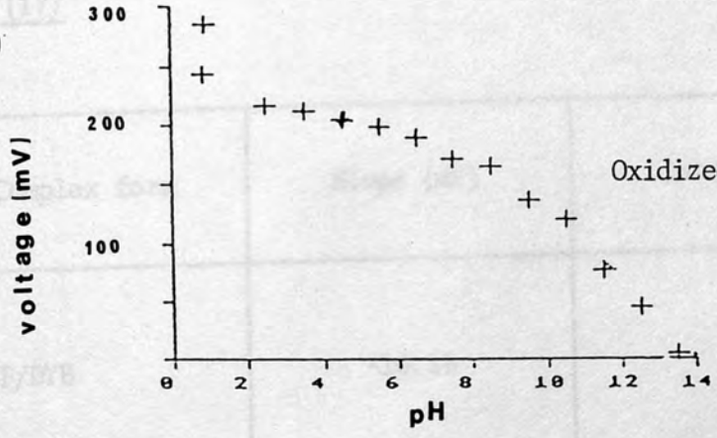

Oxidized form of TTF/DYE

(c)

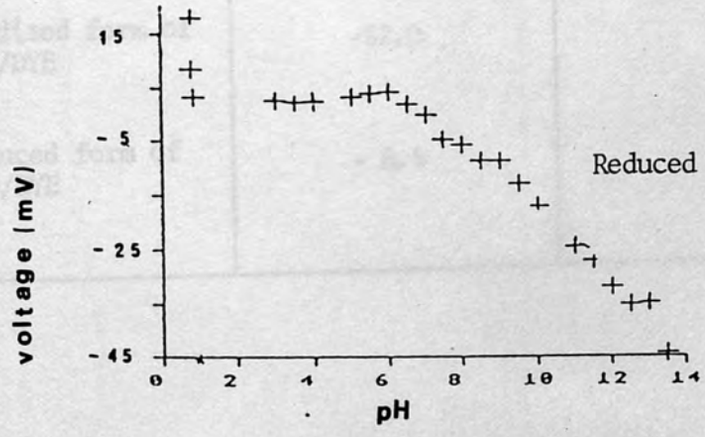

Reduced form of TTF/DYE

(d)

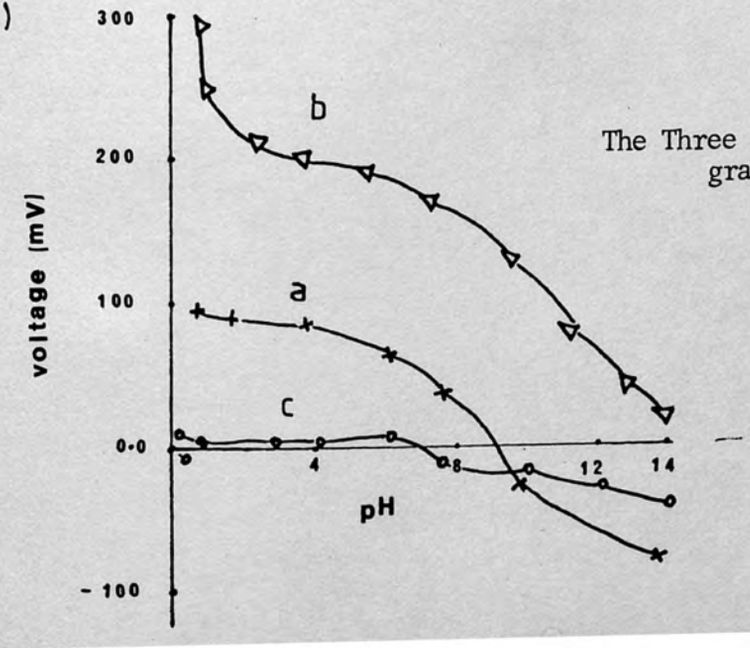

The Three Forms in one graph.

Slope and Intercept Values Calculated from pH/Voltage Curves for three Forms of TTF/DYE Complexes.

Table (17)

Complex form	Slope (mV)	Intercept (mV)
TTF/DYE	-16.16	156.7
Oxidized form of TTF/DYE	-32.0	444.5
Reduced form of TTF/DYE	- 6.5	46.6

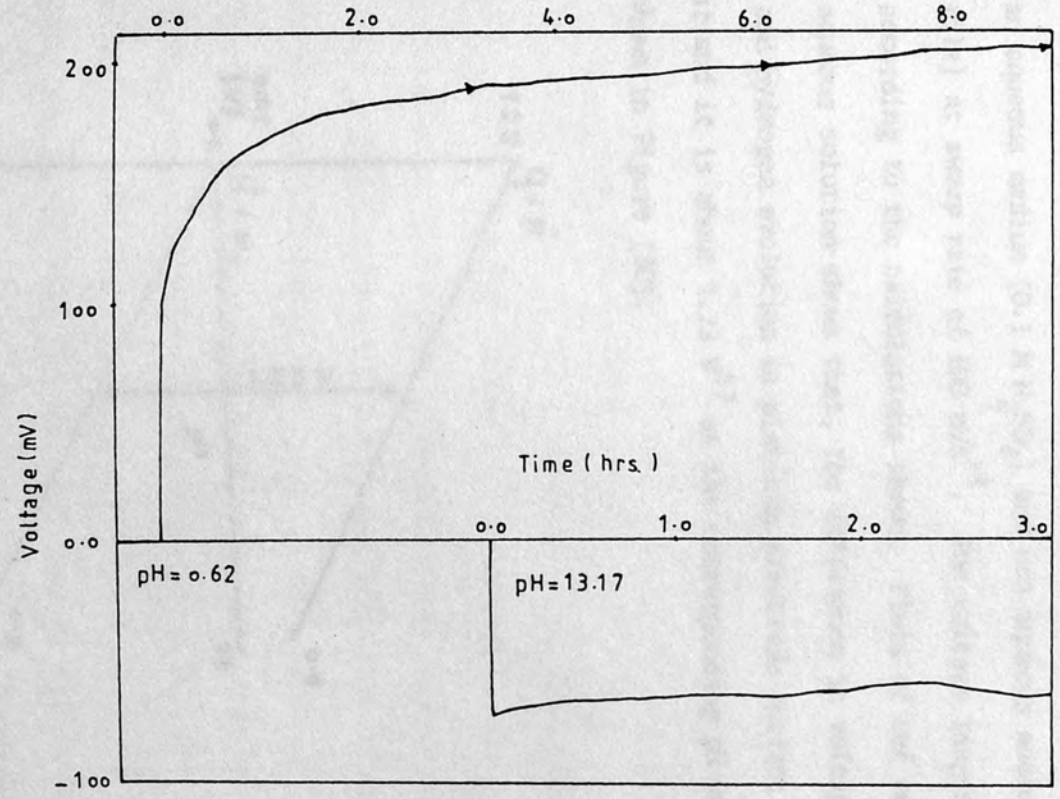

Figure (29) 4.6 Change of Voltage with time for pt mesh/TTF/DYE Electrode at Constant pH of 0.62 and 13.17.

4.7 Cyclic-Voltammagram of pt mesh/TTF-DYE Complex.

The cyclic-voltammogram of the electron-donor TTF and the anionic oxonol dye were discussed in Chapter 3. It would be of interest in this section to show the voltammograms of the complex coated on the surface of platinum mesh electrode. The experiment was run in an aqueous medium (0.1 M H_2SO_4) and non-aqueous medium (dry actonitrile) at sweep rate of 100 mVs^{-1}. The voltage ranges were chosen according to the calculations shown. Plots of emf versus pH for an aqueous solution shows that, the difference in voltage between oxygen and hydrogen evolution in platinum electrode surface is almost constant and it is about 1.23 V[87] at the corresponding pH value as it is shown in Figure (30).

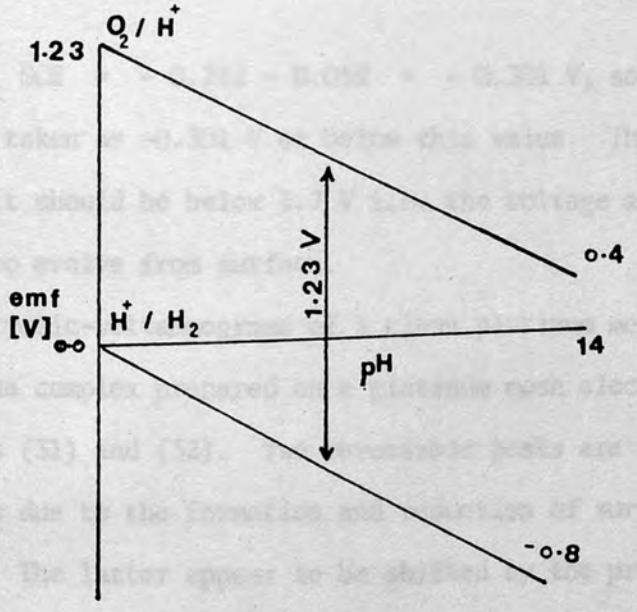

Figure (30).

Following the Nernst equation for a simple hydrogen reduction process ($2H^+ + 2e = H_2$), the voltage can be calculated as:

$$E = E^o + \frac{RT}{2F} \ln |H^+|^2$$

$$= o + 2.303 \frac{RT}{F} \log H^+$$

Since $pH = -\log H^+$ and $2.303 \frac{RT}{F} \sim 0.059V$

$$E = -0.059 \text{ pH V at } 298 \text{ K}$$

which shows that, the emf is linearly dependent on the pH.

For 0.1 M H_2SO_4, pH = 1

$$\therefore E_{w.r.t \text{ SHE}} = -0.059 \text{ V}$$

$E_{w.r.t \text{ SCE}} = -0.242 - 0.059 = -0.301$ V, so the lower limit should be taken as -0.301 V or below this value. The choice of the upper limit should be below 1.7 V i.e. the voltage at which oxygen expected to evolve from surface.

The cyclic-voltammograms of a clean platinum mesh together with that of the complex prepared on a platinum mesh electrode are shown in Figures (31) and (32). Two reversible peaks are found overlaid with peaks due to the formation and reduction of surface oxides of platinum. The latter appear to be shifted by the presence of the complex to higher and lower potentials respectively. This could be simply a result of the greatly hindered diffusion of electrolyte through the layer of complex. Averages of the oxidation and reduction peaks of the complex give formal electrode potentials of 0.218 V and 0.548 V respectively. The behaviour of the complex

is seen more clearly in the non-aqueous media of acetonitrile (Figure 33) in which the complex is sparingly soluble. The values of the formal potentials are now 0.266V and 0.675 V. The cyclic-voltammogram of the complex is different from that of a mixed solution of TTF and oxonol dye, the latter being a simple sum of Figures (16b) and (16c) (see also reference no. 88).

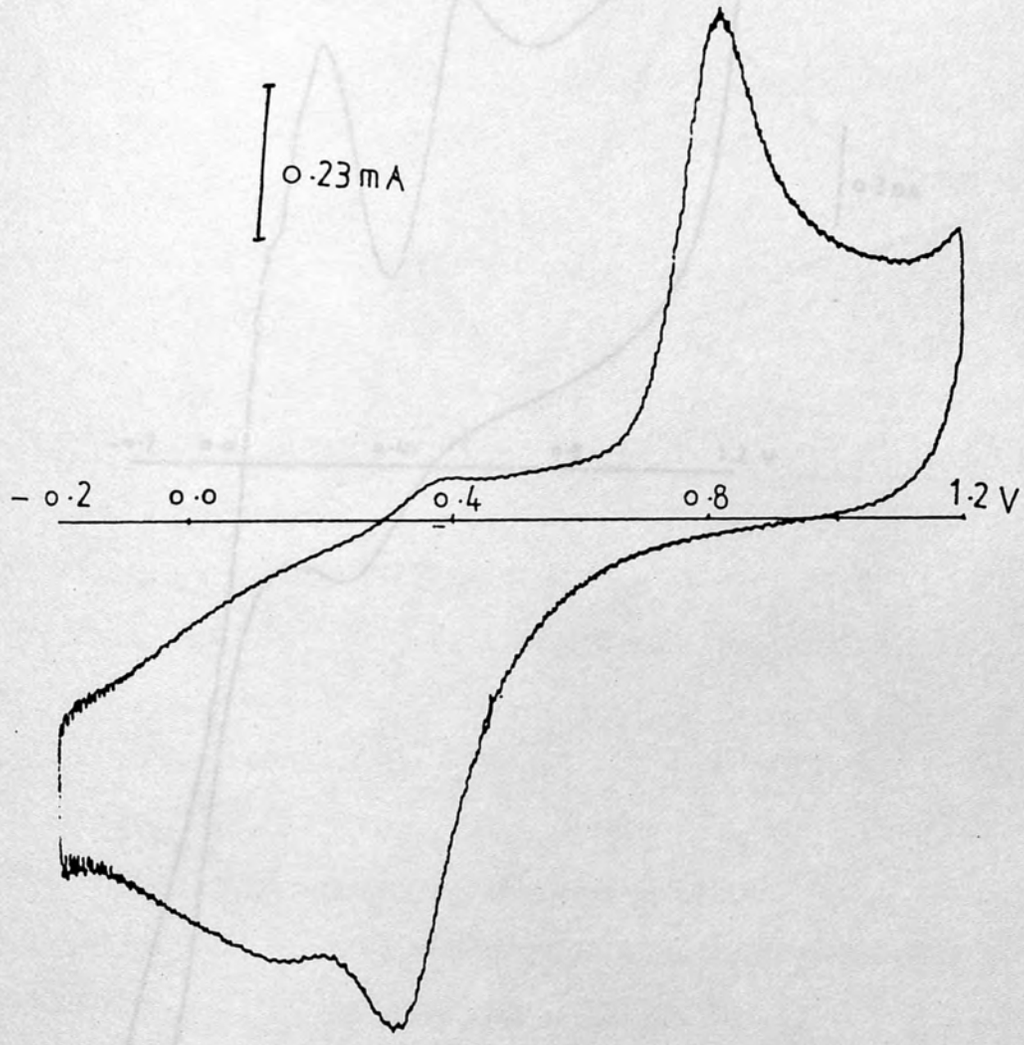

Figure (31) Cyclic-Voltammogram of pt mesh electrode (vs. SCE in 0.1 M H_2SO_4 at sweep rate of 100 mVs^{-1}).

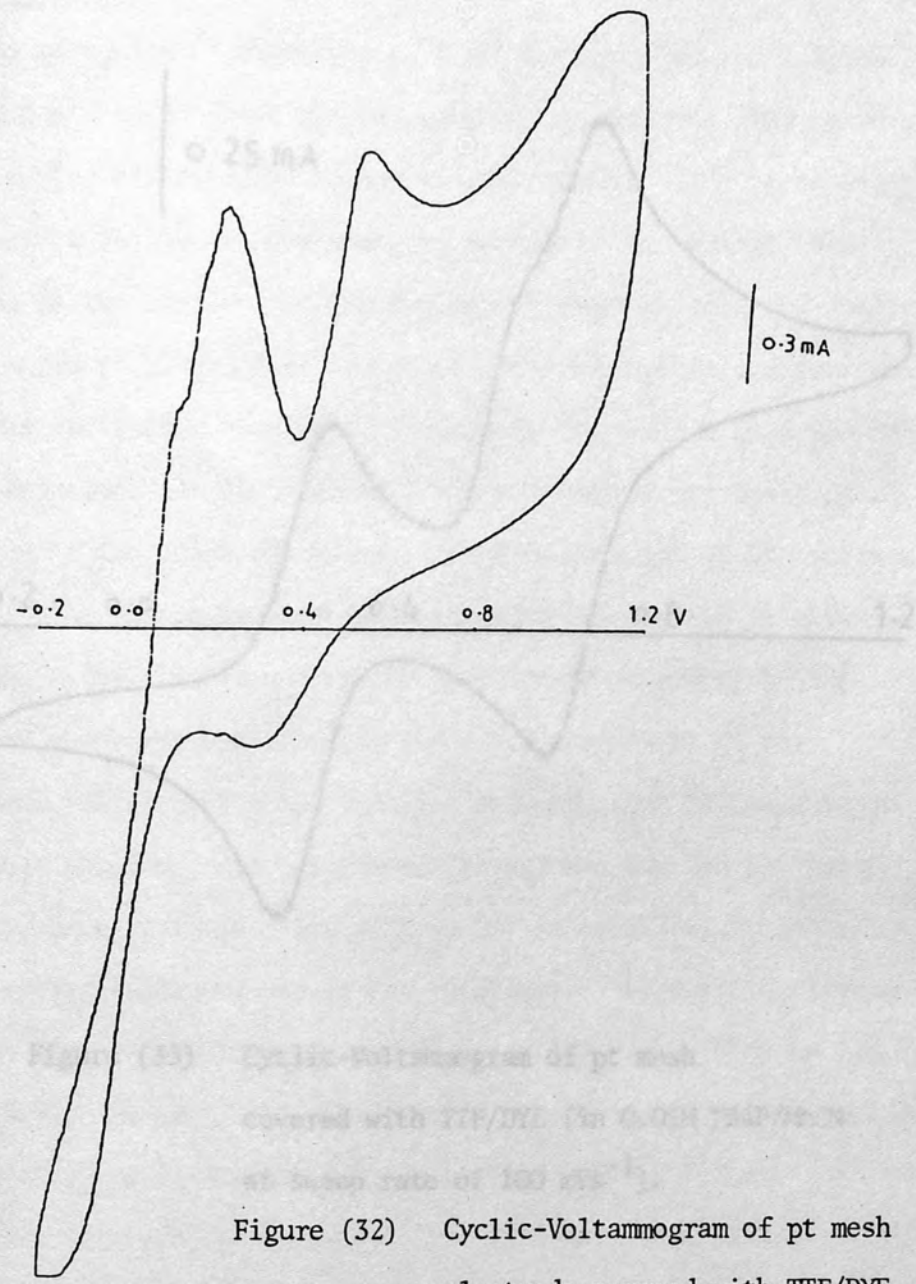

Figure (32) Cyclic-Voltammogram of pt mesh electrode covered with TTF/DYE (vs. SCE in 0.1 M H_2SO_4 at sweep rate of 100 mVs^{-1}).

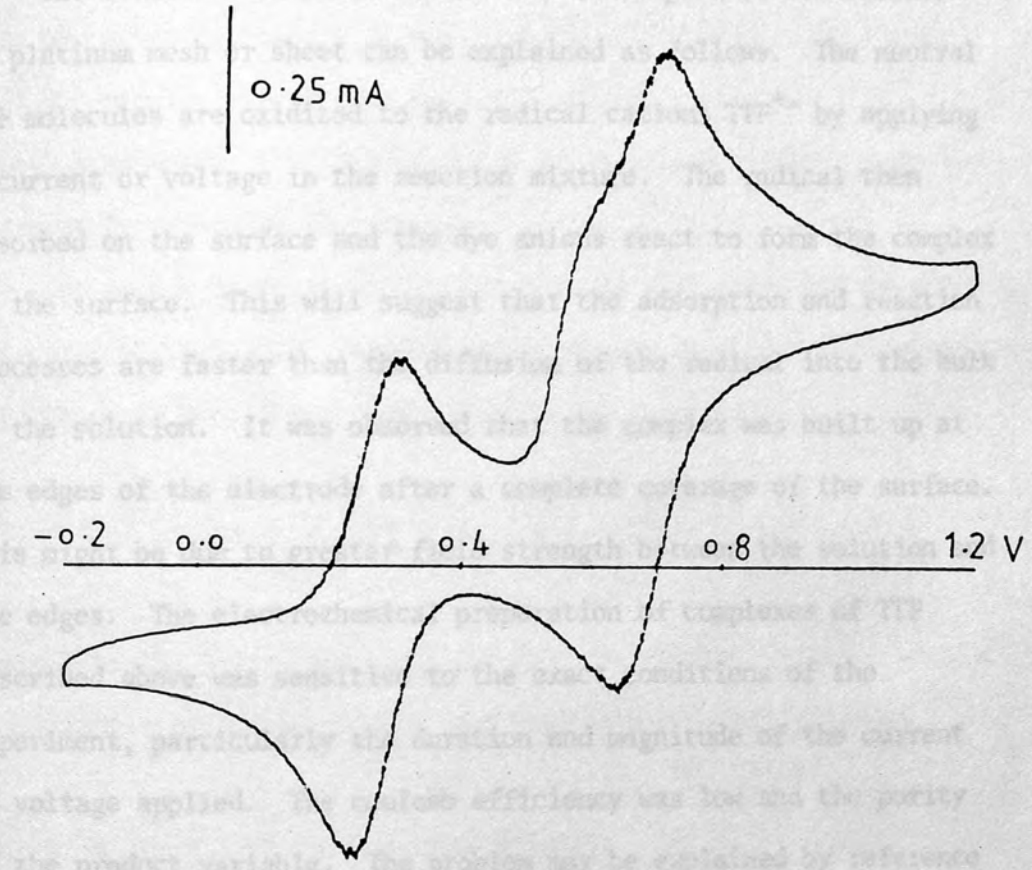

Figure (33) Cyclic-Voltammogram of pt mesh covered with TTF/DYE (in 0.05M TBAP/MeCN at sweep rate of 100 mVs^{-1}).

4.8 Discussion

The mechanism of formation of TTF/DYE complex on the surface of platinum mesh or sheet can be explained as follows. The neutral TTF molecules are oxidized to the radical cations $TTF^{+\cdot}$ by applying a current or voltage in the reaction mixture. The radical then adsorbed on the surface and the dye anions react to form the complex on the surface. This will suggest that the adsorption and reaction processes are faster than the diffusion of the radical into the bulk of the solution. It was observed that the complex was built up at the edges of the electrode after a complete coverage of the surface. This might be due to greater field strength between the solution and the edges. The electrochemical preparation of complexes of TTF described above was sensitive to the exact conditions of the experiment, particularly the duration and magnitude of the current or voltage applied. The coulomb efficiency was low and the purity of the product variable. The problem may be explained by reference to the cyclic voltammograms of the reactants. The only electrochemical reaction that is required to take place is $TTF \rightarrow TTF^{+\cdot} + e$ ($E = 0.302$ V versus SCE). However $TTF^{+\cdot}$ is oxidized to the inactive (in terms of the formation of molecular conductors) TTF^{2+} ($E = 0.77$) and the oxonol anions are irreversibly oxidized. The application of indiscriminate anodic currents results in unwanted side reactions. Time is also an important factor. For longer deposition times at a constant current the conductivity of the complex fell from $1.13 \times 10^{-4}\ \Omega\ cm^{-1}$ after one hour (1 mA constant current) to $7.4 \times 10^{-7}\ \Omega\ cm^{-1}$ after 6 hours and $< 10^{-8}\ \Omega^{-1}\ cm^{-1}$ after 12 hours. Microanalysis also suggested that after 12 hours preparation time the stoichiometry of the product

had moved away from that expected for the 1:1 complex (calculated C 54.45%, H 3.86%, N 9.41%, found after 1 hour C 54.01%, H 3.98%, N 9.70%, after 12 hours C 51.06%, H 4.05%, N 10.07%). The change does not simply reflect a move to 2:1 complex containing TTF^{2+} but probably indicates the incorporation of oxidation products into the material deposited on the anode.

The oxonol anion is a base and through this property the equilibrium potential of TTF-oxonol complex electrode may be expected to show some dependence on pH. A possible reaction may be written:

$$TTF^{+}D^{-} + H^{+} + e = TTF + DH$$

where D is the oxonol dye. If all the species that interact with H^{+} are immobilized in the surface and thus have constant activity

$$E = E^{o} + RT/F \ln(s) + RT/F \ln(aH^{+})$$

where s is the ratio of ionized complex to the neutral protonated form. The equation predicts a linear fall in E with pH with a slope of -59 mV per pH unit. Reduction in acid medium will favour the neutral protonated form, decreasing s and hence the value of the intercept of the E versus pH graph. Conversely oxidation should lead to a greater value of s and intercept. Qualitatively these features are shown in Figure (28). The slopes of the graphs (a) and (b) are near 30 mV towards higher values of pH and the reduced form shows only a small pH dependence. The above equation only holds if equilibrium can be established and if s is indeed a constant. If a local corrosion cell were established with the equation representing

one half cell then H^+ would essentially titrate the basic form of the complex. No pH dependence would then be seen since changes in s would compensate for the effect of the changing pH. A contribution of this type of mechanism would decrease the slopes of the curves in the manner observed.

The formal electrode potentials calculated for the complex were comparable to the values obtained by Lamanche et al.[55]. They analysed the cyclic voltammograms of TTF-carbon paste electrodes in different electrolytes and concluded that $E^o(TTF^{+\cdot}, TTF)$ = 0.25 V versus SCE in aqueous media and that TTF^{2+} was unstable in water.

CHAPTER 5

Electrical and Electronic Properties

of some Molecular Conductors

5.1 Electrical Conductivities of Oxonol Dyes/TTF Complexes

A TTF/Dye complex prepared as described before was placed in a glass tube of internal diameter 0.34 cm and pressed between two steel rods. The amount of pressure applied (∿ 20 kgf) was measured using a Salter Pocket Balance connected to the system as shown in Figure (34). The electrical conductivity of the pressed disc was measured by connecting a conductance bridge to the steel rods terminals. The electrical conductivity of the four compounds measured is shown in Table (18). Dielectric loss measurements have been made on the precursor oxonol dyes[89], showing them to be insulators or semi-insulators. The effect of the applied pressure on these measurements is also shown in Figure (35) using the better conducting TTF/TCNQ complex.

Table (18) Electrical Conductivity of Oxonol Dyes/TTF Complexes.

DYE Complex	Conductivity (Ω^{-1} cm^{-1})
N-Et oxonol DYE/TTF	9.8×10^{-4}
N-Et oxonol DYE/Benzo TTF	4.1×10^{-4}
N-Bu^n oxonol DYE/TTF	4.4×10^{-4}
Monomethine oxonol DYE/TTF	7.6×10^{-5}
Pentamethine oxonol DYE/TTF	4.3×10^{-4}

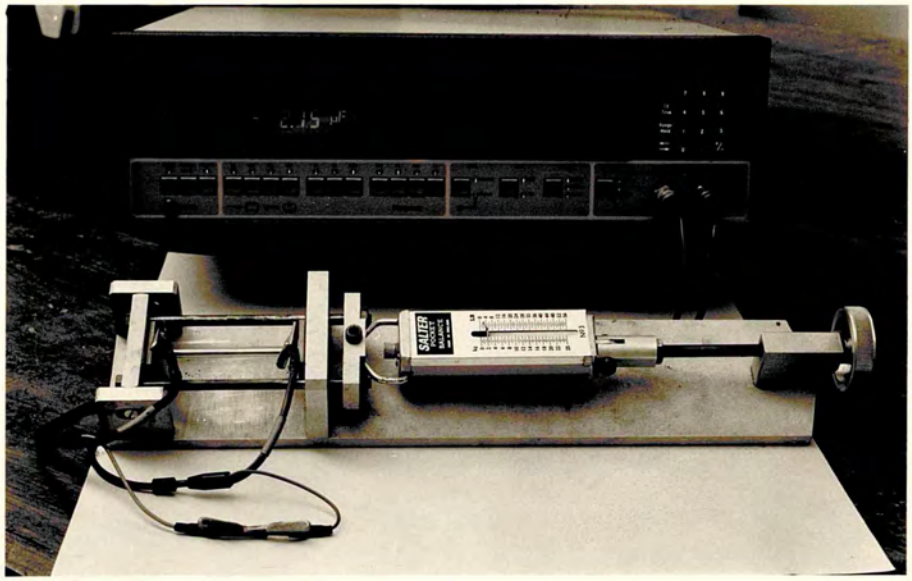

Figure (34): A pressure apparatus for measuring the conductivity of an organic solid powder

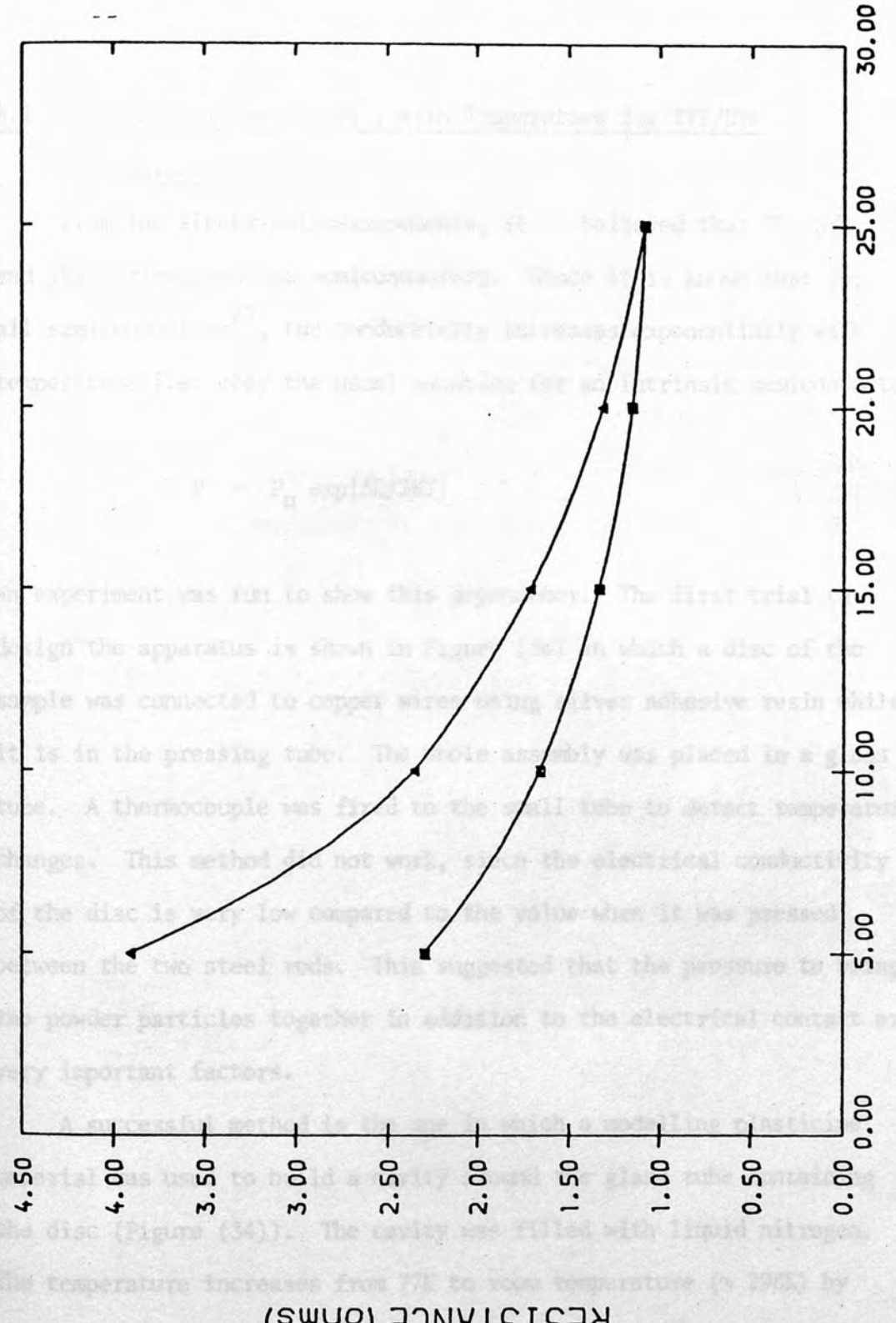

Figure (35) EFFECT OF PRESSURE ON TTF/TCNQ DISC RESISTANCE

5.1.2 Change of Conductivity with Temperature for TTF/DYE Complexes

From the electrical measurements, it is believed that TTF/DYE and its derivatives are semiconductors. Since it is known that for all semiconductors[27], the conductivity increases exponentially with temperature i.e. obey the usual equation for an intrinsic semiconductor:

$$P = P_o \exp|\Delta E/2KT|$$

an experiment was run to show this dependency. The first trial to design the apparatus is shown in Figure (36) in which a disc of the sample was connected to copper wires using silver adhesive resin while it is in the pressing tube. The whole assembly was placed in a glass tube. A thermocouple was fixed to the small tube to detect temperature changes. This method did not work, since the electrical conductivity of the disc is very low compared to the value when it was pressed between the two steel rods. This suggested that the pressure to bring the powder particles together in addition to the electrical contact are very important factors.

A successful method is the one in which a modelling plasticine material was used to build a cavity around the glass tube containing the disc (Figure (34)). The cavity was filled with liquid nitrogen. The temperature increases from 77K to room temperature ($\sim$ 298K) by allowing liquid nitrogen to evaporate slowly. The temperature changes were detected by a thermocouple fixed to the glass tube. A blank experiment was run to show the validity of the system. The change of conductivity with temperature was recorded for different dye complexes.

The data recorded for TTF/N-Et oxonol dye, monomethine/TTF and dibenzo TTF/N-Et oxonol dye are shown in Tables (19), (20) and (21). A plot of conductivity change with temperature in addition to logarithm of conductivity versus 1/T for the TTF/DYE complex are also shown in Figures (37) and (38). The activation energy Ea in the semiconductor equation mentioned was calculated from the slope of Figure (38) and it is recorded for some dye complexes. It is observed that the change in conductivity is very small in the range of temperature between 77 to 173 K, but it is remarkable in the range 173 to 298 K. This is shown in Figure (39).

5.1.3 Construction of TTF/DYE Electrode for Measuring Conductance Change with Temperature

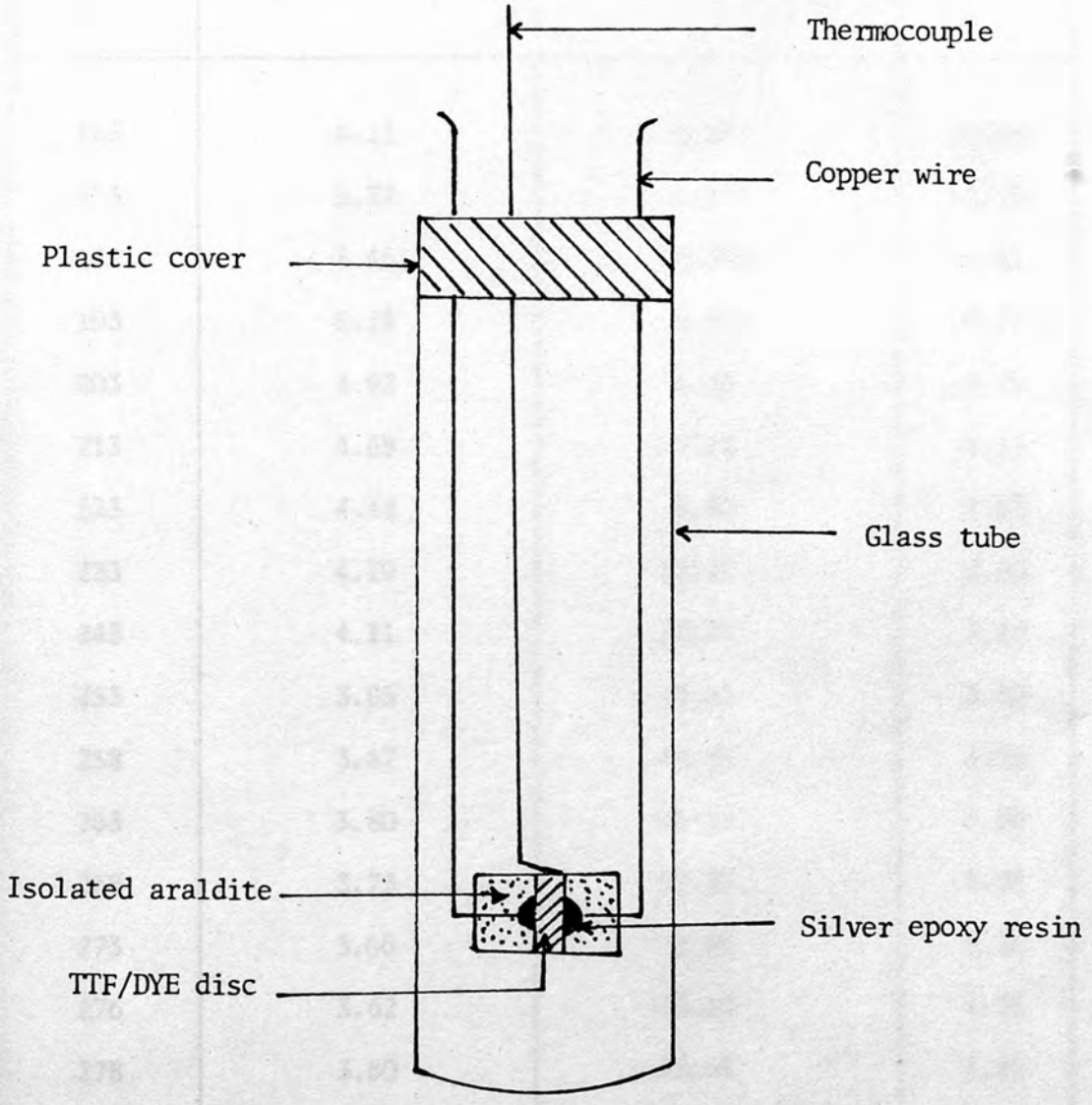

Figure (36)

Table (19) Data Obtained from Change of Conductance with Temperature for TTF/DYE Complex.

$T(K^o)$	$1/T\ (K^{-1})x10^{-3}$	Conductance (μs)	$\log_e \sigma$
163	6.13	0.107	-2.26
173	5.77	0.173	-1.75
183	5.46	0.0444	-0.81
193	5.18	0.840	-0.17
203	4.92	1.33	0.29
213	4.69	3.15	1.15
223	4.48	6.80	1.92
233	4.29	13.47	2.60
243	4.11	22.22	3.10
253	3.95	33.60	3.50
258	3.87	40.89	3.71
263	3.80	49.17	3.90
268	3.73	59.29	4.08
273	3.66	70.69	4.26
276	3.62	78.60	4.36
278	3.60	83.98	4.43
283	3.53	100.87	4.61
288	3.47	119.70	4.78
298	3.35	176.40	5.17

$\Delta E = 0.516$ eV

Table (20) Data Obtained from Change of Conductance with Temperature for TTF/monomethine Oxonol Dye Complex.

$T(K^o)$	$1/T\ (K^{-1})x10^{-3}$	Conductance (ns)	$\log_e^o$
133	7.51	26.2	3.27
143	6.99	26.7	3.28
153	6.53	27.5	3.31
163	6.13	28.8	3.36
173	5.77	30.6	3.42
183	5.46	34.8	3.55
193	5.18	44.2	3.79
203	4.92	61.9	4.13
213	4.69	94.0	4.54
223	4.48	154.5	5.04
233	4.29	260.0	5.56
243	4.11	444.3	6.10
248	4.03	572.4	6.35
253	3.95	737.7	6.60
258	3.87	948.1	6.85
263	3.80	1196.0	7.09
268	3.73	1466.0	7.29
273	3.66	1845.0	7.52
278	3.60	2297.0	7.74
283	3.53	278.0	7.93
288	3.47	3474.0	8.15
298	3.35	5880.0	8.68

$\Delta E = 0.397$ eV

Table (21) Data Obtained from Change of Conductance with Temperature for Dibenzo TTF/DYE.

$T(K^o)$	$1/T\ (K^{-1})x10^{-3}$	Conductance (σ)	$\log_e^o$
93	10.0	17.6 ns	2.86
103	9.69	19.3 ns	2.96
113	8.84	25.0 ns	3.22
123	8.13	33.0 ns	3.50
133	7.50	41.9 ns	3.74
153	6.53	59.0 ns	4.08
163	6.13	91.4 ns	4.52
173	5.77	170.0 ns	5.14
183	5.46	331.0 ns	5.80
193	5.18	699.0 ns	6.55
203	4.92	1.26 µs	7.14
213	4.69	2.20 µs	7.70
223	4.48	3.71 µs	8.22
233	4.29	6.10 µs	8.72
243	4.11	9.09 µs	9.11
253	3.95	12.93 µs	9.47
258	3.87	15.40 µs	9.64
268	3.73	21.62 µs	9.98
273	3.66	25.51 µs	10.15
278	3.60	29.96 µs	10.31
283	3.53	35.20 µs	10.47
288	3.47	41.00 µs	10.62
298	3.35	57.93 µs	10.97

$\Delta E = 0.413$

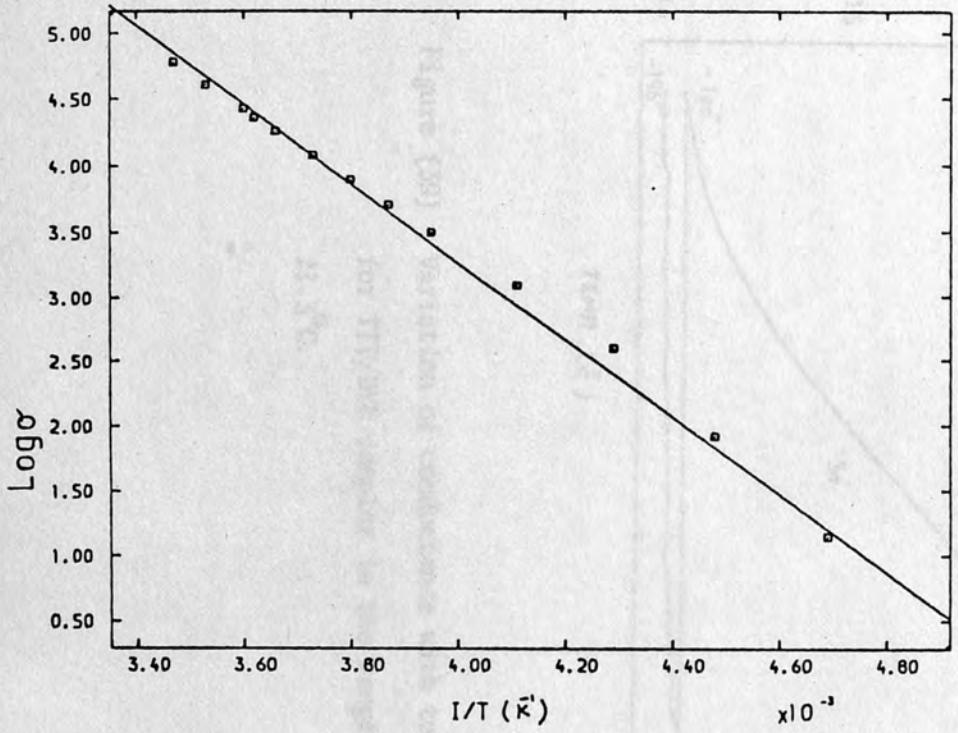

Figure (38) Graph of log conductance (σ) versus 1/T for TTF/DYE complex.

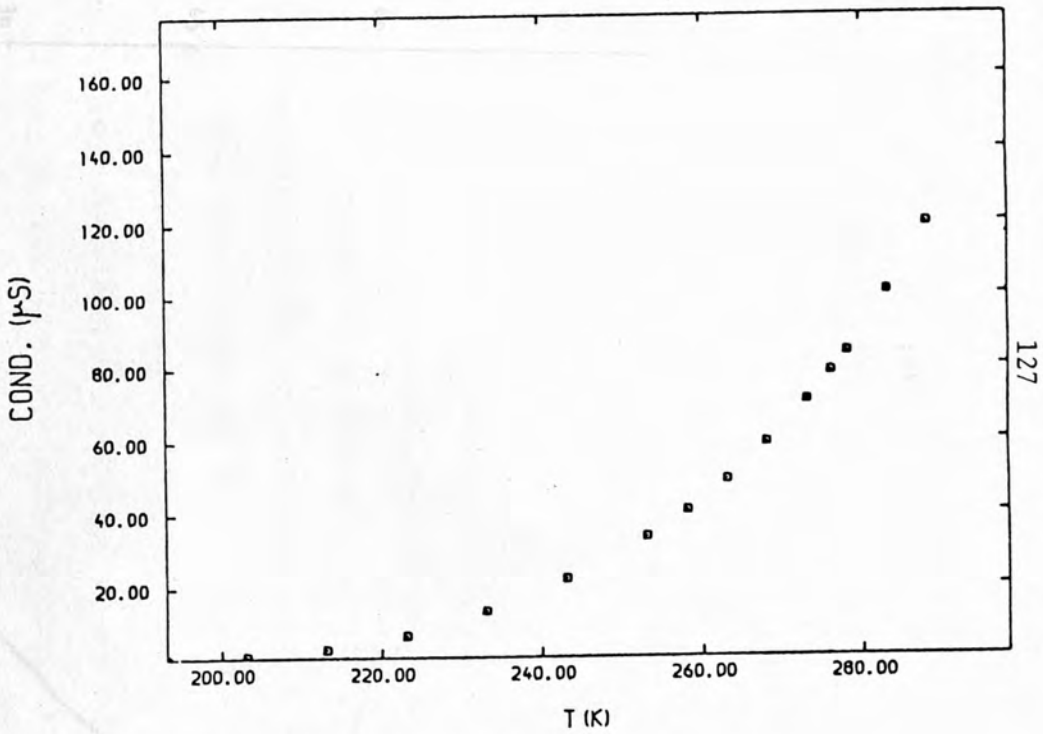

Figure (37) Graph of conductance versus temperature for TTF/DYE complex.

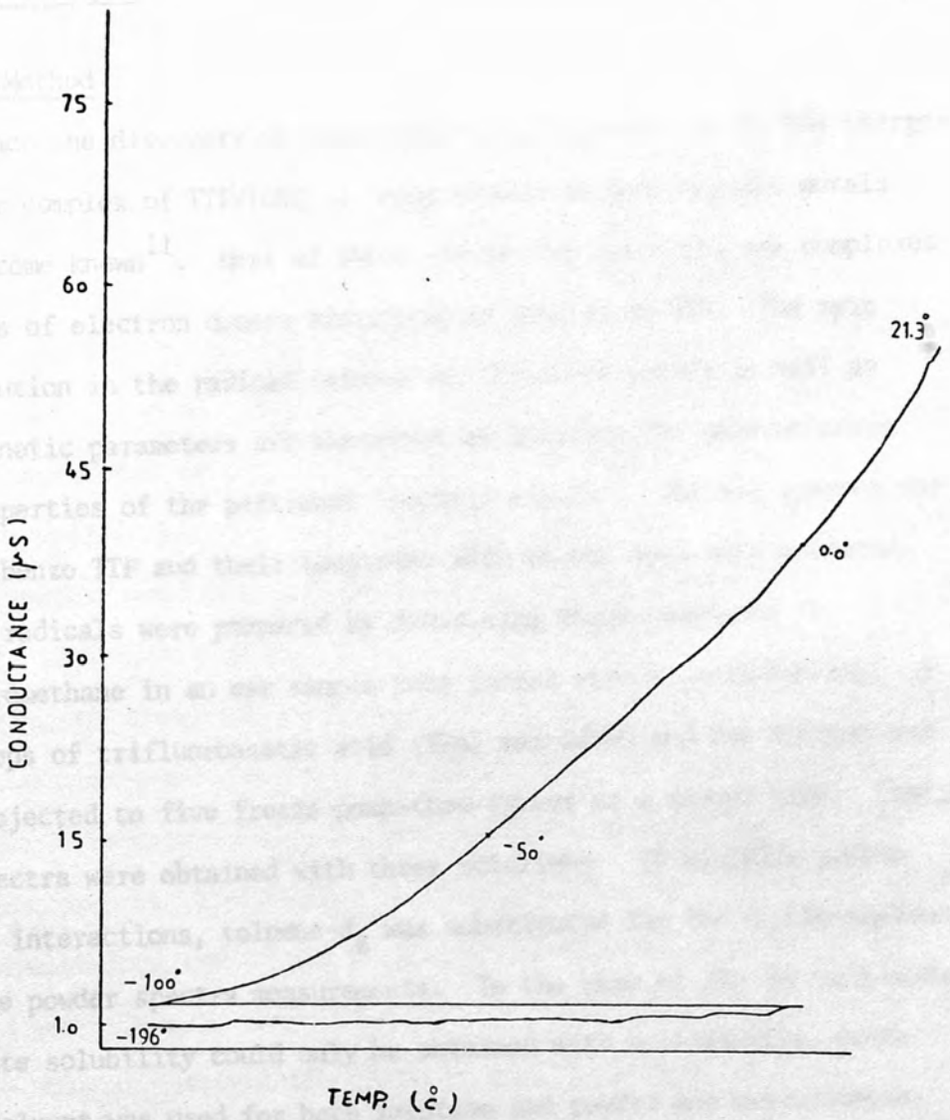

Figure (39) Variation of conductance with temperature for TTF/DYE complex in the range -196 to 21.3°C.

5.2 ESR Studies of TTF, Dibenzo TTF and their Complexes with Oxonol Dyes.

5.2.1 Method

Since the discovery of high electrical conductivity in the charge-transfer complex of TTF/TCNQ, a large number of such organic metals have become known[11]. Most of these conducting materials are complexes or salts of electron donors structurally related to TTF. The spin distribution in the radical cations of TTF-based donors as well as some kinetic parameters are therefore of interest for understanding the properties of the pertinent 'organic metals'. The esr spectra for TTF, dibenzo TTF and their complexes with oxonol dyes were measured. Cation radicals were prepared by dissolving these compounds in dichloromethane in an esr sample tube fitted with a greaseless tap. A few drops of trifluoroacetic acid (TFA) was added and the mixture was then subjected to five freeze-pump-thaw cycles on a vacuum line. Isotropic esr spectra were obtained with these solutions. To minimize proton dipole interactions, toluene-d_8 was substituted for the dichloromethane for the powder spectra measurements. In the case of the dye complexes adequate solubility could only be obtained with acetonitrile, hence this solvent was used for both solution and powder esr measurements.

5.2.2 Measurements

Esr spectra were obtained with a Varian E-4 spectrometer: g-factors were measured with the aid of a Bruker ER035M 1000 gaussmeter used in conjunction with a Marconi type 2440 microwave frequency counter. Sample temperatures were measured with a Comark type 5215 digital thermometer.

5.2.3 Results and Discussion

The esr spectrum of the TTF radical (CH_2Cl_2, -35°C) is a quintet (Figure (40)) indicating four equivalent protons; a_H = 0.1262 ± 0.0023 mT. The hyperfine splitting agrees with that measured recently by Gerson (0.125 mT)[90]. The isotropic g-factor is large indicating that a substantial proportion of the unpaired spin density resides on the sulphur atoms. The large amount of an isotropy in the system is reflected in the wide spread values of g_{xx}, g_{yy} and g_{zz}. The difference between the average of these values <g> and g_{iso} may be attributable to the large widths of the lines in the powder spectra. Figure (41) shows the powder spectrum of TTF radical along with that of dibenzo TTF at the freezing conditions, while Figure (42) shows the sulphur[33] satellite in dibenzo TTF at -30°C.

Table (22) shows the data obtained for TTF, dibenzo TTF and their oxonol dye complexes. The esr spectrum of the TTF/oxonol dye complex in acetonitrile showed the expected five lines arising from the four equivalent protons, a hyperfine splitting constant of 0.1190 ± 0.0005 mT was evaluated from the second derivative spectrum (Figure 43). This value is very close to that found for $TTF^{+\cdot}$ in dichloromethane. However, from the sulphur[33]-satellites there is some difference in the a_s values. The sulphur[33]-satellites spectrum for TTF/DYE complex is shown in Figure (44), while a powder spectrum of the complex at a freezing condition is shown in Figure (45). The solution spectrum of the cation radical of the dibenzo TTF/DYE complex in acetonitrile could not be resolved but a single narrow line of half-height width of 0.105 mT was observed. The narrowness of the line suggests that the two a_H values are smaller than those observed for dibenzo $TTF^{+\cdot}$ in dichloro-

methane. Generally, the powder spectra for the dye complexes in acetonitrile are rather different from those of $TTF^{+\cdot}$ and dibenzo $TTF^{+\cdot}$ in toluene-d_8. However, this is to be expected since the proton and nitrogen nuclei in acetonitirle will cause problems. Tentative values of g-factors obtained from the cation radical of the TTF/DYE complex in acetonitrile at -146^{o}C are shown in Table (22).

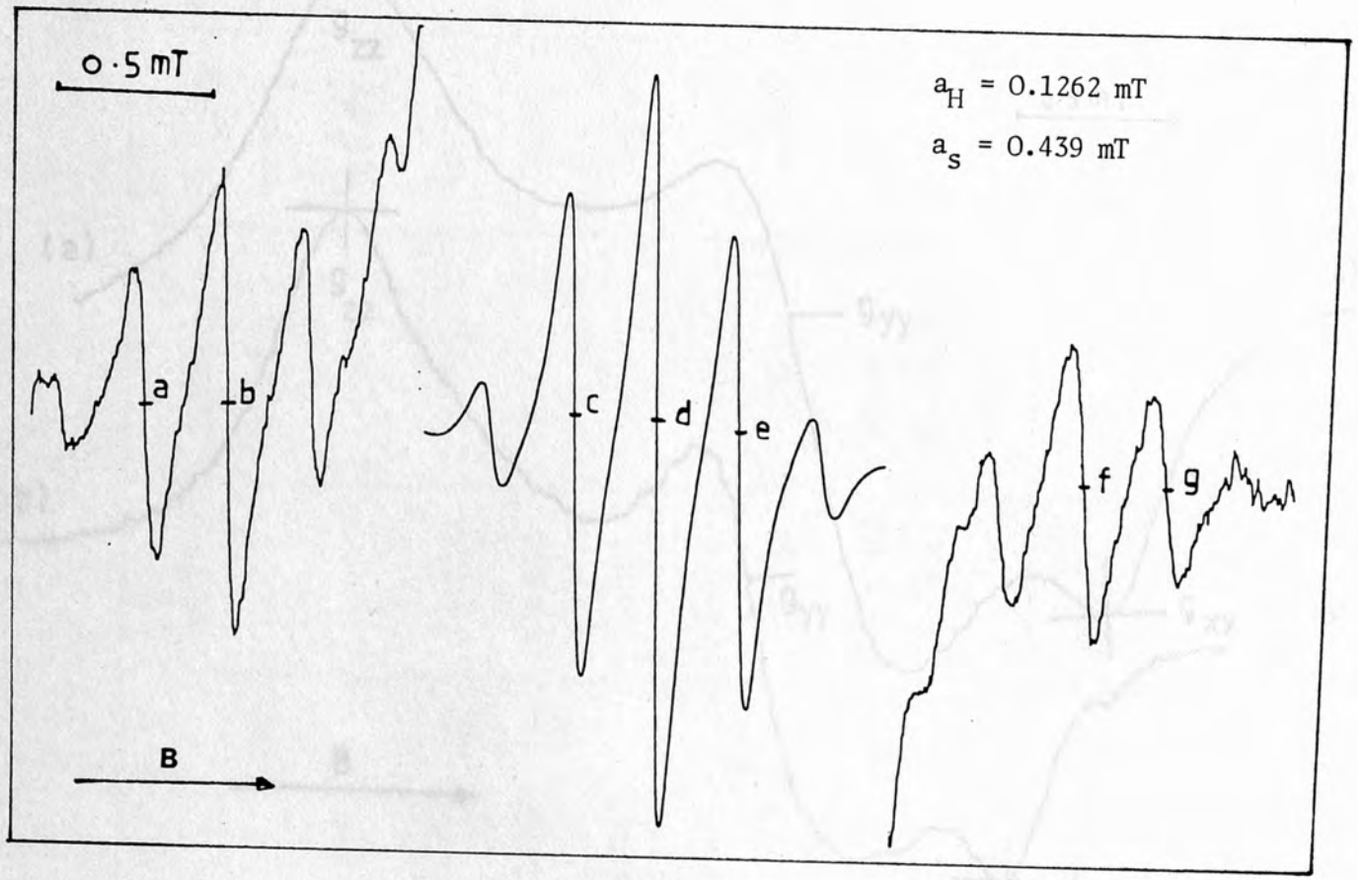

Figure (40) ESR Spectrum of $TTF^{+\cdot}$ Radical and its Amplification (x 10^2) at the sides, solvent (CH_2Cl_2 + TFA) at -35°C.

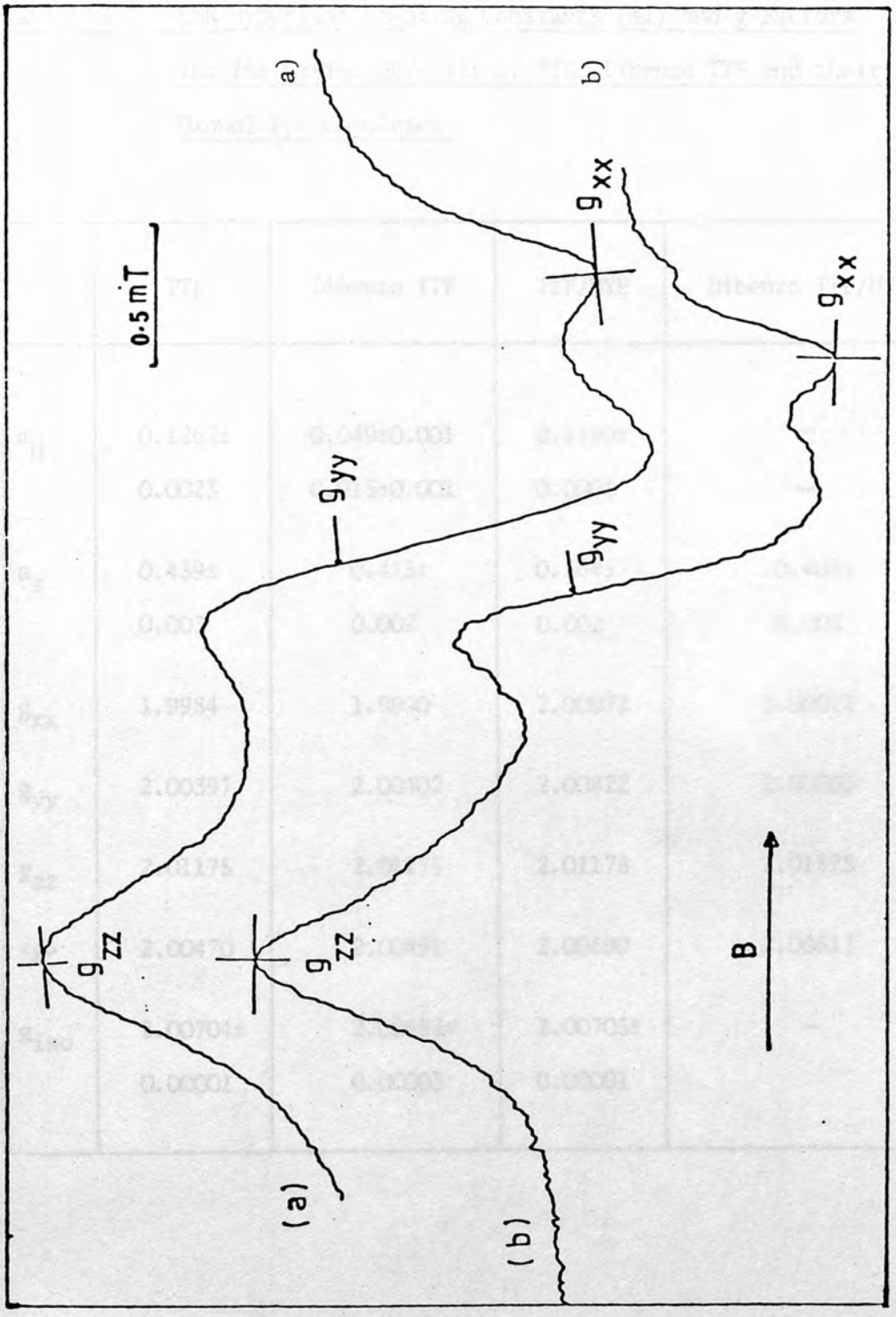

Figure (41) ESR Spectra for a) TTF radical in toluene-d_8 at -135°C
b) Dibenzo TTF in CH_2Cl_2 at -150°C.

Table (22) ESR Hyperfine Coupling Constants (mT) and g-Factors for the Cation Radicals of TTF, Dibenzo TTF and their Oxonol Dye Complexes.

	TTF	Dibenzo TTF	TTF/DYE	Dibenzo TTF/DYE
a_H	0.1262±	0.049±0.001	0.1190±	–
	0.0023	0.015±0.001	0.0005	–
a_s	0.439±	0.415±	0.564±	0.408±
	0.003	0.002	0.002	0.003
g_{xx}	1.9984	1.9990	2.00072	2.00072
g_{yy}	2.00397	2.00402	2.00822	2.00303
g_{zz}	2.01175	2.01175	2.01178	2.01175
<g>	2.00470	2.00491	2.00690	2.00517
g_{iso}	2.00704±	2.00683±	2.00705±	–
	0.00001	0.00003	0.00001	

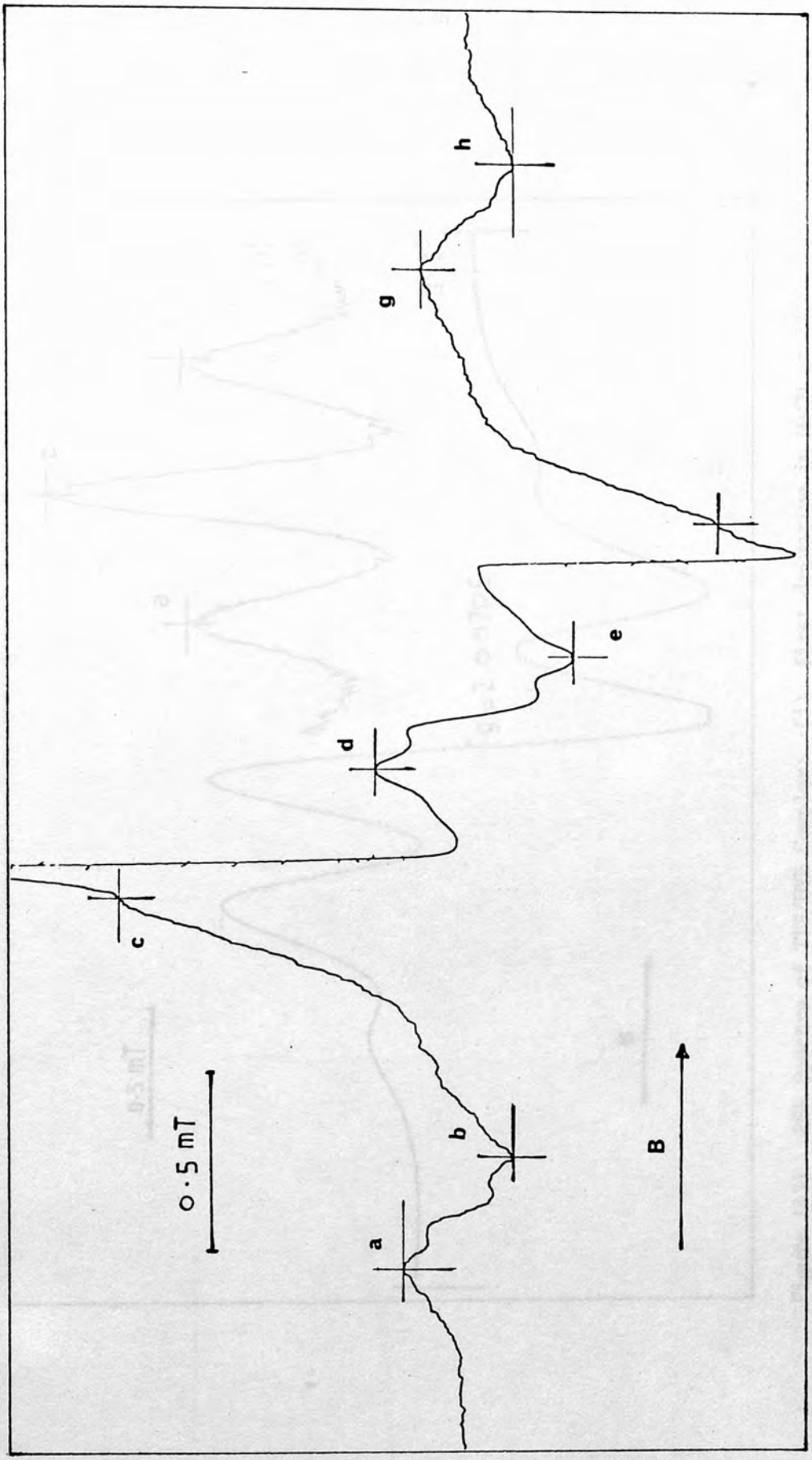

Figure (42) ESR Spectrum of Dibenzo TTF and its Amplification (x 10^2) at the sides showing s^{33}-satellite in CH_2Cl_2 at -30°C

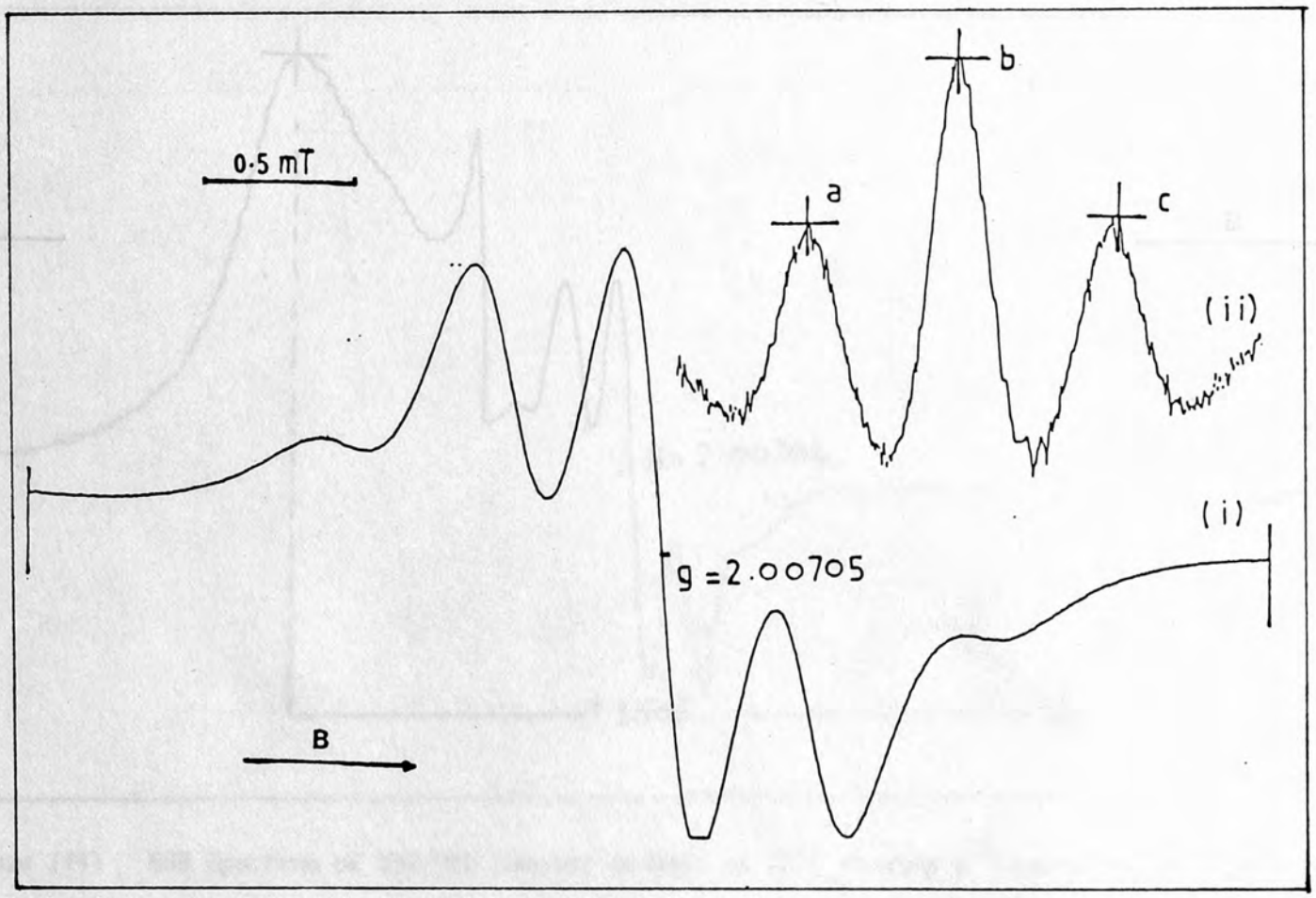

Figure (43) ESR Spectra of TTF/DYE Complex: (i) first drivative in MeCN at 22°C

(ii) central three lines of second derivative used to measure coupling constant.

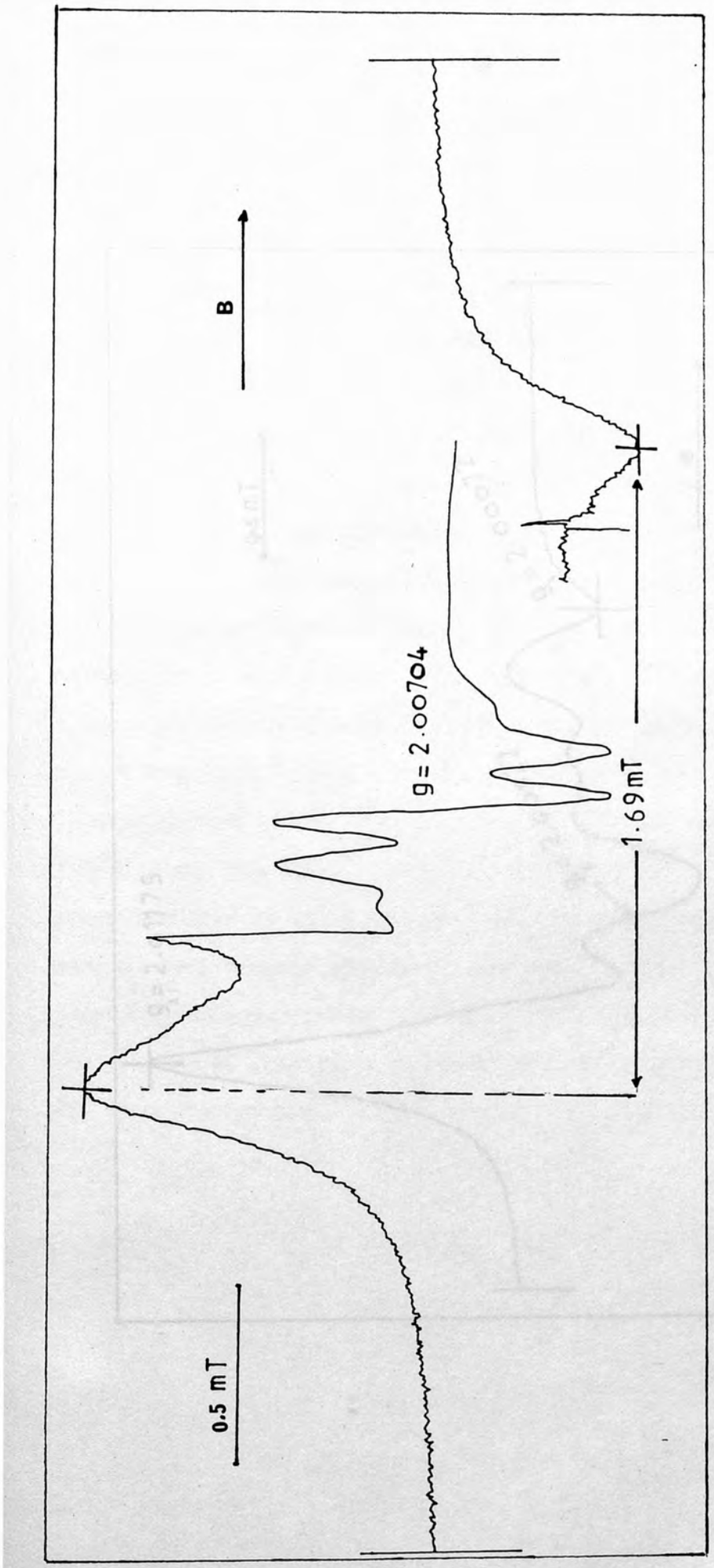

Figure (44) ESR Spectrum of TTF/DYE Complex in MeCN at 21°C showing s^{33}-satellite at Higher Amplification.

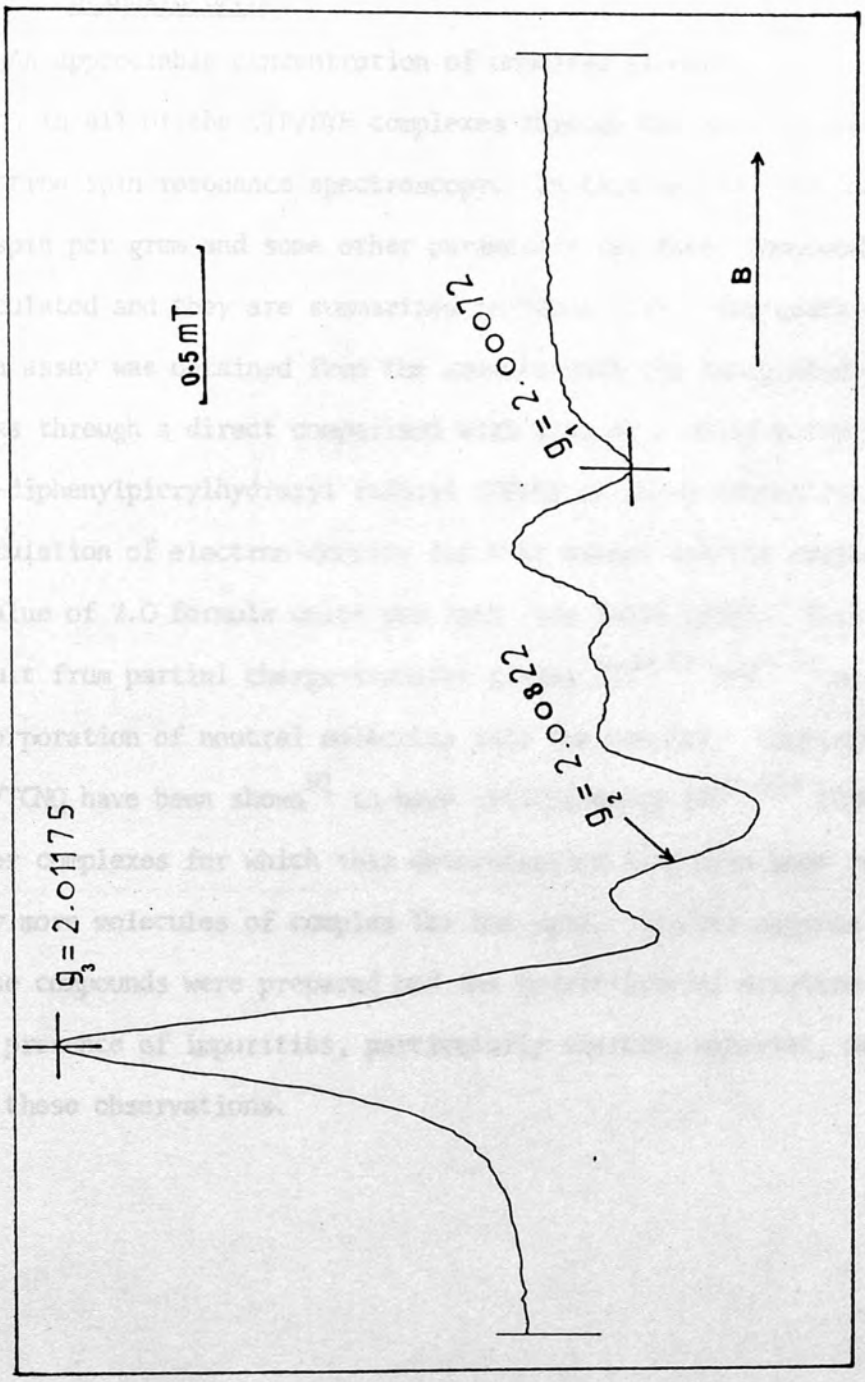

Figure (45) ESR Spectrum of TTF/DYE Complex in Acetonitrile at -146°C.

5.2.4 Calculation of Electron Density for TTF Complexes using Standard DPPH.

An appreciable concentration of unpaired electrons has been found in all of the TTF/DYE complexes through the application of electron spin resonance spectroscopy. In this section the number of spin per gram and some other parameters for these compounds were calculated and they are summarized in Table (23). The quantitative spin assay was obtained from the area beneath the integrated absorption peaks through a direct comparison with that of a solid polycrystalline 1,1-diphenylpicrylhydrazyl radical (DPPH) of known concentration. Calculation of electron-density for N-Et oxonol dye/TTF complex gave a value of 2.0 formula units per spin (see Table (23)). This may result from partial charge-transfer giving $TTF^{0.5+}$ $DYE^{0.5-}$ or the incorporation of neutral molecules into the complex. Complexes of TTF/TCNQ have been shown[91] to have stoichiometry $TTF^{0.59+}$ $TCNQ^{0.59-}$. Other complexes for which this determination have been made require many more molecules of complex for one spin. Smaller amounts of these compounds were prepared and the possibility of dilution by the presence of impurities, particularly starting material, may account for these observations.

Table (23) Data Calculated from ESR Spectra of TTF/DYE Complexes.

Compound	Spin/g	Average MW/s	No. of Molecules per spin
DPPH	1.53×10^{21}	4.5×10^{2}	1.0
N-Me DYE/TFF	1.30×10^{20}	4.6×10^{2}	1.3
N-Et DYE/TTF	4.75×10^{20}	1.2×10^{3}	2.0
N-Bu^{n} DYE/TTF	2.71×10^{19}	2.2×10^{4}	34.1
N-Et DYE/Benz TTF	2.37×10^{19}	2.5×10^{4}	36.7
Monomethine/TTF	1.94×10^{19}	3.1×10^{4}	57.3

5.2.5 Thermal Stability of TTF/DYE Complex as Measured by ESR.

Bulk powder spectra of TTF/DYE complex was measured as a function of temperature. The decay of the esr signal was used to monitor the stability of the complex. No decay was observed below about 150°C and the reaction was irreversible. A sample held at 170°C for 1.0 minute had its esr signal reduced to zero which remained so on taking the temperature back to room temperature. 150°C is considerably lower than the temperature at which the complex decomposes (256°C). Figures 46a and 46b show the decay at different temperatures as well as the reactions are irreversible. Wudl discusses the metal-to-insulator transition for molecular crystals. In compounds with many equivalent positions in the unit cell reorientation of anions leads to an insulator. Other mechanisms arise from electron-phonon interactions (charge density waves) and magnetic interactions (spin density waves). The size of the dye anion may rule out easy reorientation although without knowledge of the crystal structure a conclusive statement cannot be made. The integrated absorption signal was used as a measure of the active amount of complex remaining. Figure (47) shows a first order plot of the decay at 163°C. The peak height and peak area at specific times are tabulated in Table (24) and they are plotted in Figures (48a) and 48b). The rate at which the compound loses its esr signal is calculated from the slope of Figure (48b) and it was found to be $-3.54 \times 10^{-2} \pm 0.0025\ s^{-1}$. Since the esr signal decreases gradually, change of crystal form is less probable while decomposition or other processes had mostly occurred. An infra red spectra showed the same peaks for the complex after and before heating with a lesser intensity for the heated form. It may be concluded that decomposition process has occurred.

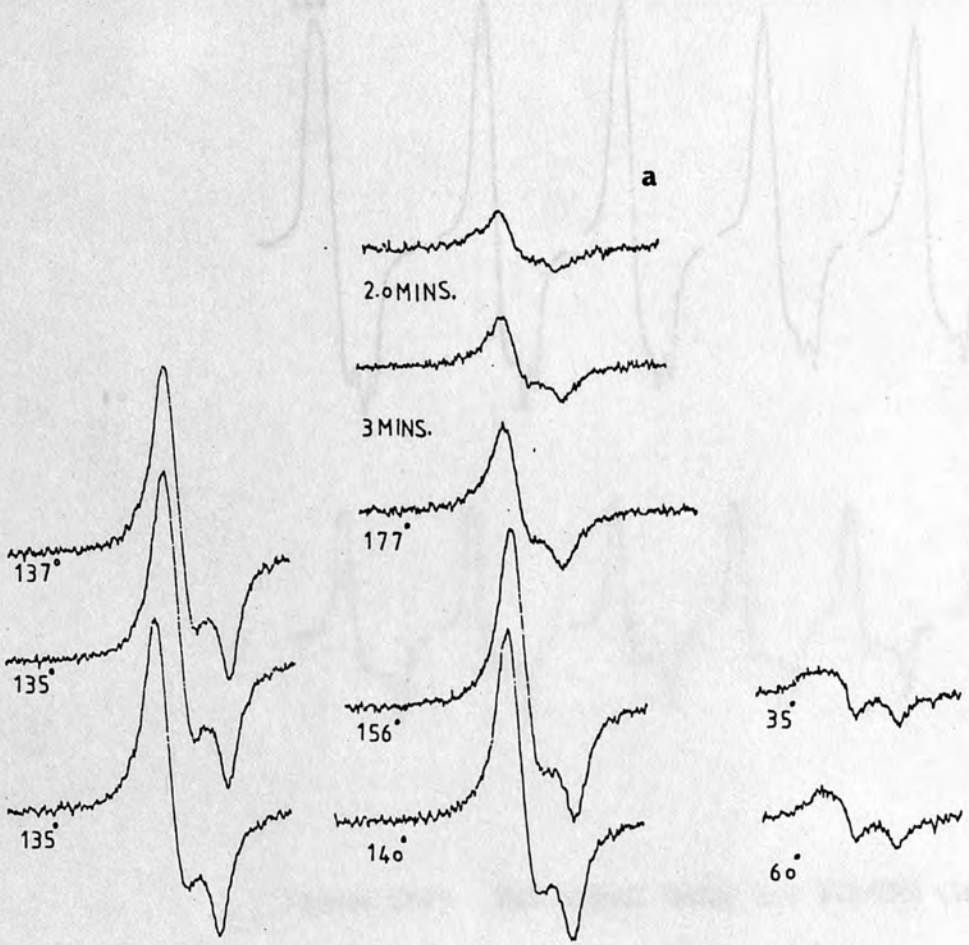

Figure (46) a) ESR Spectra for TTF/DYE Complex at Different Temperatures.

b) ESR Spectra for TTF/DYE Complex at Two Extreme Temperatures.

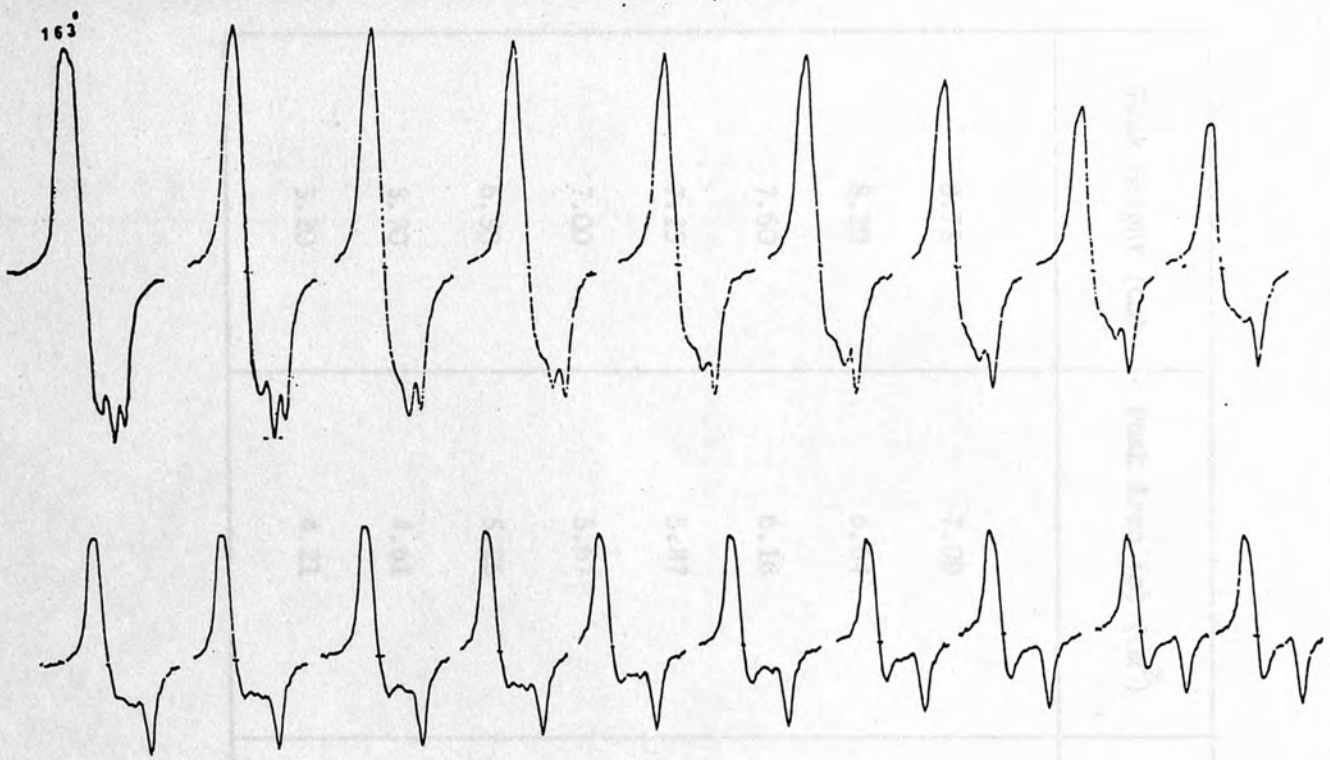

Figure (47) ESR Signal Decay for TTF/DYE Complex at 163°C and in 2 Minutes Intervals.

Table (24) Data Calculated from the Rate of Unpaired Electron Loss Using esr for TTF/DYE Complex.

Peak Height (cm)	Peak Area (a) (cm^2)	log (a)	Time (min)
8.75	7.09	1.96	0.0
8.20	6.64	1.89	2.0
7.60	6.16	1.81	4.0
7.25	5.87	1.77	6.0
7.00	5.67	1.74	8.0
6.50	5.26	1.66	10.0
5.70	4.61	1.53	12.0
5.20	4.21	1.44	14.0

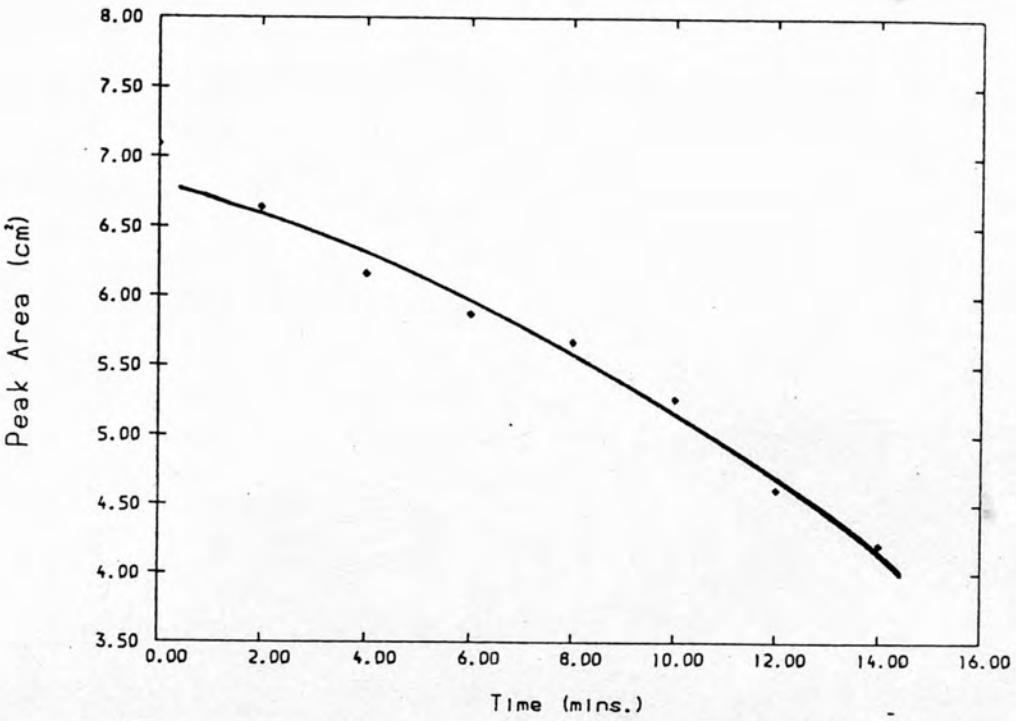

(a) Graph of peak area versus time for TTF/DYE decomposition using esr

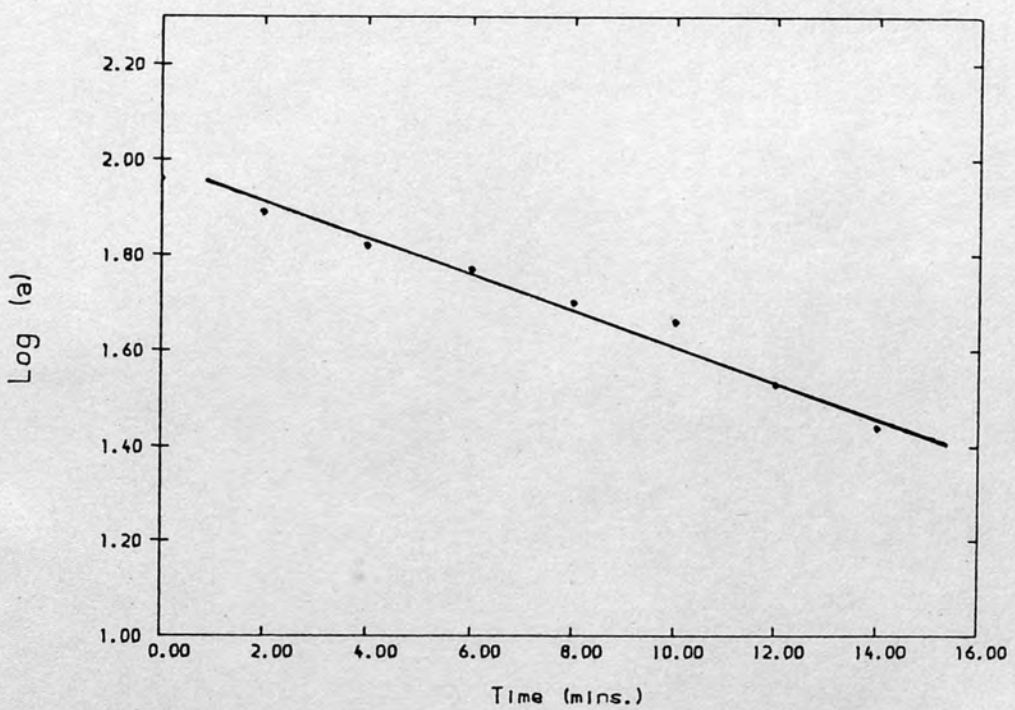

(b) Graph of Log(a) versus time for TTF/DYE

Figure (48)

5.2.6 Interconversion of the Mono- and Dication Radicals of TTF as Followed by esr.

The reversibility of formation of TTF mono- and dication radicals in the form of a simple chloride was examined using the esr technique. The salt was prepared by the action of chlorine gas on a carbon tetrachloride solution of the neutral TTF.[9] A stoichiometric amount of chlorine must be employed to avoid further oxidation to the dication. In this experiment the chlorine gas was passed through the carbon tetrachloride solution of TTF while it was in the esr machine cell. After TTFCl salt was formed (deep purple), an esr spectrum was run (Figure 49(i)a). An additional amount of chlorine was added to convert the salt to the dication (yellow precipitate). The spectrum was run again. It was reduced in intensity (Figure 49(i)b). The solution was left in the cell overnight and the esr spectra was run again. It was found that the esr spectra increases in intensity, but it did not reach the starting intensity (Figure 49(i)c). This result suggests that the dication can equilibriate with the monocation i.e. certain degree of reversibility exists. The possible mechanism is shown in Figure (49)(ii).

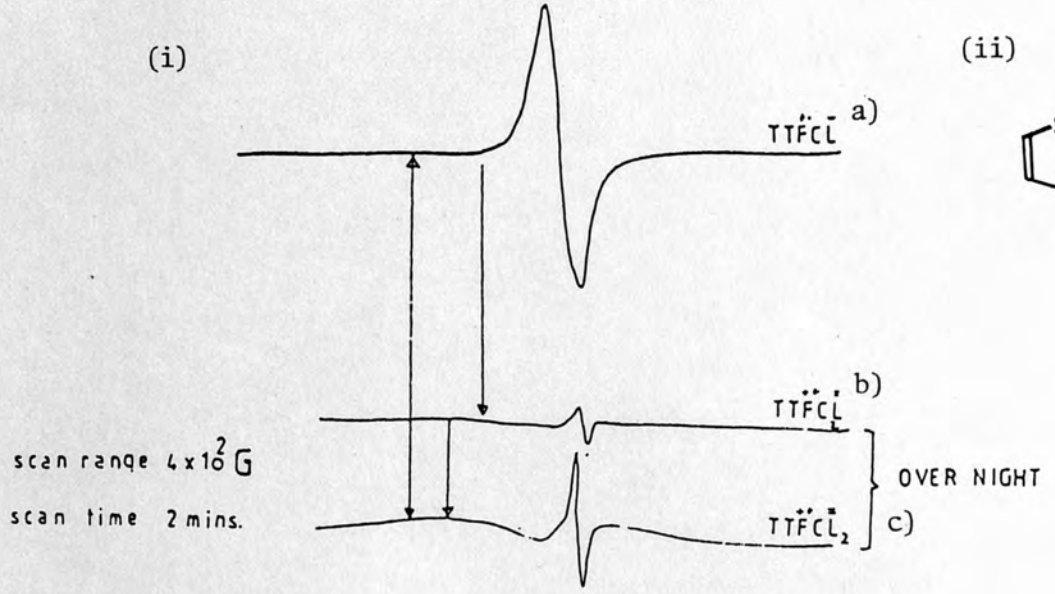

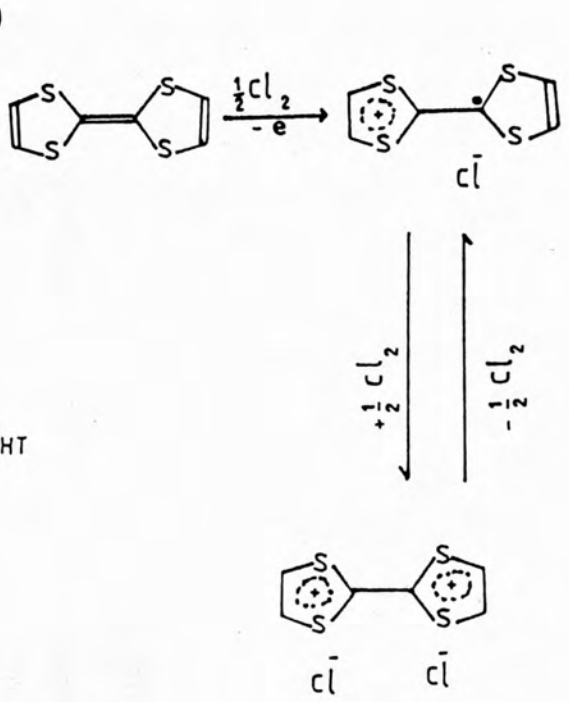

Figure (49) (i) TTF Simple Salt Mono- and Dication Radicals Interconversion as shown by esr.

(ii) Possible Mechanism for the Reaction.

5.3 Quantum Mechanical Calculations

The semi-empirical method MNDO (Modified neglect of diatomic overlap) was used to determine the equilibrium molecular geometries, enthalpies of formation at these geometries, ionization potentials and molecular charge distribution for TTF, dibenzo TTF and their mono- cation radicals. Geometries were defined in terms of bond lengths, angles and dihedral angles[93]. The experimental reported data for TTF neutral molecule[94] and the optimized geometry using MNDO are shown in Figures (50a) and (50c). To make sure that the data given are from the correct structure of each molecule, an optimized geometry of dibenzo TTF was plotted. The atoms position, which are in a correct order are shown in Figure (51). Enthalpies of formation, ionization potentials and charge distribution are shown in Tables (25) and (26).

Figure (50a) Experimental Geometries Taken from Reference 95.

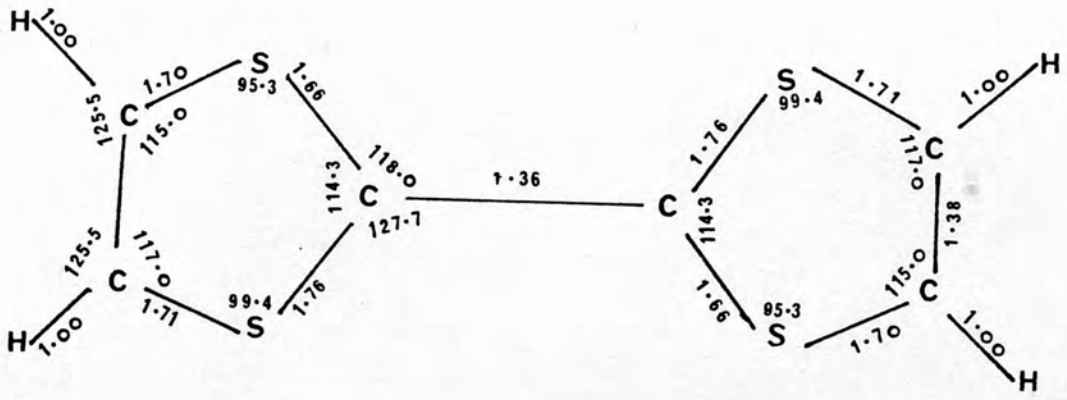

(b)

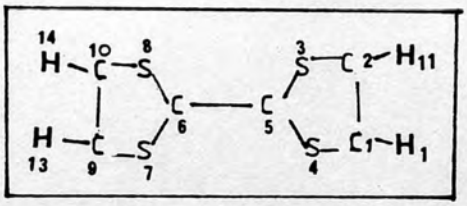

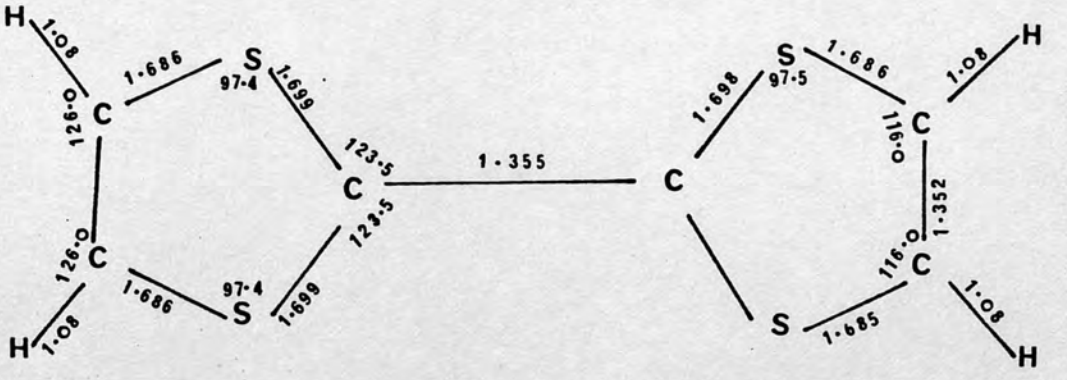

Figure (50c) Optimized Geometries as Predicted by MNDO Method.

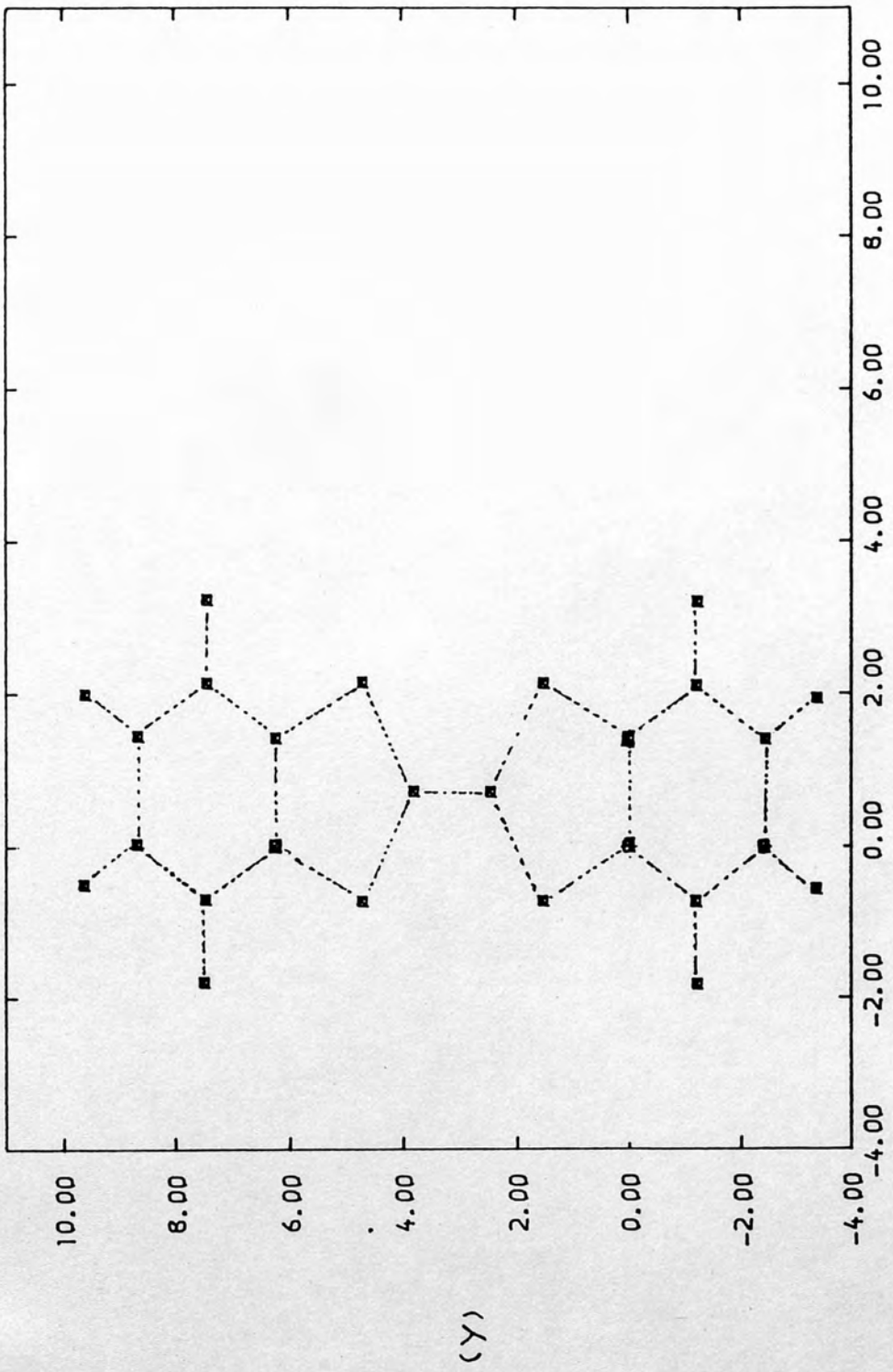

Figure (51) Atoms position in dibenzo TTF molecule.

Table (25) Calculated Enthalpies of Formation and Ionization Potentials for TTF, Dibenzo TTF and their Mono-Radical Cation Using MNDO Method.

	ΔH_f/KJ mol^{-1}	I.P/KJ mol^{-1} (neutral molecules)
TTF	171.54	779.21
$TTF^{+\cdot}$	901.04	-
$\Delta(\Delta H_f)$	729.50	-
DBTTF	241.41	774.39
$DBTTF^{+\cdot}$	950.18	-
$\Delta(\Delta H_f)$	708.77	-

Table (26) Charge Distribution for TTF Neutral Molecule as Predicted by MNDO Method.

Atom Number	Atoms	Charge Distribution
1	C	-0.2290
2	C	-0.2291
3	S	0.2935
4	S	0.2929
5	C	-0.3470
6	C	-0.3468
7	S	0.2936
8	S	0.2937
9	C	-0.2291
10	C	-0.2291
11	H	0.1092
12	H	0.1092
13	H	0.1090
14	H	0.1090

It was observed that MNDO reproduces the experimental condition that the C-C bond-length between the outer ring carbon atoms (C_1-C_2 and C_9-C_{10}, see Figure 5Ob) of TTF are comparatively less than that of the carbons between the rings (C_5-C_6), without recourse to the use of d-orbitals, a requirement suggested by Cooper et al.[95]. This trend mirrors the results obtained for heptafulvalene[96] where the bridging double bond (1.373A) was shown to be longer than the ring double bond (1.332-1.343A). The importance of empty sulphur d-orbitals in organosulphur compounds is one of continuing controversy. Coffen[84] and Mcloer[97] found independently that unless d-orbitals are included in the molecular orbital calculations of TTF, neither spectroscopic[84], nor molecular structure[97] could be correlated with theory. This might be the reason for some of the differences between the calculated and experimental values.

All values of ionization potentials are greater than experimental following a trend reported by Dewar and McKee[98] who note that calculated ionization potentials of sulphur to be about 1 eV (96.5 KJ mol^{-1}) too high.

The small differences between the calculated ionization potentials of the neutral molecules and the enthalpy difference of formation ($\Delta H_f(M^+) = \Delta H_f(M)$) is reflected in the similar geometries of neutral molecules and cations. MNDO put most of the positive charge on sulphur and hydrogen with the carbons of the fulvalene rings acquiring negative charge. The charge distribution for TTF is shown in Table (26). This result is different from that obtained by MINDO/3[99] in which the positive charge is largely located on the central carbon atoms with a small positive or even negative charge on sulphur.

5.4 Photoelectron Spectroscopy Studies.

5.4.1 Introduction

A photoelectron spectrum is a distribution curve of the kinetic energies of electrons emitted from a substance whilst under the impact of monochromatic radiation[100]. The first such spectra to be obtained from the vapours of atoms and molecules were recorded late in 1961 by Al-Joboury and Turner[101] and by Vilesov et al.[102].

Adsorption of certain frequencies of far ultra violet light brings about transitions of electrons between orbitals. The analysis of the resulting spectra gives a picture of the relative spacing of the orbitals. This information can also be obtained by measuring how much energy is needed to remove an electron from an orbital. This energy is one of the ionization potentials of the molecule. Measuring the ionization potentials of electrons in various orbitals of the molecule gives a picture of the orbital energies. Radiation in the far ultra violet region ($\lambda < 1700$ Å) can cause electronic excitation, ionization or even bond rupture in a molecule. If a photon of frequency (ν) collides with a single molecule, the kinetic energy of the ejected electron is given by:

$$h\nu = \frac{1}{2} m_e \nu^2 + I_i$$

where (I_i) is the ionization potential of the ejected electron. The index (i) labels the orbital occupied by the electron and hence the electrons ejected have various kinetic energies depending on the orbital they occupy. The ejected electrons are called photoelectrons, and the determination of their spectrum of energies gives rise to the

name photoelectron spectroscopy (p.e.s.). If a molecular photoelectron experiment is carried out at room temperature, we can safely assume that the molecule is in its ground electronic and vibrational state. When the molecule is converted into the positive ion it may end up in an excited vibrational state. This is given by:

$$E = h\nu - I_{elec.} - E_{vib.}$$

where $I_{elec.}$ denotes the ionization potential without vibrational changes i.e. the ionization potential. The electromagnetic radiation is essentially in the U.V region of the spectrum. A great deal of work has been done with light generated by a discharge through helium: this gives a strong line at 58.4 nm ≡ 21.22 eV, i.e. this only ejects electrons with ionization potentials less than 21.22 eV. Much higher photon energies are used for electrons deeper in the molecule and hence X-rays are used giving rise to a technique called X-ray photoelectron spectroscopy which is used for qualitative chemical analysis.

Both U.V and X-ray have proved to be a useful analytical techniques, U.V being used to detect molecules on the basis of spectral "finger prints"[103], and X-ray being used to detect atoms on the basis of characteristic binding energies[104]. Thus by combining core and valence ionization potentials data one can quantify the bonding or anti-bonding character of molecular orbitals. This is the kind of information that chemists have always hoped to obtain from photoelectron spectroscopy but which until recently has generally only been obtained from theoretical calculations.

5.4.2 Results and Discussion.

This work has been done at Sussex University using Perkin Elmer PS16. The valence ionization potentials of TTF, Dibenzo TTF and TTF/DYE compounds are recorded using helium resonance line (584Å) as the excitation source. Lower and upper limits of ionization potential are marked by helium and argon (ionization potential of 4.98 and 15.75 eV respectively). The photoelectron spectra of the three compounds as well as the first two ionization potentials are shown in Figures (52), (53), (54) and Table (27).

Table (27) First and Second Ionization Potentials and the Binding Energy for TTF, Dibenzo TTF and TTF/DYE Using P.E.S.

Compound	1st I.P±0.05 (eV)	2nd I.P±0.05 (eV)	Binding Energy (1st-2nd orbitals)
TTF	6.80	8.90	2.1
Dibenzo TTF	6.90	8.60	1.7
TTF/DYE	6.80	8.60	1.8

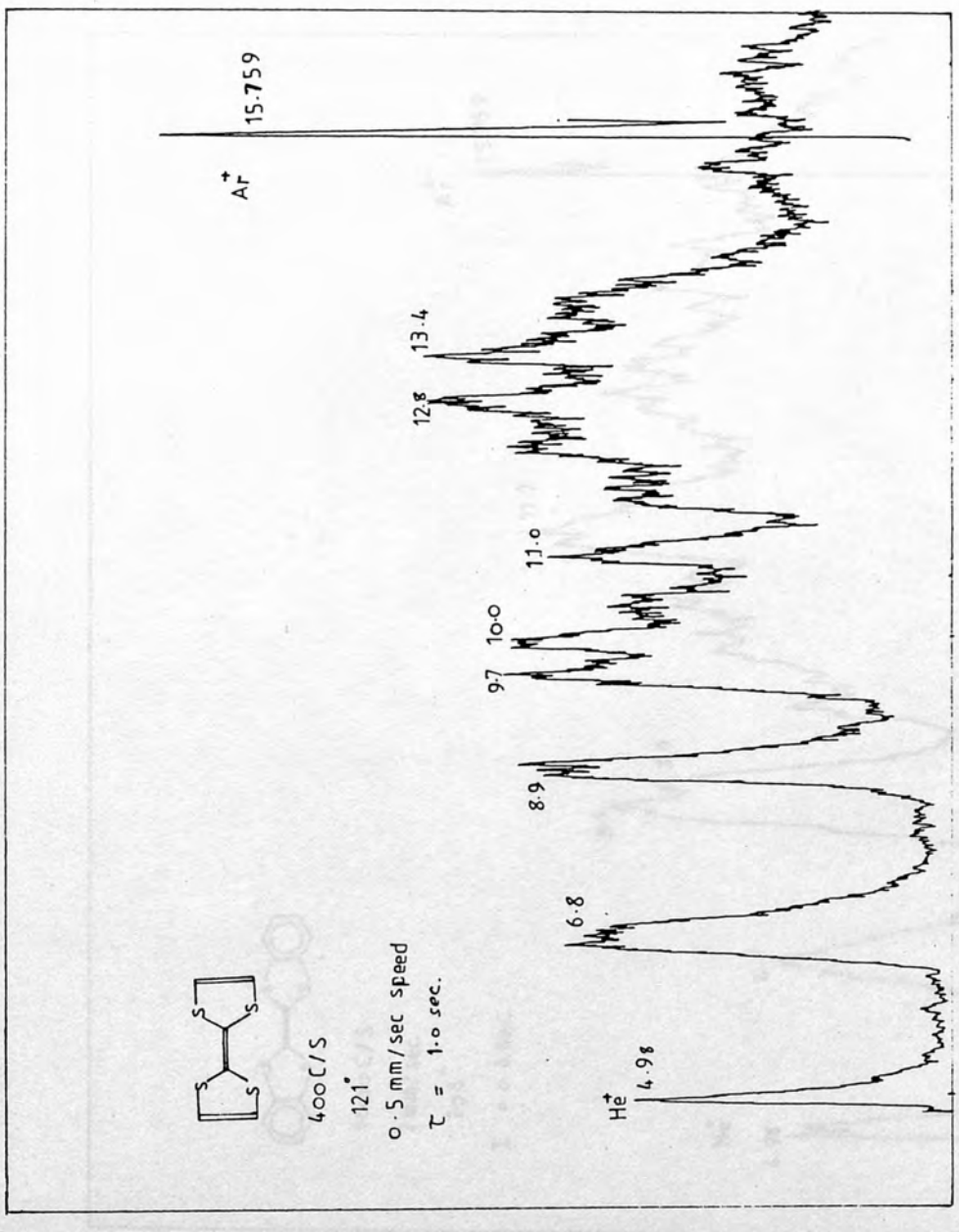

Figure (52) Photoelectron Spectrum for TTF Molecule at 121°C.

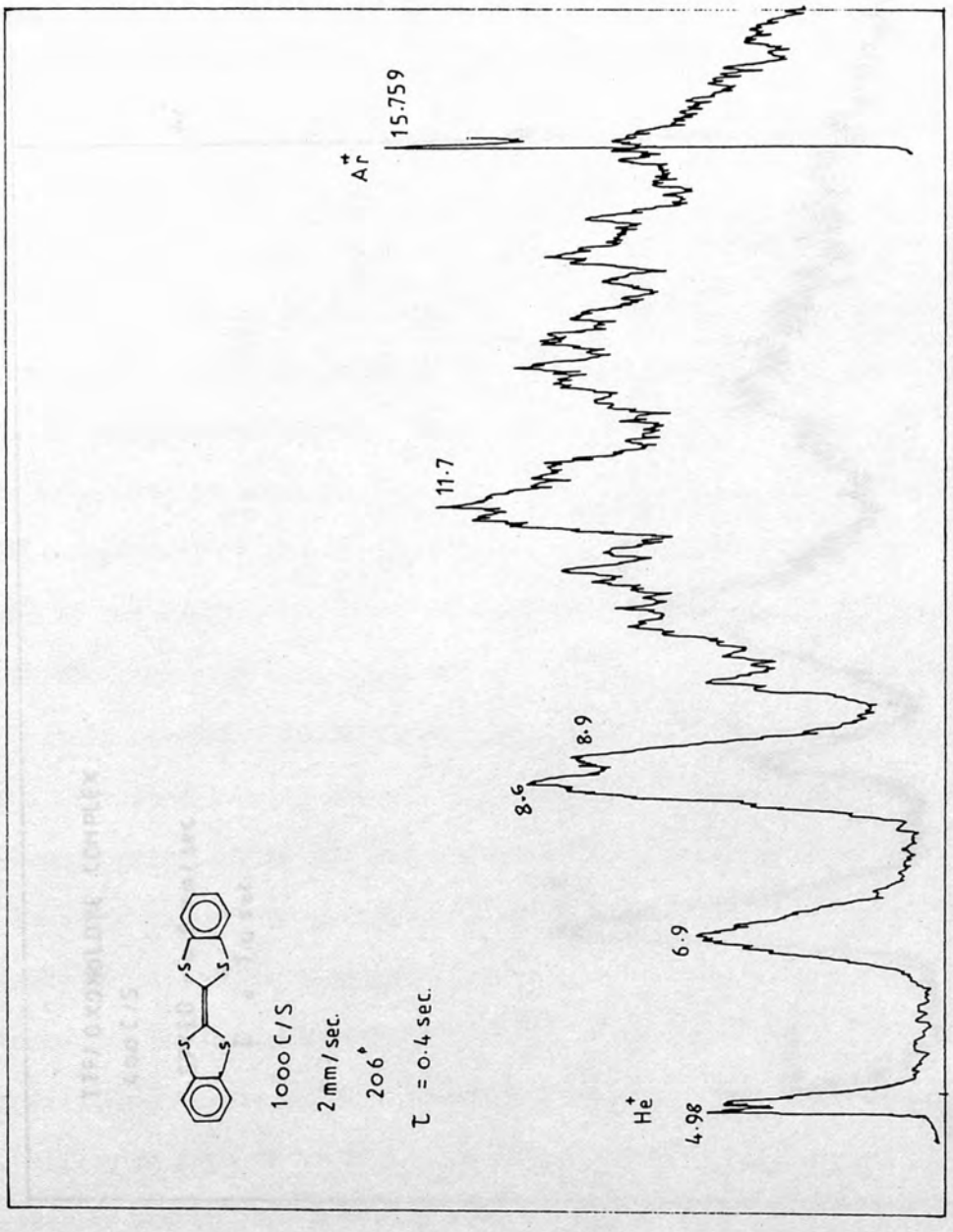

Figure (53) Photoelectron Spectrum for Dibenzo TTF Molecule at 206°C.

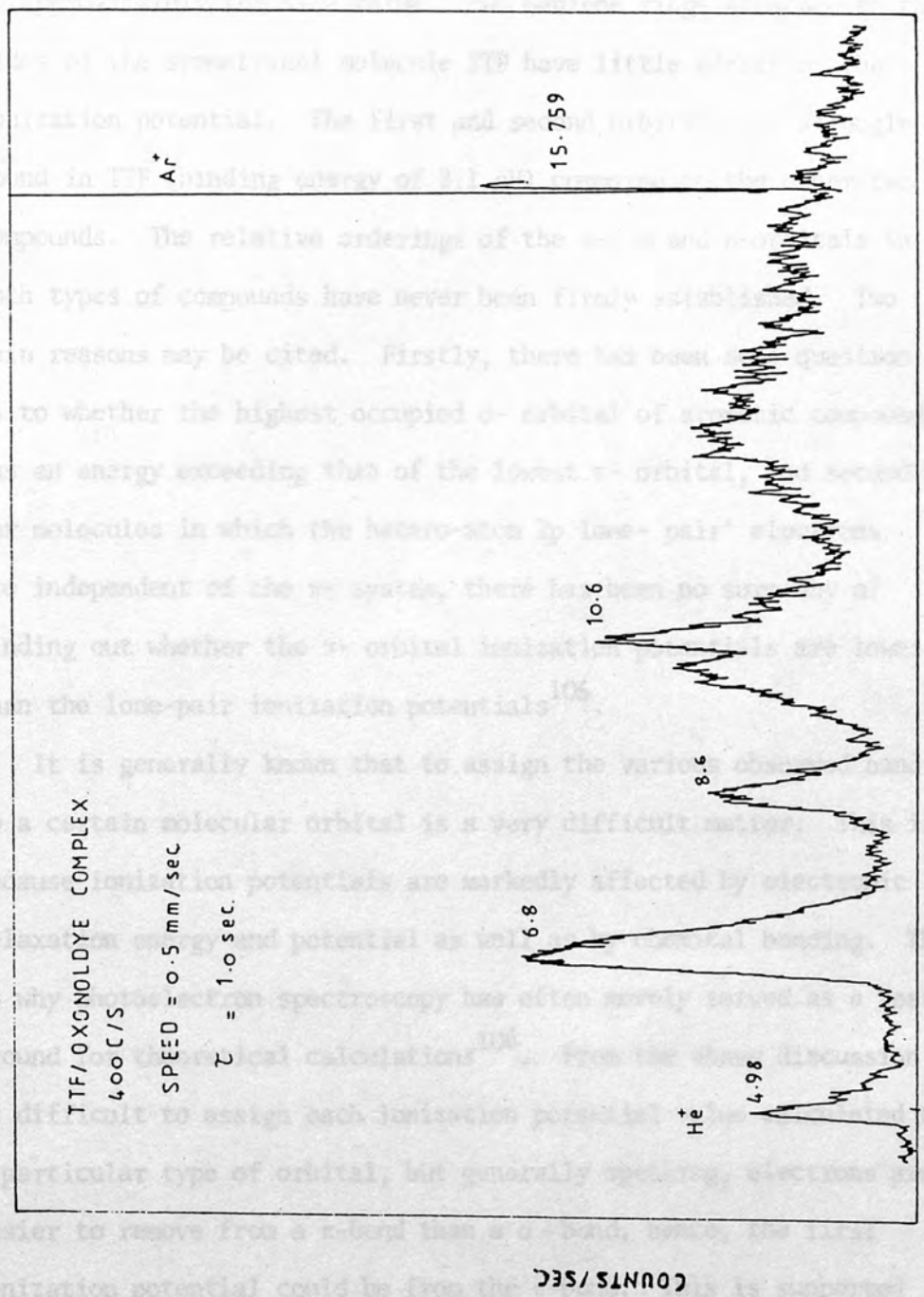

Figure (54) Photoelectron Spectrum for TTF/DYE Complex.

It is shown clearly that TTF, Dibenzo TTF and TTF/DYE photoionized at approximately the same value. Two benzene rings attached to the sides of the symmetrical molecule TTF have little effect on the ionization potential. The first and second orbitals are strongly bound in TTF (binding energy of 2.1 eV) compared to the other two compounds. The relative orderings of the π-, σ and n-orbitals in such types of compounds have never been firmly established. Two main reasons may be cited. Firstly, there has been some question as to whether the highest occupied σ- orbital of aromatic compounds has an energy exceeding that of the lowest π- orbital, and secondly, for molecules in which the hetero-atom 2p lone- pair' electrons are independent of the π- system, there has been no sure way of finding out whether the π- orbital ionization potentials are lower than the lone-pair ionization potentials[105].

It is generally known that to assign the various observed bands to a certain molecular orbital is a very difficult matter. This is because ionization potentials are markedly affected by electronic relaxation energy and potential as well as by chemical bonding. That is why photoelectron spectroscopy has often merely served as a testing ground for theoretical calculations[106]. From the above discussion it is difficult to assign each ionization potential value calculated to a particular type of orbital, but generally speaking, electrons are easier to remove from a π-bond than a σ - bond, hence, the first ionization potential could be from the π-bond. This is supported by the fine structure appearing in each of the three spectra.

CHAPTER 6

Preliminary Investigation of the use of Charge-Transfer Compounds as Gas Sensors.

6. Introduction

It has long been known that adsorbed gases can have a marked effect on the electrical conductivity of semiconductors. The effect has been reported in transition metal oxides[107], anionic dyes[108], phthalocyanine films[109] and a range of organic solids[27].

It has been shown that the electrical conductivity of β-carotene varies with oxygen pressure[110], while studies by Labes[111] and Labes and Rudyi[112] on the iodine-anthracene and chloranil-amine systems and by Misra[113] on β-carotene show the potential of these materials as the basis of gas detecting systems. The conductivity of organic semiconductors can change by many orders of magnitude when a gas adsorbs on their surfaces, which makes them ideal for detecting very low concentrations of pollutants. When a gas molecule chemisorbs on the surface of a semiconductor, an electron or electrons may be transferred from one to the other, the direction of this transfer depending upon the electronegativity of the gas and the work function of the solid[114].

Very recently an ionomer-film modified electrode was introduced into the sensing process[115]. An ionomer is a linear or branched organic polymer which contains covalently attached ionizable groups[116]. Ion-exchange selectivity coefficients for a series of alkyl-substituted pyridinium cations in Na/ion have been measured. The large value of these coefficients are attributed to the hydrophobic effects; a free-energy relationship relating the coefficients to the size of the ion has been described.

A semiconductor for use as the basis of a gas sensor must have the following properties[114]:

1. Its conductivity must vary with the concentration, in ambient air, of the gas to be measured. This effect must be reversible, i.e. in the absence of the gas the conductivity must return to its original value, as well as reproducible if the sensor is to be used in instruments.

2. The material must be stable when heated to temperatures high enough for the reaction of interest to take place quickly and reversibly, and to temperatures > 100°C in order to minimize water condensation effects.

Although not essential it is desirable, from the point of view of providing cheap instrumentation, that the fabrication of sensors using the material is easy and cheap. It would also be an advantage to be able to modify the structure of the semiconductor in order to vary its sensitivity to different gases.

The phthalocyanines satisfy most of these conditions. Various gases have been shown to affect the electrical conductivity of these materials[27]. Although the reversibility of these effects have not been fully investigated, at least a degree of reversibility has been reported[117]. In this section sensors are described in which the conductivity changes in some charge-transfer compounds (TTF/TCNQ, TTFCl, LiTCNQ and TTF/DYE) thin discs and films are used as a possible means of detecting some pollutant gases (SO_2, H_2S, NO_2, CO, O_2, CH_4).

6.1 Preparation of Electrodes for Gas Sensors

Phthalocyanines and their derivatives are the major organic materials used as gas sensors as mentioned before. In this section, the use of some charge-transfer compounds as gas sensors were tested. Different methods were used to construct the electrodes of which the printed circuit comb-shaped electrode is the most successful. These methods can be summarized:

a. Impregnating the electroactive material into the silica gel coated plastic electrode.
b. A microscopic slide glass with a rough surface on which a thin layer of the electroactive material was coated.
c. A pressed disc of the conducting powder.
d. Polytetrafluoroethylene/alumina porous mixture as substrate for conducting powder.
e. A comb-shaped copper electrode formed from a printed circuit board.

All methods (a-d) give an electrode of high resistance, which are not suitable to be used as detectors. The last method (e) seems to work if certain parameters, such as the coated layer thickness could be controlled.

6.1.1 Printed Circuit Copper Electrode

A single side epoxy glass copper-clad board of thickness 1.6 mm was used in constructing this electrode. The comb-shape of copper layer on the surface (thickness $\sim$ 30 μm) was formed using an etch resist ink pen. The whole assembly was dipped in concentrated solution of ferric chloride (2.0 M) for about 2.0 hours and then removed from the solution, and rinsed with distilled water. The ink

was washed out using ethyl alcohol. The two terminals were welded to tinned-copper wires for connection. This is shown is Figure 55a. The organic substance under test was pressed in a form of a thin disc on the surface of the copper electrode, Figure 55b.

6.2 Change of Surface Conductivity for Different Electrode Materials on Passing Set of Different Gases.

The electrode prepared was encapsulated in a glass tube with the thin layer surface of the electroactive material facing an air inlet (Figure 55c). The two terminals were connected to an Automatic Precision Bridge B905 to measure change of surface conductivity during gas flow. The gas was allowed to flow over the electrode surface with a flow rate of 24 cm^3/min. Change of conductivity with time was recorded during gas flow and after gas stopped flowing. The first compound tested was TTF/TCNQ. SO_2, H_2S, Cl_2, CH_4, NO_2 and O_2 pure gases were tested. Figure (56) showed that on passing SO_2 gas, the conductance decreased with time, but it increased when the gas stopped flowing which indicates that the response is reversible. On the other hand oxygen decreased the conductivity and no recovery was observed even when the gas stopped. Figure (57) showed oxygen gas compared to methane which has the same effect. On diluting SO_2 and CO gases, the effect is very small as it was shown in Figure (58).

To show that which component of the complex TTF/TCNQ has the largest effect on gas adsorption, an experiment was run with TTF and TCNQ simple salts using dilute gases. Figures (59) and (60) show the

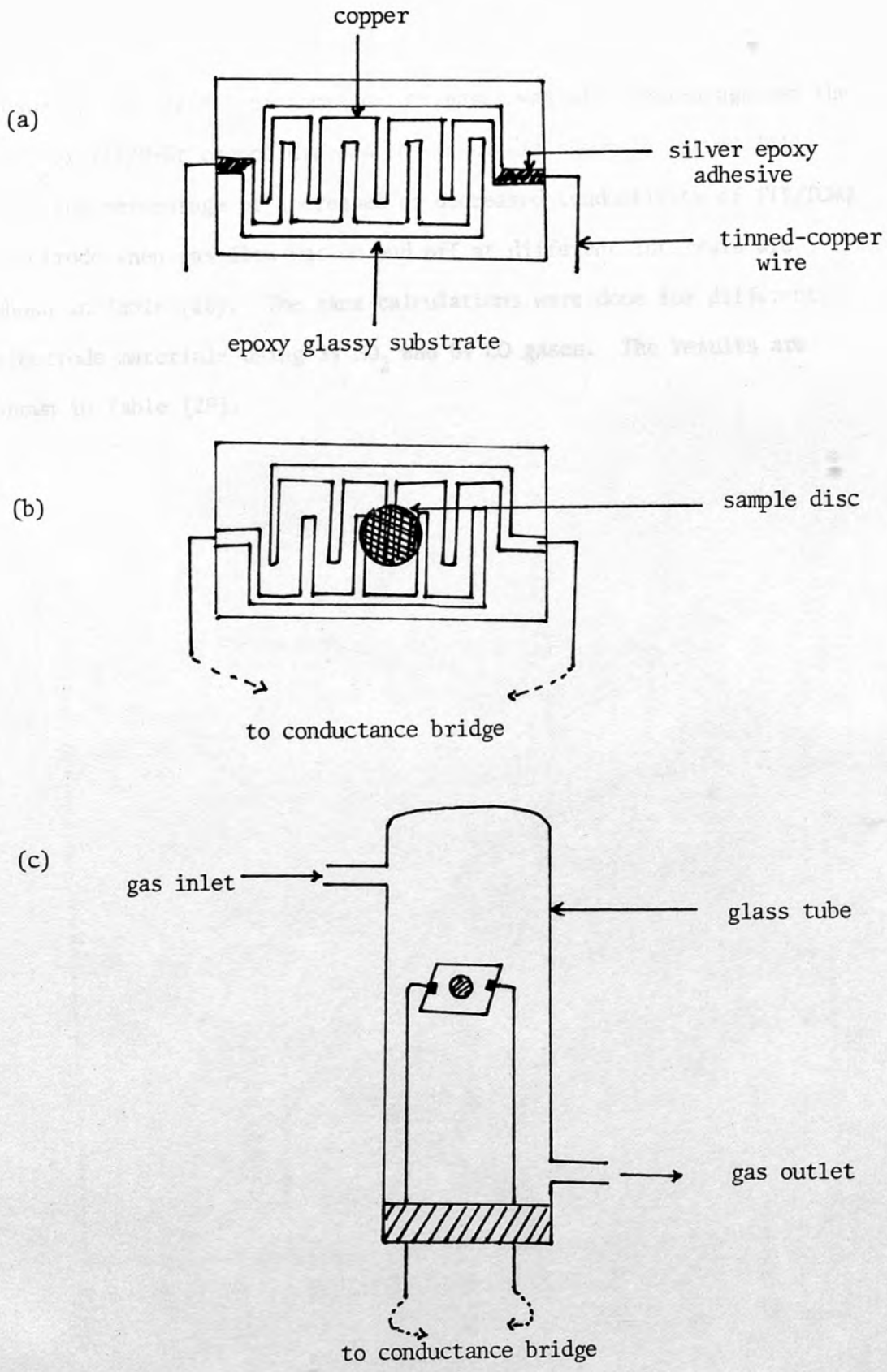

Figure (55) Assembly for electrical contact (a) and (b) and for gas sensor (c).

results. The effect of these dilute gases was also tested against the complex TTF/N-Et oxonol dye and the result is shown in Figure (61).

The percentage of increased or decreased conductivity of TTF/TCNQ electrode when gas flow was on and off at different intervals are shown in Table (28). The same calculations were done for different electrode materials using 5% SO_2 and 8% CO gases. The results are shown in Table (29).

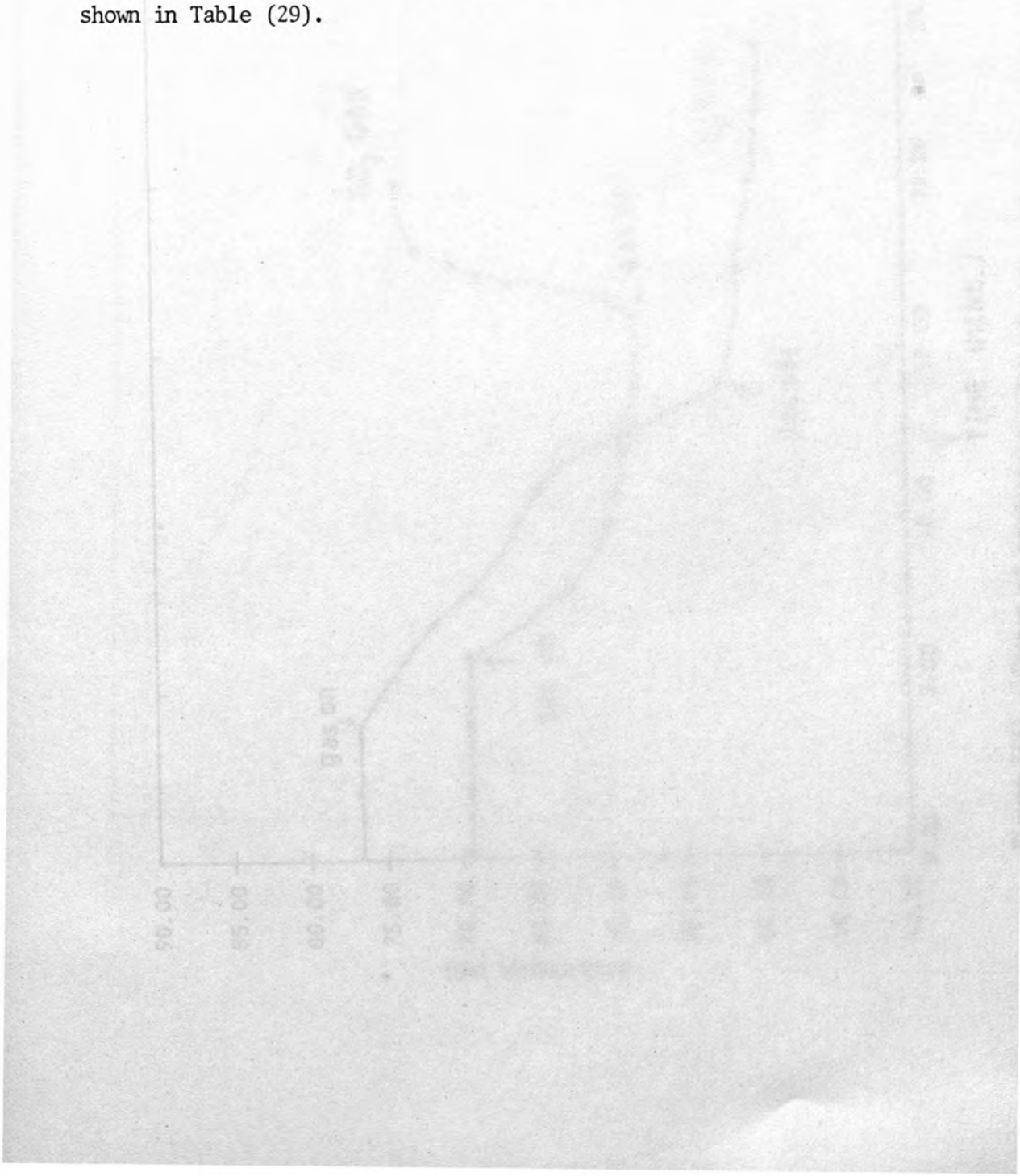

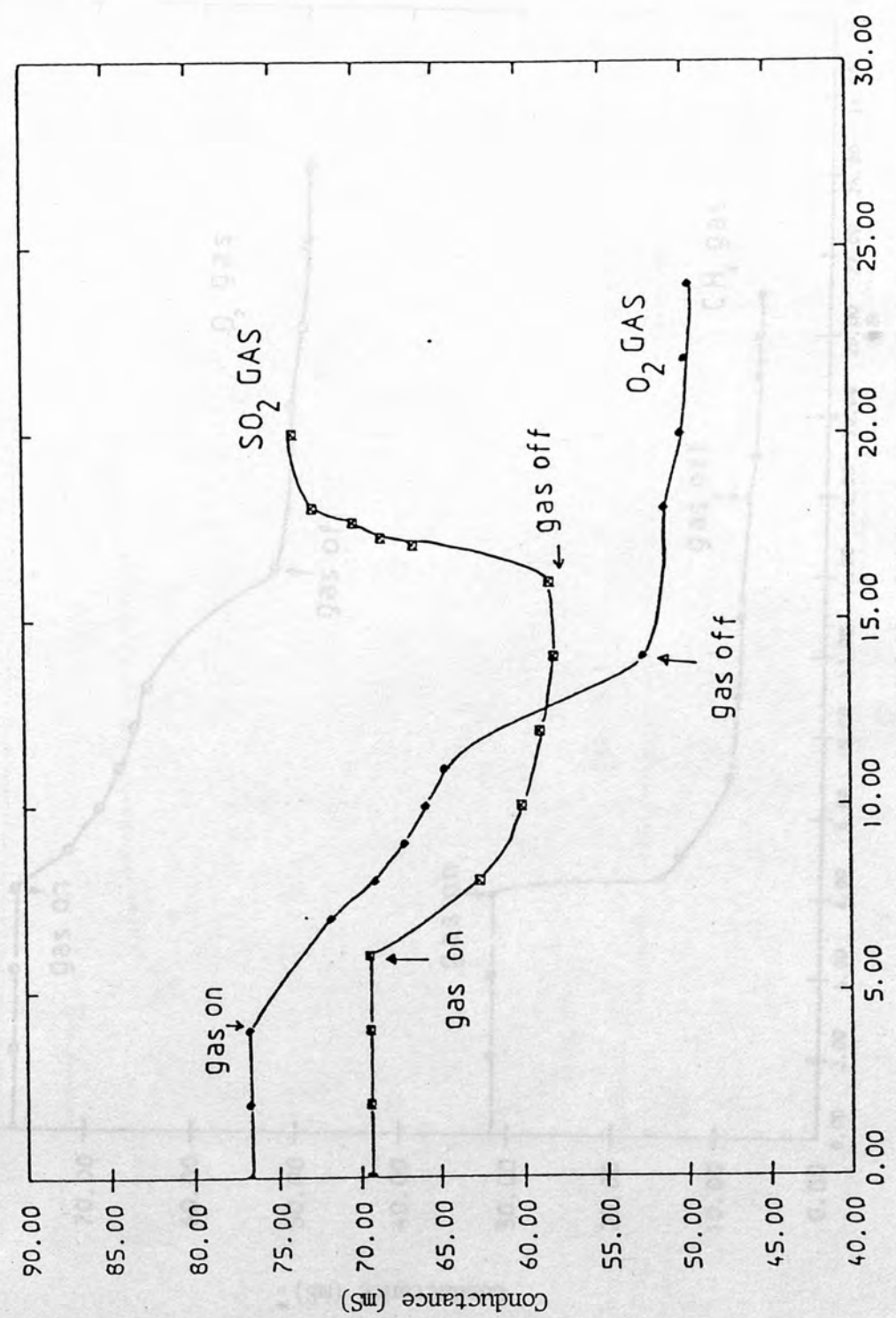

Figure (56) Change of conductance with time when SO_2 and O_2 gases adsorbed on TTF/TCNQ electrodes.

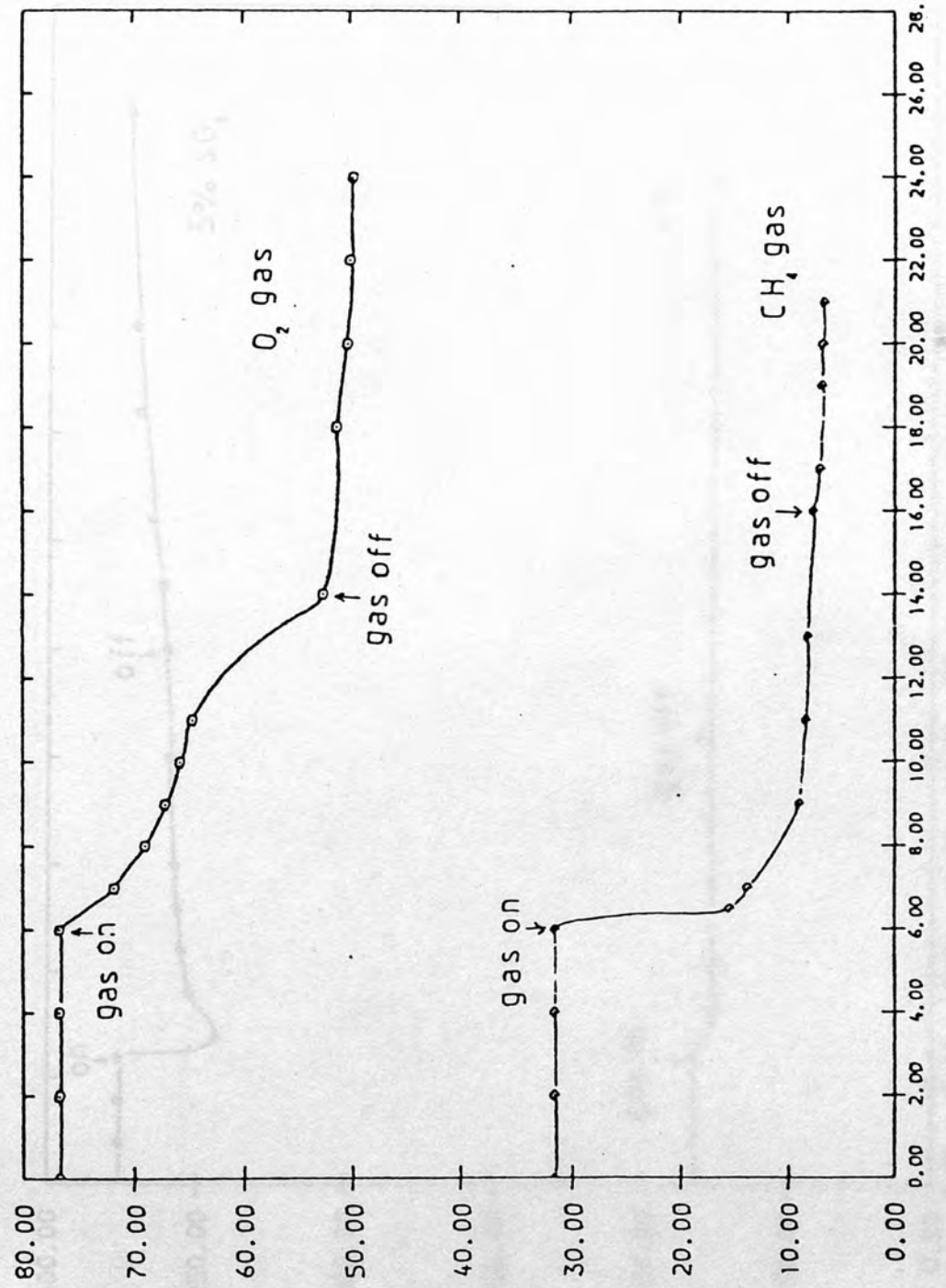

Figure (57) CHANGE OF SURFACE CONDUCTIVITY WITH TIME FOR O_2, CH_4 GASES ACT ON TTF/TCNQ ELECTRODES.

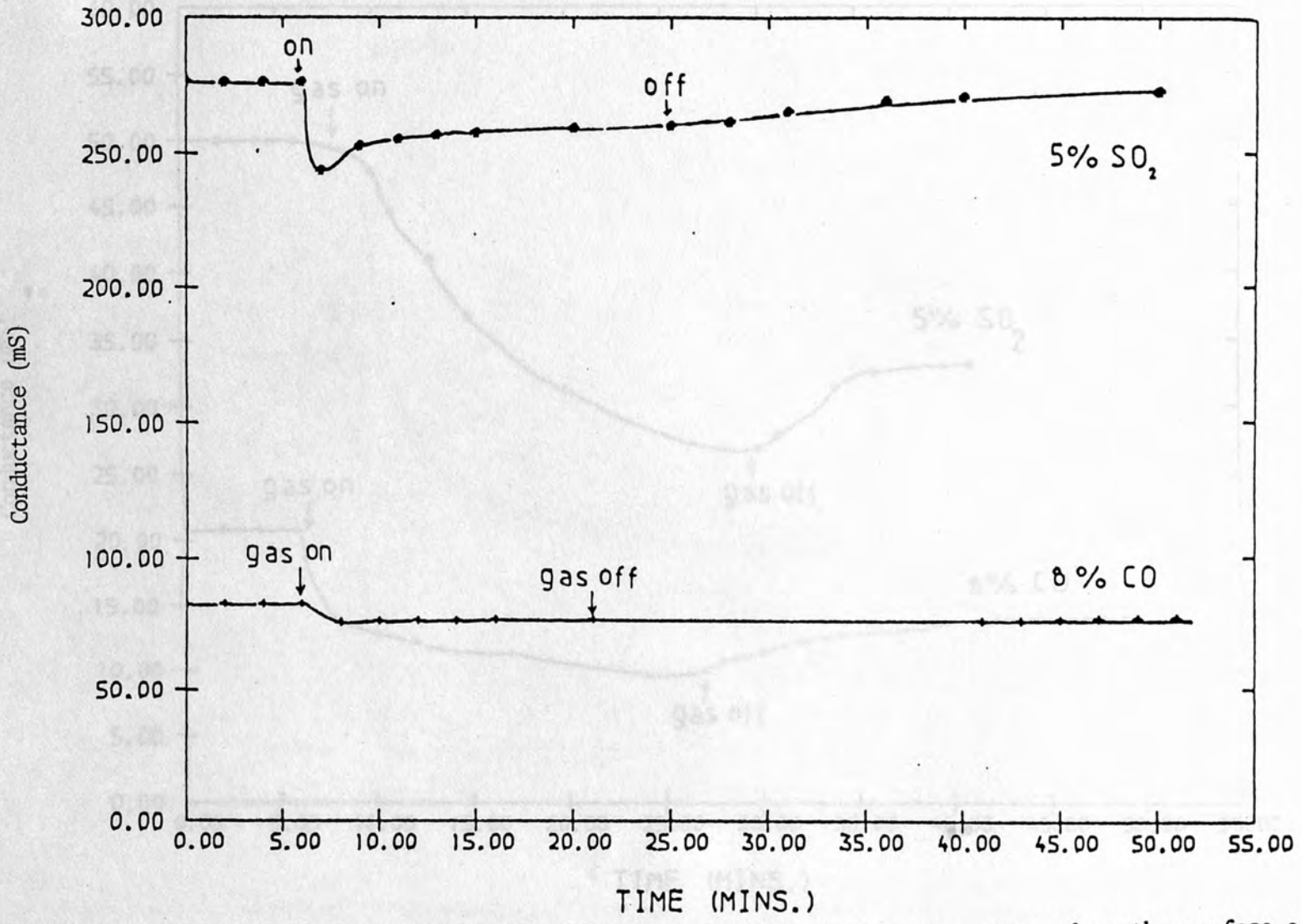

Figure (58) Change of conductance with time when 5% SO_2, 8% CO gases passed on the surface of TTF/TCNQ electrodes.

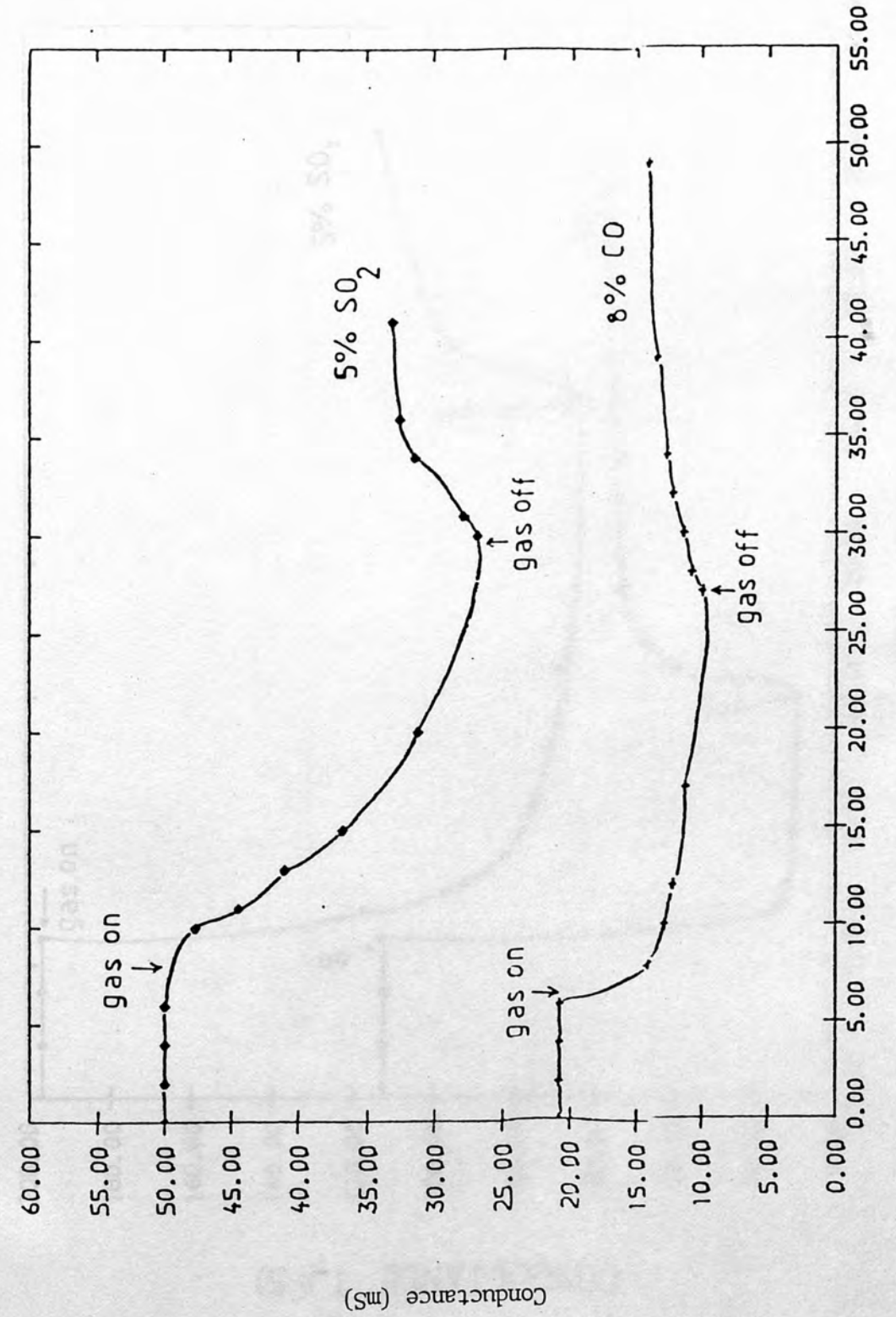

Figure (59) CHANGE OF SURFACE CONDUCTANE WITH TIME FOR 5% SO_2, 8%CO GASES PASSED ON TTFCL ELECTRODES.

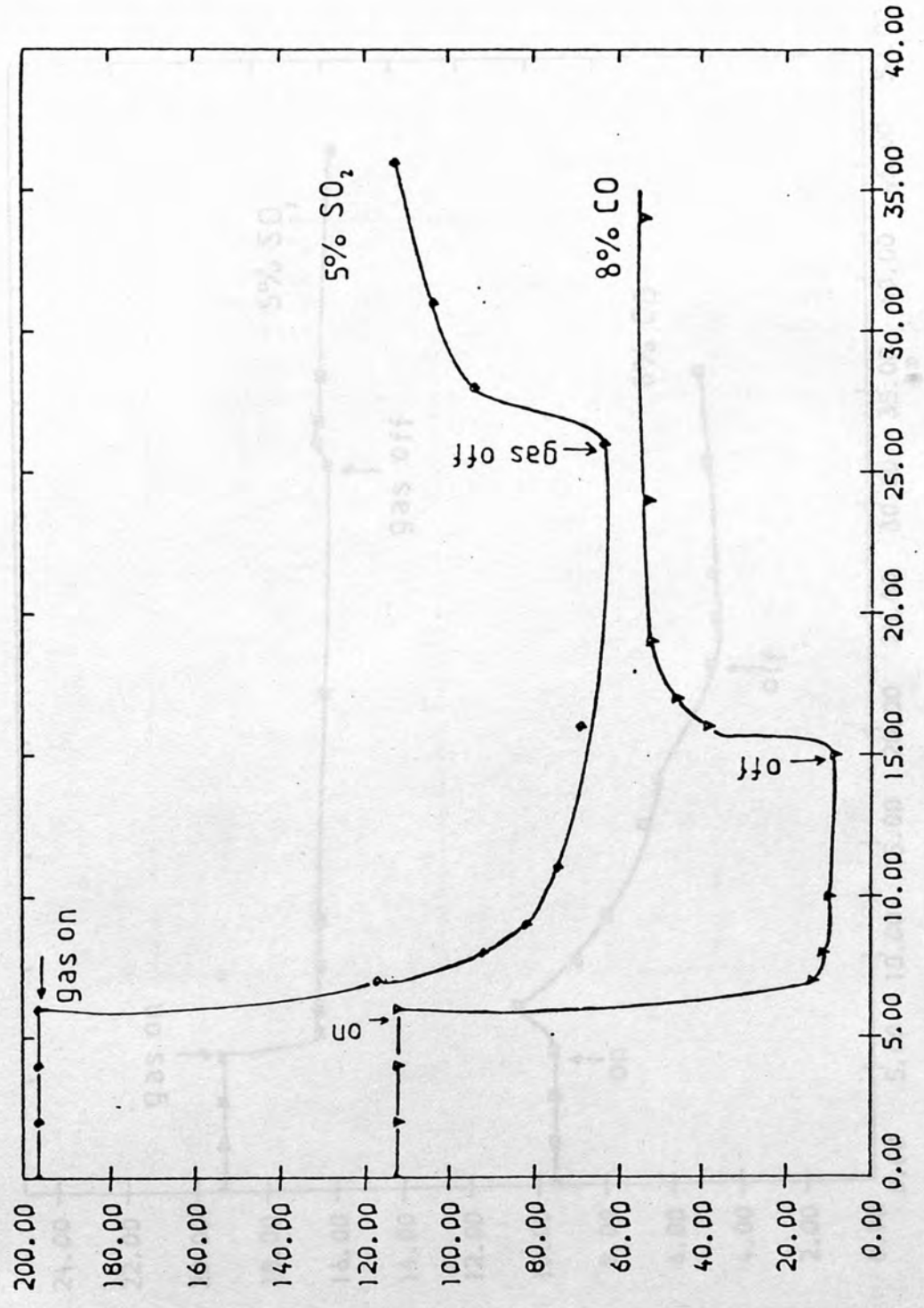

Figure (60) Change of conductance with time when 5% SO_2, 8% CO gases passed on the surface of LiTCNQ electrodes.

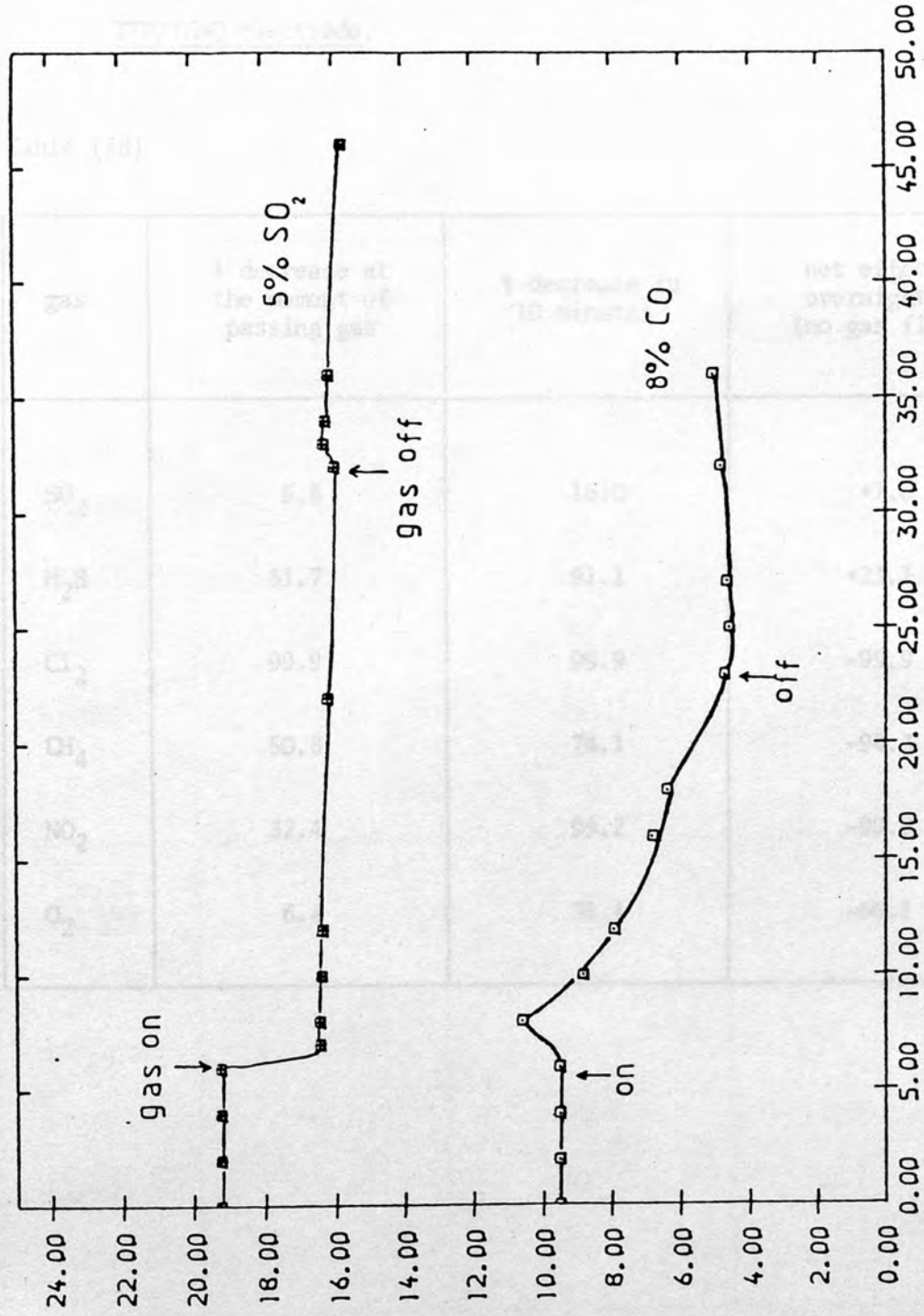

Figure (61) Change of conductance with time when 5% SO_2, 8% CO gases passed on the surface of TTF/DYE electrodes.

6.2.1 Effect of different gases on the surface conductivity of TTF/TCNQ electrode.

Table (28)

gas	% decrease at the moment of passing gas	% decrease in 10 minutes	net effect overnight (no gas flow)
SO_2	9.8	16.0	+7.0
H_2S	31.7	91.1	+23.1
Cl_2	99.9	99.9	-99.9
CH_4	50.8	74.1	-94.3
NO_2	32.4	99.2	-99.9
O_2	6.4	31.4	-66.1

6.2.2 Effect of 8% CO gas and 5% SO_2 gas (in N_2) on different electrode material conductivity.

Table (29)

electrode material	at the moment of gas flow	after 10 minutes of gas flow	net effect overnight (no gas)
CO gas			
TTF/TCNQ	-8.7	-7.3	-51.6
TTF/DYE	+11.5	-28.5	-76.2
TTFCl	-32.1	-46.2	59.2
LiTCNQ	-87.7	-92.1	-10.3
SO_2 gas			
TTF/TCNQ	-11.9	-6.8	-1.3
TTF/DYE	-14.4	-15.8	
TTFCl	+11.8	-26.4	-70.3
LiTCNQ	-40.3	-64.7	-30.7

6.3 Vacuum Sublimation Thin Film Electrode.

A thin film of TTF/TCNQ was coated on the surface of a comb-shaped copper electrode by the vacuum sublimation process. The sample sublimed under vacuum (∿ 60 mmHg) and heating (∿ 110-120°C) on to a surface of the electrode already fixed above the sample and connected to a Conductance Bridge via tungsten pinch-seated copper wires (Figure (62)). The thickness of the layer evaporated was followed by the drop on resistivity. When a reasonable reading was reached (∿ 600 Ω), the electrode was disconnected from the sublimation chamber. This electrode was used for detection of SO_2 at different concentrations. The change of conductivity with gas percentage is shown in Figure (63).

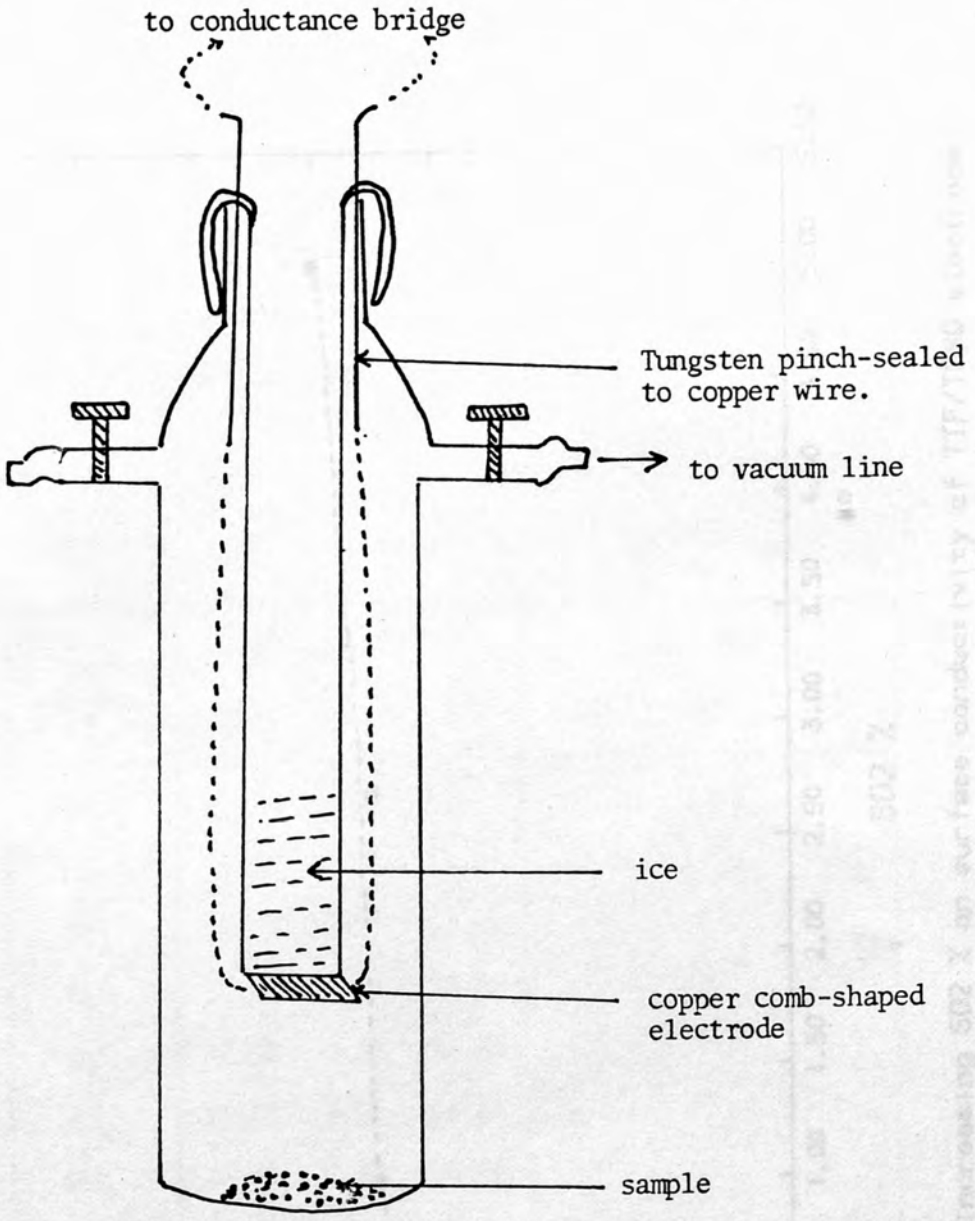

Figure (62) 6.3.1 Apparatus used for vacuum sublimation of TTF/TCNQ.

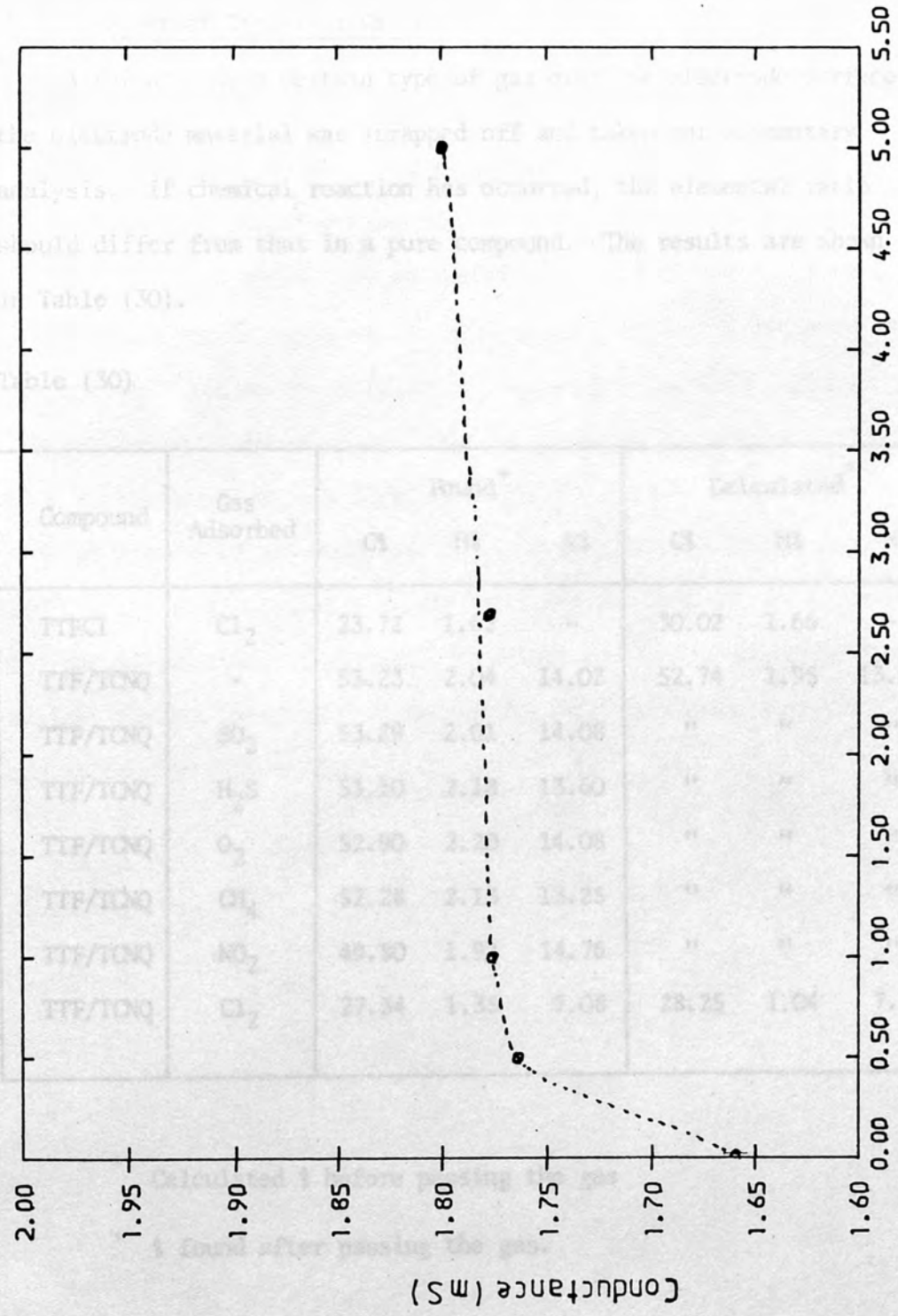

Figure (63) Effect of increasing SO2 % on surface conductivity of TTF/TCNQ electrode

6.3.3 Microanalysis of TTF/TCNQ Electrode Material after Passing a set of Different Gases.

After passing a certain type of gas over the electrode surface, the electrode material was scrapped off and taken for elementary analysis. If chemical reaction has occurred, the elemental ratio should differ from that in a pure compound. The results are shown in Table (30).

Table (30)

Compound	Gas Adsorbed	Found+			Calculated*		
		C%	H%	N%	C%	H%	N%
TTFCl	Cl_2	23.72	1.62	-	30.02	1.66	-
TTF/TCNQ	-	53.23	2.04	14.02	52.74	1.95	13.67
TTF/TCNQ	SO_2	53.29	2.01	14.08	"	"	"
TTF/TCNQ	H_2S	53.10	2.18	13.60	"	"	"
TTF/TCNQ	O_2	52.90	2.20	14.08	"	"	"
TTF/TCNQ	CH_4	52.28	2.13	13.25	"	"	"
TTF/TCNQ	NO_2	49.80	1.92	14.76	"	"	"
TTF/TCNQ	Cl_2	27.34	1.35	7.08	28.25	1.04	7.32

* Calculated % before passing the gas

\+ % found after passing the gas.

6.4 Adsorption of SO_2 Gas on the Surface of TTF/TCNQ Electrode Under Vacuum.

The adsorption measurements were done in a vacuum line already constructed by a colleague. Figure (64) showed the parts of the vacuum line used. The sample was weighed using a vacuum electronic micro-balance (C.I. Electronics Limited). The pressure of the gas entering the system was measured by a manometer connected to the right of the assembly and the pressure which acted on the sample was measured with the one connected at the left. The high vacuum was maintained using a Diffusion and a Rotary pump. The low pressure of the gas measured by a Vacuum Gauge, Pirani Type, Model 8/2.

To get rid of any moisture on the sample, it was heated to around 100^{o}C using an Electronic Furnace Type LMF4 and then cooled before the gas passed over. The change in weight of the sample was measured against the gas pressure and the results were tabulated in Table (31), and plotted in Figure (65).

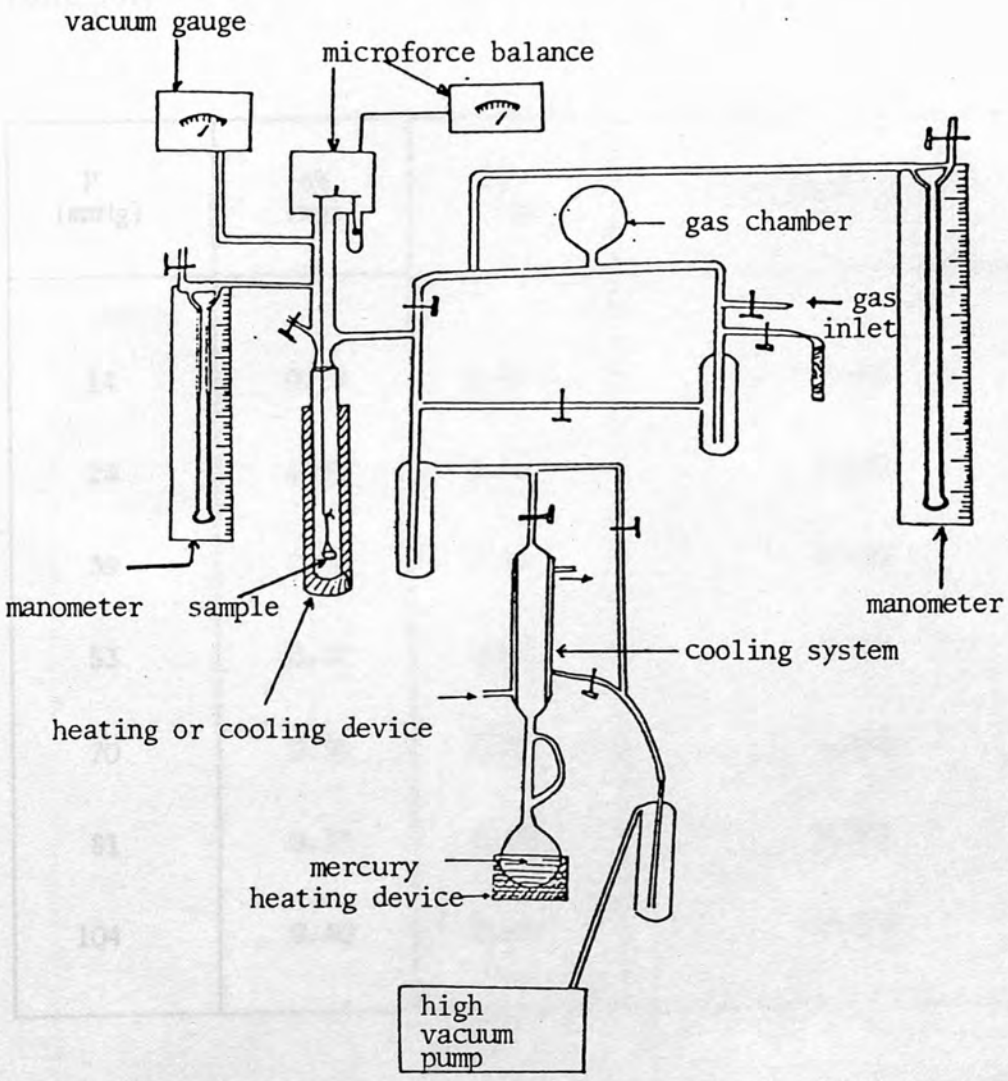

Figure (64) 6.4.1 Vacuum Line used for adsorption measurements.

6.4.2 Calculated Parameters from BET Equation, for SO_2 Gas Adsorbed on TTF/TCNQ Electrode[118].

Table (31)

P (mmHg)	ΔW (mg)	$P/_{po}$	$(1/W[(P/po)-1]\,(mg^{-1})$
14	0.18	0.02	0.104
24	0.20	0.03	0.163
39	0.30	0.05	0.180
53	0.32	0.07	0.234
70	0.36	0.09	0.282
81	0.37	0.106	0.322
104	0.40	0.137	0.396

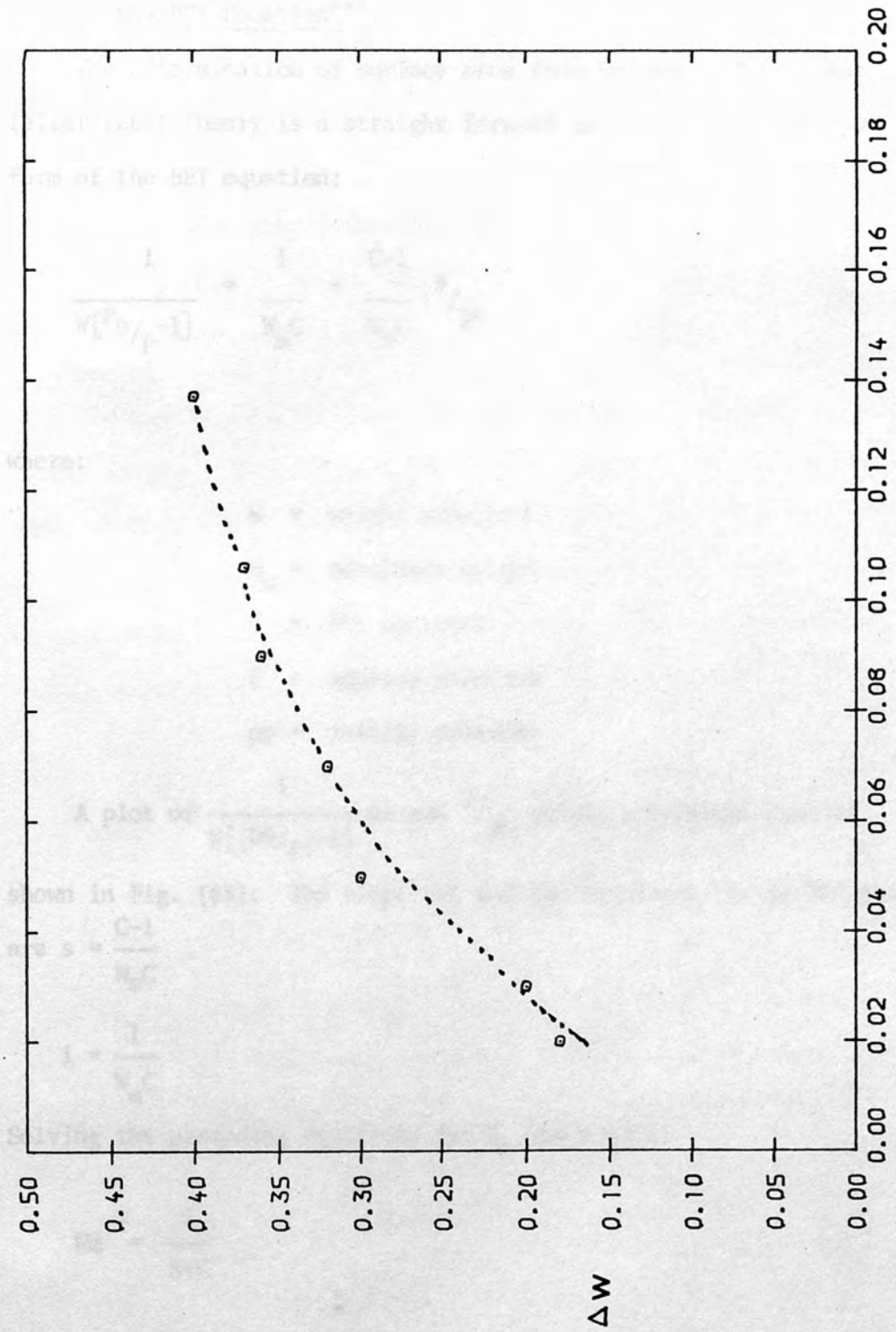

Figure (65) Graph of Δw versus p/p_o for SO_2 Gas act on TTF/TCNQ Electrode

6.4.3 Calculation of Specific Surface Area of TTF/TCNQ from the BET Equation[118].

The determination of surface area from Brunauer, Emmett and Teller (BET) Theory is a straight forward application of the final form of the BET equation:

$$\frac{1}{W[P_o/_p - 1]} = \frac{1}{W_m C} + \frac{C-1}{W_m C} P/_{po} \qquad (1)$$

where:

W = weight adsorbed

W_m = monolayer weight

C = BET constant

P = applied pressure

po = initial pressure

A plot of $\frac{1}{W[(po/_p)-1]}$ versus $P/_{po}$ yields a straight line as shown in Fig. (65). The slope (s) and the intercept (i) of BET plot are $s = \frac{C-1}{W_m C}$

$$i = \frac{1}{W_m C}$$

Solving the preceding equations for W_m and C gives:

$$Wm = \frac{1}{S+C} \qquad (2)$$

$$C = \frac{S}{C} + 1 \qquad (3)$$

The total surface area can be calculated from the Langmuir equation:

$$S_t = \frac{W_m N^- \alpha}{M^-} \qquad (4)$$

where: α is the cross-sectional area,

M^- is the molecular weight of an adsorbate molecule and

N^- is Avogadro's number.

The specific surface area can be determined by dividing S_t by the sample weight. To do so, the area for one molecule of the adsorbate must be known. This was calculated from sulphur dioxide molecules in which the area occupied by one molecule was calculated from sulphur-oxygen radius i.e. assuming the sulphur atom at the centre of the circle occupied by one molecule as shown below:

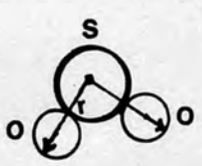

The area occupied by one SO_2 molecule was found to be equal 25.2×10^{-20} m^2. The monolayer weight = 0.1604×10^{-3} gram substitution in equation (4) yield a total surface area of 0.380 m^2. Dividing by the weight of the complex used (0.0995 gr) gives the specific surface area of 3.82 $m^2 g^{-1}$.

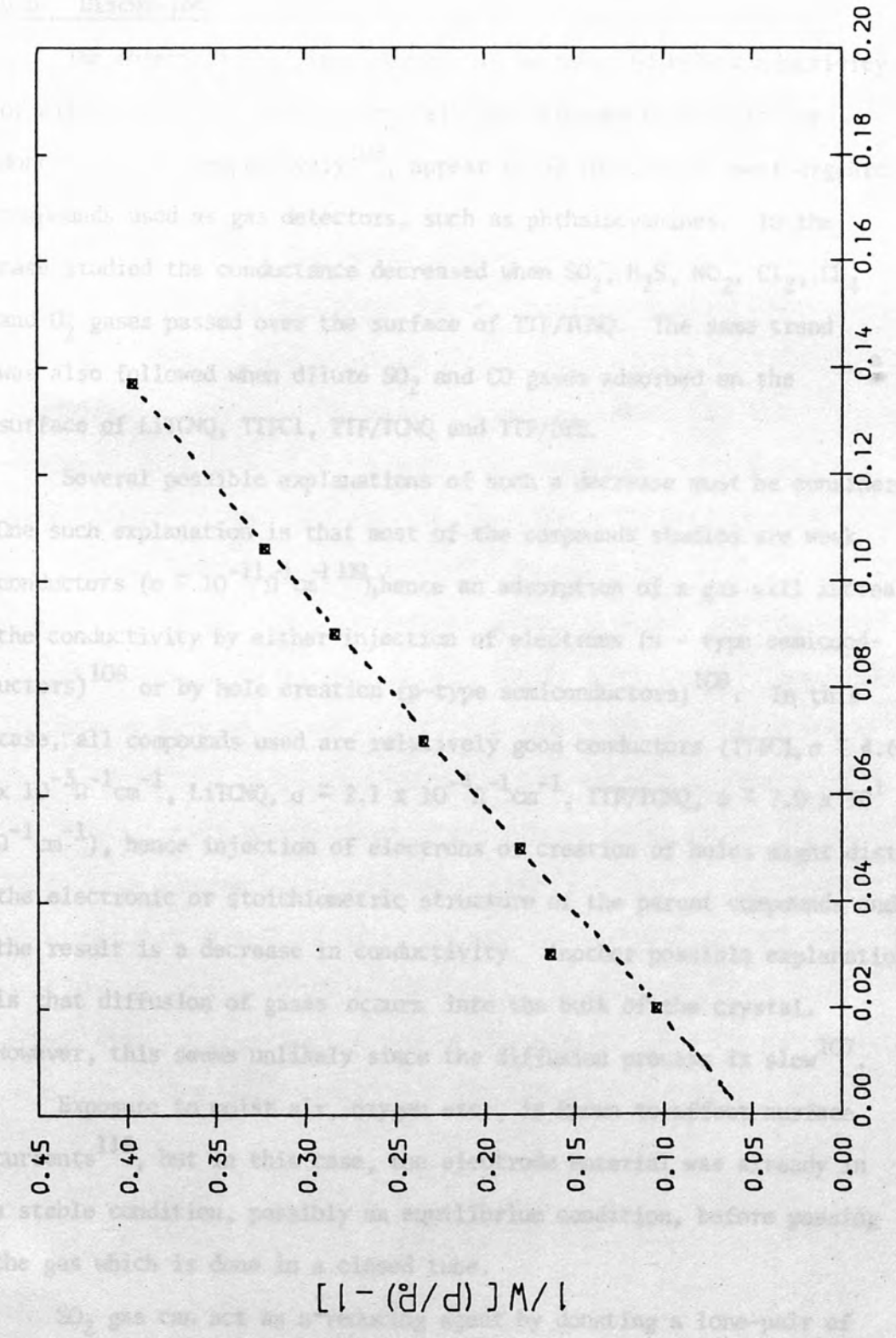

Figure (66) Grapg of 1/W[(P/P)-1] versus P/P. for SO_2 Gas Adsorbed on TTF/TCNQ Electrode

6.5 Discussion

The observation of the increase in surface and bulk conductivity of either doner or acceptor crystals when exposed to acceptor or doner vapours, respectively[108], appear to be the case in most organic compounds used as gas detectors, such as phthalocyanines. In the case studied the conductance decreased when SO_2, H_2S, NO_2, Cl_2, CH_4 and O_2 gases passed over the surface of TTF/TCNQ. The same trend was also followed when dilute SO_2 and CO gases adsorbed on the surface of LiTCNQ, TTFCl, TTF/TCNQ and TTF/DYE.

Several possible explanations of such a decrease must be considered. One such explanation is that most of the compounds studied are weak conductors ($\sigma \simeq 10^{-11} \Omega^{-1} cm^{-1}$ [119]),hence an adsorption of a gas will increase the conductivity by either injection of electrons (n - type semiconductors)[108] or by hole creation (p-type semiconductors)[109]. In this case, all compounds used are relatively good conductors (TTFCl, $\sigma \simeq 4.6 \times 10^{-3} \Omega^{-1} cm^{-1}$, LiTCNQ, $\sigma \simeq 2.1 \times 10^{-4} \Omega^{-1} cm^{-1}$, TTF/TCNQ, $\sigma \simeq 7.0 \times 10^{1} \Omega^{-1} cm^{-1}$), hence injection of electrons or creation of holes might disturb the electronic or stoichiometric structure of the parent compounds and the result is a decrease in conductivity. Another possible explanation is that diffusion of gases occurs into the bulk of the crystal. However, this seems unlikely since the diffusion process is slow[107].

Exposure to moist air, oxygen etc., is known to affect surface currents[115], but in this case, the electrode material was already in a stable condition, possibly an equilibrium condition, before passing the gas which is done in a closed tube.

SO_2 gas can act as a reducing agent by donating a lone-pair of electrons from oxygen or sulphur atoms, hence it can act in a process

of electron injection as well as hole creation by accepting electrons into its sulphur d-orbital. NO_2, CH_4, O_2, Cl_2 and H_2S gases reduce the conductivity of TTF/TCNQ irreversibly, while the only possible reversible process is adsorption of SO_2.

Microanalysis of TTF/TCNQ as electrode material before and after passing most of the gases, give almost the same atomic percentage which might indicate that there are no chemical reactions taken place. In case of chlorine gas passed on the surface of TTFCl or TTF/TCNQ electrodes, a change in the element analysis (Table (30)) was observed. This is what was expected to happen, since chlorine can form dication of TTF. Ten chlorine atoms seems to interact with TTF/TCNQ as shown by the microanalysis results.

From the SO_2% versus conductance curve, it seems that the amount of gas for monolayer coverage is very small, since there is not much increase or decrease in conductivity in increasing gas % from 0.5 to 5. This is supported by the small specific surface area calculated from BET Theory. The small increase in conductance using a thin film of TTF/TCNQ by sublimation on passing SO_2 gas of different concentrations indicates that thin films have different structures from thin discs used before, or the effect of moisture is more pronounced in thin films, since moisture on the surface can interact with SO_2 gas to form an acidic medium which leads to an increase in conductance.

CHAPTER 7

General Conclusion and Discussion

7. General Conclusion and Discussion

The electrochemistry of formation of TTF/DYE complex was investigated by cyclic-voltammetry to determine the optimum conditions for its preparation. A narrow range of potential is available to the reaction forming the TTF radical cation (0.30 - 0.77 V versus SCE). Each of these latter reactions will reduce the yield or give unwanted products as a result of indiscriminate anodic currents. The only reaction required to take place is TTF ⟶ $TTF^{+\cdot}$ + e (E^{ϕ} = 0.302 V versus SCE). The electrochemical preparation of TTF/DYE complexes were sensitive to the conditions of the experiment, particularly the duration and magnitude of the current and voltage applied. Formal electrode potentials obtained for TTF/DYE complex in aqueous and non-aqueous media were lower than the values obtained for the two separate precursors.

The first two ionization potentials of TTF and dibenzo TTF, measured from the photoelectron-spectroscopy are close in value, and the formation of a complex with an oxonol dye equally leads to little change. The similarity between the spectra of neutral and complexed TTF suggests that in each case the species observed is the same, namely neutral TTF. Chemical analysis of the salts did not reveal neutral TTF as an impurity in the complex and therefore it is concluded that the TTF vapour arises from the complex itself. It is of interest to note that electrochemical potentials from cyclic-voltammetry measurements are more sensitive to changes in the molecules than either esr or pes although in all techniques it is possible to detect separate features due to TTF and its ions when complexed with the oxonol dye.

TTF/DYE complexes are semiconductors and the trend towards lower conductivity appear to follow the smaller numbers of unpaired electrons. If the number of spins could be increased greater conductivities may be expected. The complex started to lose its unpaired electron at a temperature lower than its decomposition temperature and the loss is irreversible. The isotropic g-factor calculated from esr measurements is large for TTF indicating that a substantial proportion of the unpaired spin density resides on the sulphur atoms, but MNDO calculations for charge-density distribution gives sulphur atoms large positive charge. This might be a defect of MNDO which does not include d-orbitals in its basis set. The same reason may be applied to the observation that ionization potentials predicted by MNDO method are higher than the experimental values by approximately 1 eV.

Charge-transfer complexes show different degrees of response towards some pollutant gases. The response is low for dilute gases which is not desirable for a compound to be used as a gas sensor. The result may be improved if better electrical contact and certain modifications in structure could be made, in addition to control of material thickness.

REFERENCES

1. Garito, A.F., Heeger, A.J., Acc.Chem.Res., 1, 232 (1974).

2. Akamatu, H., Inokuchi, H., Matsunaga, Y., Nature, 173, 168 (1954).

3. Bryce, M.R. and Murphy, L.C., Nature, 309, 119 (1984).

4. Schlenk, W., Justus Liebigs Ann.Chem., 368, 277 (1909).

5. Foster, R. (ed.) "Molecular Complexes", vols. 1,2 (Elek Science, London, 1973, 1974).

6. Acker, D.S. and Hertler, W.R., J.Am.Chem.Soc., 84, 3370 (1962).

7. Melby, L.R., Harder, R.J., Hertler, W.R., Mahler, W., Benson, R.E., and Mochel, W.E., J.Am.Chem.Soc., 84, 3374 (1962).

8. Little, W.A., Phys.Rev., A 134, 1416 (1964).

9. Wudl, F., Smith, G.M. and Hufnagel, E.J., J.C.S.Chem.Commun., 13, 1453 (1970).

10. Wudl, F., Wobschall, D. and Hufnagel, E.J., J.Am.Chem.Soc., 94, 670 (1972).

11. Ferraris, Jr., Cowan, D.O., Walatka, V. and Perstein, J.H., J.Am.Chem.Soc., 95, 948 (1973).

12. Coleman, L.B., Cohen, M.J., Sandman, D.J., Yamagish, F.G., Garito, A.F. and Heeger, A.J., Solid Stat.Commun., 12, 1125 (1973).

13. Coleman, L.B., Cohen, J.A., Garito, A.F. and Heeger, A.J., Phys.Rev., B 7, 2122 (1973).

14. Jerome, D., Mazaud, A., Ribault, M., Bechgaard, K., J.Phys.Lett., 41, 2195 (1980).

15. Shirikawa, H., Louis, E.J., MacDiarmid, A.G., Chiang, C.K. and Heeger, A.J., J.C.S. Chem.Commun., 13, 578 (1977).

16. Chiang, C.K., Fincher, C.R., Jr., Park, Y.W., Heeger, A.J., Shirakawa, H., Louis, E.J., Gau, S.C. and MacDiarmid, A.G., Phys.Rev.Lett., 39, 1098 (1977).

17. Chiang, C.K., Druy, M.A., Gau, S.C., Heeger, A.J., Louis, E.J., MacDiarmid, A.G., Park, Y.W. and Shirakawa, H., J.Am.Chem.Soc., 100, 1013 (1978).

18. Gibson, H.W., Bailey, F.C., Epstein, A.J., Rommelmann, H., Kaplan, S., Harbour, J., Yang, X.Q., Tanner, D.B. and Pochan, J.M., J.Am.Chem.Soc., 105, 4417 (1983).

19. Labes, M.M., Love, P. and Nichols, L.F., Chem.Rev., 79, 1 (1979).

20. Underhill, A.E. and Watkins, D.M., Chem.Soc.Rev., 9, 429 (1980).

21. Soos, Z.G., Ann.Rev.Phys.Chem., 25, 121 (1974).

22. Peristein, J.H., Angew.Chemie, 16, 519 (1977).

23. Torrance, J.B., Acc.Chem.Res., 12, 79 (1979).

24. David, B., "Chemistry in Britain", 19, No. 9,8 (1983).

25. Becker, J.Y., Bernstein, J., Bittner, S., Levi, N. and Shaik, S.S., J.Am.Chem.Soc., 105, 4468 (1983).

26. Trasatti, S. (ed.), "Electrodes of Conductive Metallic Oxides", Elsevier Scientific Publishing Company (Part A), (1980).

27. Gutmann, F., Lyons, L.E., "Organic Semiconductors", John Wiley and Sons, Inc., 1967.

28. Potember, R.S., Poehler, T.O. and Benson, R.C., Appl.Phys.Lett., 41, 548 (1982).

29. Chiang, C.K., Gau, S.C., Fincher, C.R., Jr., Park, Y.W., MacDiarmid, A.G. and Heeger, A.J., Appl.Phys.Lett., 33, 18 (1978).

30. Jaegar, C.D. and Bard, A.J., J.Am.Chem.Soc., 102, 5435 (1980).

31. Delhaes, P., Lussan, C., Valiron, O.M. and Amiell, J., FEBS Lett., 69, 252 (1976).

32. Meguro, K. and Esumi, K., J.Colloid Interface Sci., 59, 93 (1977).

33. Elseoud, A.O., Dasilva, J.M. and Elseoud, I.M., J.Colloid Interface Sci., 62, 119 (1977).

34. Bechgaard, K. and Jerome, D., Scient.Am. 247, 50 (1982).

35. Jacobsen, C.S., Mortensen, K., Andersen, J.R. and Bechgaard, K., Phys.Rev. B18, 905 (1978).

36. Andrieux, A., Duroure, C., Jerome, D. and Bechgaard, K., J.Phys.Paris Lett., 40, 1-381 (1979).

37. Hardebusch, U., Gerhardt, W., Shilling, J.S., Bechgaard, K., Weger, M., Miljack, M. and Cooper, J.R., Solid Stat.Commun., 32, 1151 (1979).

38. Peierls, E.R., "Quantum Theory of Solids", (Oxford Unversity Press, 1955).

39. Frohlich, H., Proc.R.Soc., A223, 296 (1954).

40. Inokuchi, H., Bull.Chem.Soc.Jpn., 24, 222 (1951).

41. Hatano, M., J.Polym.Sci., 51, S26 (1961).

42. Siemons, W.J. Bierstedt, D.E. and Kepler, R.G., J.Chem.Phys. 39, 3523 (1963).

43. Sharp, M., Johansson, G., Anal.Chim.Acta., 54, 13 (1971).

44. Le Blanc, O.H., Jr., J.Chem.Phys., 42, 4307 (1965).

45. Begun, G.M., Compton, R.N., J.Chem.Phys., 58, 2271 (1973).

46. Klots, C.E., Compton, R.N. and Raaen, V.F., J.Chem.Phys., 60, 1177 (1974).

47. Compton, R.N. and Nalley, J.S., Chem.Phys.Lett., 9, 529 (1971).

48. Engler, E.M., Kaufman, F.B. and Green, D.C., J.Am.Chem.Soc., 97, 2921 (1975).

49. Pauling, L., "The Nature of the Chemical Bond", 3rd ed., Cornell University Press, Ithaca, N.Y., P. 59 (1960).

50. Johnson, D.A., "Sulphur in Organic and Inorganic Chemistry", Vol. 2,A. Senning, ed. Marcell Deckker, New York, N.Y., P. 37 (1972).

51. Wheland, R.C., J.Am.Chem.Soc., 99, 291 (1977).

52. Wheland, R.C., J.Am.Chem.Soc., 98, 3962 (1976).

53. Jæger, C.D.,Bard, A.J., J.Am.Chem.Soc., 101, 1690 (1979).

54. Kaufman, F.B., Schroeder, A.H., Engler, E.M., Kramer, S.R. and Chambers, J.Q., J.Am.Chem.Soc., 102, 483 (1980).

55. Lamache, M., Menet, H. and Moradpour, A., J.Am.Chem.Soc., 104, 4520 (1982).

56. Henning, T.P., White, H.S. and Bard, A.J., J.Am.Chem.Soc., 104, 5862 (1982).

57. Arden, W., Phys.Chem., 82, 868 (1978).

58. Williams, J.M., Beno, M.A., Wang, H.H., Leung, P.C.W., Emge, T.J., Geiser, U. and Carlson, K.D., Acc.Chem.Res., 18, 261 (1985).

59. Kini, A.M., Cowan, D.O., Gerson, F and Mocket, R., J.Am.Chem.Soc., 107, 556 (1985).

60. Johnson, A.S.W. and Tseung, A.C.C., J.Appl.Electrochem., 7, 445 (1977).

61. Anti-Corrosion Manual, "Scientific Surveys Ltd.", 84 (1964).

62. Kingery, W.D., "An Introduction to Ceramics", John Wiley and Sons, Chichester (1960).

63. Tseung, A.C.C., "Special Ceramics in Fuel Cells and Batteries in Special Ceramics", Vol.4, (ed. Popper, P.) British Ceramics Res.Assoc., 283 (1968).

64. Scket, J.B., "Crystal Chemistry and Semiconduction", Academic Press, London (1971).

65. Rao, C.N.R. and Subba Rao, G.V., Physica Status Solidi, 1, 597, (1970).

66. Borom, M.P., Longwell, J.A. and Pask, J.A., J.Am.Ceram.Soc., 50, 61 (1967).

67. Pask, J.A. and Fulrath, R.M., J.Am.Ceram.Soc., 45, 592 (1962).

68. King, B.W., Trip, H.P. and Duckworth, W.H., J.Am.Ceram.Soc., 42, 504 (1959).

69. Tseung, A.C.C. and Jasem, S.M., J.Electrochem.Soc., 126, 1353 (1979).

70. Hibbert, D.B., J.C.S.Chem.Commun., 202 (1980).

71. Rasiyah, P. and Tseung, A.C.C., J.Electrochem.Soc., 129, 1724 (1982).

72. Tseung, A.C.C. and Jasem, S.H., Electrochimica Acta., 22, 31 (1977).

73. Adams, R.N., "Electrochemistry at Solid Electrodes", Marcel Dekker, Inc., New York (1969).

74. Gary, A.M., J.Chem.Educ., 60, 697 (1983).

75. Kissinger, P.T., J.Chem.Educ., 60, 705 (1983).

76. Bard, A.J. and Faulkner, L.R., "Electrochemical Methods Fundamentals and Applications", John Wiley and Sons (1980).

77. Bajwa, G.S. and Barrell, K.J., J.Org.Chem., 41, 145 (1976).

78. Farmery, D.L., British Patent, 1, 512 863 (1978).

79. Pletcher, D., "Advanced Instrumental Methods in Electrode Kinetics", Southampton University, 1975.

80. Nicholson, R.S., Anal.Chem., 37, 1351 (1965).

81. Malhotra, S.S. and Whiting, M.C., J.Chem.Soc., 3812 (1960).

82. Reich, C., Pandolfe, W.D. and Bird, G.R., Phot.Sci.Eng., 17, 334 (1973).

83. Wheland, R. and Gibson, J., J.Am.Chem.Soc., 98, 3916 (1976).

84. Coffen, D.L., Chambers, J.O., Williams, D.R., Garraett, D.E. and Canfield, N.D., J.Am.Chem.Soc., 93, 2258 (1971).

85. Baldwin, R.P., Ravichandran, K. and Johnson, R.K., J.Chem.Educ., 61, 821 (1984).

86. Nicholson, R.S. and Shain, I., Anal.Chem., 36, 706 (1964).

87. Bockris, J.O'M. and Reddy, A.K.N., "Modern Electrochemistry", Vol. 2, Plenum Press (1977).

88. Edwards, D., Grossel, M.C., Hamedelniel, A.E., Hibbert, D.B., Postle, J.R. and Webb, T.C., J.Chem.Soc.Chem.Commun., submitted 1986.

89. Edwards, D., Grossel, M.C., Cheetham, A.K. and Eddy, M.M., J.Chem.Soc.Chem.Commun., submitted 1986.

90. Cavara, L., Gerson, F., Cowan, D.O. and Lerstrup, K., Helv.Chem.Acta., 69, 141 (1986).

91. Metzger, R., J.Chem.Phys., 66, 2525 (1977).

92. Wudl, F., Acc.Chem.Res., 17, 227 (1984).

93. Rzepa, H.S., MNDO Quantum Chemistry Package, University of London Computer Centre (1984).

94. Kasper, J.S. and Interrante, L.V., Acta.Cryst., B32, 2914 (1976).

95. Cooper, W.F., Kenny, N.C., Edmonds, J.W., Nagel, A., Wudl, F. and Coppens, P., J.Chem.Soc.Chem.Commun., 889 (1971).

96. Visser, G.J. Heeres, G.J., Wolters, J. and Vos, A., Acta.Cryst., B24 467 (1968).

97. Celver, J.W., GINDO Fortran Program, Chemistry Department, State University of New York at Buffalo.

98. Dewar, M.J.S. and McKee, M.L., J.Comput.Chem., 4, 84 (1983).

99. Hibbert, D.B., Hamedelniel, A.E. and Sutcliffe, L.H., J.Mol.Spec., submitted 1987.

100. Baker, A.D., Ph.D. Thesis, University of London, 1968.

101. Al-Joboury, M.I. and Turner, D.W., J.Chem.Phys., 37, 3007 (1962).

102. Vilesov, F.I., Kurbatov, B.L. and Tererin, A.N., Doklady. Akad.Nauk.SSR., 138, 1329 (1961).

103. Bock, H. and Solouki, B., Angew.Chem., 20, 427 (1981).

104. Muilenberg, G.E., "Handbook of X-Ray Photoelectron Spectroscopy", Perkin Elmer, Eden Prairie, MN, 1978.

105. Turner, D.W., Baker, A.D., Baker, C. and Brundle, C.R., "Molecular Photoelectron Spectroscopy", Wiley Interscience (1970).

106. Jolly, W.L., Acc.Chem.Res., 16, 370 (1983).

107. Stetter, R.J., J.Colloid and Interface Science, 65, 432 (1978).

108. Vartanyan, T.A., Acta Physiochem.USSR, 22, 201 (1947).

109. Bornmann, A.J., J.Chem.Phys., 27, 604 (1957).

110. Rosenberg, B., J.Chem.Phys., 34, 812 (1961).

111. Labes, M.M. Conference on surface effects detection, Washington D.C., 173 (1964).

112. Labes, M.M. and Rudyi, N.O., J.Am.Chem.Soc., 85, 2055 (1963).

113. Misra, N.T., Rosenberg, B. and Switzer, R., J.Chem.Phys., 48, 2096 (1968).

114. Bott, B. and Jones, A.T., Sensors and Actuators, 5, 43 (1984).

115. Espenscheid, M.W., Ghatak, R., Moore, R.B., Penner, R.M., Szentirmay, M.N. and Martin, C.R., J.Chem.Soc., Faraday Trans.I, 82, 1051 (1986).

116. Eisenberge, A. (ed.), "Ion in Polymers, Advances in Chemistry Series 187 (American Chemical Society, Washington, 1980).

117. Van Ewyck, L.R., Ph.D. Thesis, University of Kent, Canterbury, 1978.

118. Lowell, S., "Introduction to Powder Surface Area", John Wiley and Sons, Inc. (1979).

119. Jones, A.T. and Bott, B., "Proceeding of the International Conference on Solid-State Sensors and Actuators-Transducers, Boston, Massachusetts, 1985.

Publications

1. D. Edwards, M.C. Grossel, D.B. Hibbert and A.E. Hamedelniel, A tetrathiafulvalene salt of a photographic dye: A bleachable organic conductor., J.Chem.Soc.Chem.Commun., submitted 1986.

2. D.B. Hibbert, A.E. Hamedelniel, M.C. Grossel and D. Edwards, The electrochemistry of some novel organic conductors and their precursors, Electrochimica Acta, submitted 1986.

3. D.B. Hibbert, A.E. Hamedelniel and L.H. Sutcliffe, ESR and theoratical study of tetrathiafulvalene and dibenzotetrathiafulvanene and their radical cations, J.Mol.Spect., submitted 1987.

Corrections

① Page 65 reactions(s) one s off

② Pages 76, 86 scale

③ Page 101 1mA for 1.0 hour

④ page 98 2 mA should be replaced by 1 mA

⑤ Page 104 n not h

⑥ Page 118 Five compounds not Four cpds